Ansto

LUCAS HEIGHTS RESEARCH LABORATORIES

A REPORT TO NERDDP ON PROJECT No. 1319

entitled

DESCRIPTION OF SYNROC DURABILITY: KINETICS AND MECHANISMS OF REACTION

by

A. JOSTSONS, K.L. SMITH, M.G. BLACKFORD, K.P. HART, G.R. LUMPKIN, P. McGLINN, S. MYHRA, A. NETTING, D.K. PHAM, R. ST. C. SMART AND P.S. TURNER

AUGUST 1990

VOL. III

4.0 KINETIC DESCRIPTION OF SYNROC DURABILITY

Objective 3 of the original project proposal specified an extensive study leading to a kinetic description of the rates of release of individual elements from single-phase minerals and Synroc. The study was to have been based on a full analysis of the data base, built up over two previous 3-year NERDDC projects jointly conducted by ANSTO and Griffith University (Segall et al, 1983; Smart et al, 1987), from leaching and dissolution testing of inactive Synroc specimens from the ANSTO Fabrication Program. The data base from the ANSTO NERDDC study of active (actinide) samples (Reeve et al, 1987) was to be included. It was also to include further study of the kinetics of elemental release to be measured on inactive specimens made for studies in this new project.

Inevitably, with the curtailment of the 3-year program to 1 year, these objectives have had to be modified. In particular, the 1 year program specified that the kinetics of elemental release would only be determined on specimens made for this study. Most of the extensive data base in objective 3 referred to Synroc rather than to predominantly single-phase specimens. Despite this modification, some limited work has been carried out on the inactive leach rate data base from previous studies and this will be described in this report. Additionally, kinetic analysis of new inactive Synroc samples prepared in this project will be described. Correlation with the results from kinetic modelling of the durability of single-phase minerals, described in Chapter 2, can now be completed following full definition of the kinetic regimes applying to the perovskite and hollandite phases.

Hence, the work reported here exceeds that projected in the curtailed 1 year program. However, it will be clear that there are major aspects of the kinetic analysis requiring completion before a full description can be published. Recommendations relating to those areas requiring completion will be considered in the report.

4.1 DEFINITIONS OF KINETIC REGIMES

The primary requirement of a high-level waste (HLW) solid material is a demonstrated ability to retain the radioactive fission products and actinides under reaction conditions in a variety of solution compositions (e.g. water, silicate solution, bicarbonate solution, brine) at temperatures up to 350°C. Testing for dissolved species yields kinetic data on the mass loss rate and the rates of release of individual elements. It has been demonstrated, however, in previous work (e.g. Myhra et al, 1988), that this measure of chemical durability taken alone can provide a misleading picture of surface reaction and elemental release. The reasons for this can be summarised as:-

- surface reaction can take place to disrupt the crystalline lattices without all reacted species entering the solution e.g. Ti, Zr, Al and other elements may be retained in the reacted surface;
- metastable species may initially form in the reacted surface with the possibility of later release into solution;
- precipitation from solution may also remove some species (suggesting retention) into metastable products deposited either on the reacted surface or on the walls if the reaction vessel.

Hence, a purely phenomenological description of Synroc leaching and dissolution, based on extrapolated leach rates, is not adequate. It is necessary to supplement this data with studies, using surface analysis and electron microscopy, of the reacted surface in order

to define the reaction mechanisms underlying the kinetics. Confidence in prediction of long-term durability can only be based on these reaction mechanisms.

It is likely that more than one reaction mechanism will be operative at any particular time in the reaction sequence. It may be possible to define the predominant reaction (and other contributing reactions) in various time periods. Hence, kinetic regimes, correlating the leach rate data with predominant reaction mechanisms, can be notionally separated to give a more complete chemical description of Synroc durability. The separation may be primarily time-based or mechanism-based depending on the utility of the description. As will be apparent, separation based on time alone is not possible.

Previous work (Segall et al, 1983; Smart et al, 1987; Smart et al, 1989; Myhra et al, 1988; Levins and Jostsons, 1988) has suggested a variety of different mechanisms of chemical attack on the Synroc surface, the bulk lattices of the Synroc phases and the intergranular films of the ceramic. In this project, more extensive consideration has been given to the evidence for each of these mechanisms. The work completed on the individual phases (Chapter 2) has considerably assisted in clarifying this consideration. It is now possible to summarise the five major mechanisms and to consider each mechanism in more detail with evidence for the factors controlling the mechanism. They can be summarised as follows:

Regime I — Instantaneous release to solution of adsorbed and disordered ions exposed at the surface of individual phases, intergranular films, defects, kink sites (i.e. low-coordination sites) and surface-intersected pores. This instantaneous release is measured by immersion in solution for less than 5 minutes. The total loss to solution comprises ≤1 monolayer normalised for each element. It results primarily from termination of crystalline lattices, exposure of defects in the ceramic and damage resulting from cutting and polishing the surface of the specimen.

Regime II — Ion exchange and reaction of metastable minor phases (e.g. metal alloys and glassy material at triple points and around alloy grains) over the first few days in solution. Ion exchange occurs predominantly in intergranular films, pores and, possibly, some minor phases but work with single phase perovskite and hollandite has shown that the major phases are unlikely to contribute significantly to this mechanism. Surface-exposed grains of minor phases, particularly metal alloys containing Mo, oxidise and dissolve relatively rapidly during this period but microencapsulation limits this loss to the surface region.

The first two kinetic regimes are primarily responsible for the relatively rapid decrease in dissolution rates for individual elements over the first few days of chemical attack in solution. This feature of Synroc dissolution has been thoroughly documented (e.g. Coles and Bazan, 1982; Ringwood et al, 1989).

Regime III — Base catalysed hydrolysis leading to breakdown of the crystalline lattice of the major titanate phases begins to predominate in dissolution rates after decline of the contributions from the first two regimes. This reaction results in the formation of a hydrolysed $Ti(OH)_x^{4-x+}$ layer in the surface of the major phases. The reaction occurs relatively fast for perovskite, slowly for hollandite and almost immeasurably slowly for zirconolite. The hydrolysed layer is of varying thickness depending on the temperature of the solution and may retain some of the cations released from their lattice positions by the reaction. At epithermal temperatures (i.e. 20-60°C), a limiting reaction layer

of amorphous hydrolysed Ti-rich material approximately 10-100nm thick is formed with diffusion of reactants and products inhibited by this layer. At hydrothermal temperatures (i.e. ≥90°C), recrystallisation of the layer in-situ on perovskite and hollandite occurs to produce TiO_2 products (brookite and anatase). At intermediate temperatures, the kinetics and thermodynamics or recrystallisation will depend critically on the particular phase, the solution conditions, temperature and the microstructure of the ceramic. The period of primary importance of this mechanism varies considerably from one element to another depending on its phase location, the relative reactivity of that phase and its ability to be retained in the hydrolysed layer.

Regime IV — Diffusion via intergranular films and pore spaces is convoluted with diffusion through the hydrolysed reacted layers (regime III). This regime is largely speculative and is based on indirect evidence from the correlation of leach rate data with microstructure and surface analysis. When the loss rates due to base catalysed hydrolysis have declined as a result of limiting layer formation and microencapsulation of perovskite and hollandite by zirconolite, diffusion will become considerable in the longer term loss of particular elements to solution. It is expected that, in addition to ion exchange deeper into the intergranular films, pores and metastable phases, some based catalysed hydrolysis may take place at the interface of grains of the major phases with the intergranular films. Based on leach rate data at longer times (i.e. >100 days) release via this mechanism is extremely slow.

Regime V — Precipitation and recrystallisation of new phases contributes to surface coverage. Precipitation of particular phases from saturated solution, e.g. carbonates, molybdates, may begin during the first day after solution immersion but other phases will contribute more slowly as solution concentrations of their elemental species build up. In addition, in-situ recrystallisation (regime III) of TiO_2 and ZrO_2 will continue to contribute crystallites to this layer. In long-term leaching (e.g. 1,000 days), this regime has been shown to form an extensive, altered Ti-rich but not continuous layer over the majority of the Synroc surface. The precipitation/recrystallisation time domain varies significantly for different elements depending on solubility relationships and the kinetics of phase formation.

As discussed above, the division of this kinetic description into different regimes is not intended to imply that these regimes occur independently of each other. In fact, significant overlap of regimes II and III is inevitable as the pH alters, and regime III, IV and V will overlap as the rate control changes to slower rate determining steps with the progress of dissolution. Nevertheless, as will be explained below, there is now significant evidence for the existence of each mechanism in a complex sequence of control of Synroc durability.

4.2 CONSIDERATION OF AVAILABLE KINETIC DATA

The kinetic data considered in this project falls into three categories:

- Inactive leach rate data from the research and development program for Synroc fabrication conducted in previous ANU/ANSTO/GU NERDDC projects (Segall et al, 1983; Smart et al, 1987; Smart et al, 1989; Reeve et al, 1983; Ringwood, 1984; Ringwood, 1986) and other ANSTO testing. This comprises a data base of thousands of analyses but many of the fabrications were unsuitable for consideration. A search sequence for this data was designed at the beginning of this project. It is set out in

TABLE 4.1: SEARCH SEQUENCE - INACTIVE DATA

I Manual pre-sort of all fabrication data to reject batches unsuitable for analysis, due to variation in:

1) Density
2) Redox control (Ti addition etc.)
3) Calcination conditions
4) Hot pressing conditions
5) Waste composition

II Manual pre-sort of fabrication data into fabrication routes, i.e. Sandia, Oxide, mixed minerals, Hydrolysis etc., and identification of Batch Nos. in each category.

III Search for all the data 0-1 day duration in each fabrication route group for each element and mass.

IV Inspection of data in each group for unsuitable:

1) Density values from output file.
2) Aberrant final pH values.
3) Mass or individual leach rates (limits will be decided after initial consideration of the data).

V Sort into disc and powder samples. The only variables significant in rate control for 0-1 day rate regime are fabrication conditions, sample form, leachant type, temperature, i.e. pH, SA/V, are not important. Suitable data for each element will be averaged for:

1) Fabrication route
2) Sample form
3) Leachant
4) Temperature

and elemental rate constants derived.

VI The same procedure will be followed for the medium duration regime 1-7 days (subject to examination of data). But with pH and Surface Area/Volume as an additional variable for consideration.

VII The same procedure will be followed for the long term duration with all of the above parameters considered and with the addition of calculating the dissolved carbonate concentration (from initial pH and its effect on Ca leach rates).

VIII It will be necessary to re-calculate rates in each kinetic regime in some cases, using raw data (i.e. solution concentrations). For instance rates in the 7-28 day regime will be obtained from subtraction of 0-7 day data from 0-28 day data.

Table 4.1. Stage I of the search sequence resulted in deletion of more than two thirds of the data from this data base. These deletions were principally due to unsuitable

fabrication conditions, resulting in non-standard Synroc C, with the major problems being: no addition of Ti powder for redox control; density ≤98% theoretical density; cold pressing; calcination at excessive temperatures leading to Cs loss; hot pressing at excessive temperatures leading to large grain sizes and local melting. In addition, a major part of the data was rejected due to incomplete recording of fabrication conditions, waste composition, or leach rate results. Other problems associated with the leach run output data from fabrications that were found to be suitable were: that most data is dominated in the early stages (i.e. 0-1 day) of testing by the instantaneous release of elements from rough surfaces (especially Cs); that there are discontinuities of results for specific specimens from the same batch over long term leach tests; that some elements at very low solution concentrations were close to the detection limit in early analyses using colorometric, AA and ICP methods before ICP/MS was introduced; that loss to solution for Ca, Al, Mo and Cs occasionally gave results showing unexplained discontinuities (i.e. major increases) in analyses probably indicating redissolution of metastable precipitates, peeling of the Ti-rich hydrolysed layer and intersections of diffusion pathways with easily leachable sources of the particular element. All four problems presented considerable difficulties with the preparation of long term plots for amounts leached of particular elements for most of the inactive leach rate data.

- Active leach data from NERDDC Project number EG87/639 (Reeve et al, 1987) comprising actinide leach rates as well as elemental loss rates for matrix species.

- New data generated using inactive Synroc C samples prepared in this project.

Data from each of these sequences will be used to illustrate the kinetic regimes. As will be explained, it has not proved possible to derive values for rate constants of individual elements in each regime due to regime overlaps and inadequate data on the effect of reaction variables.

In the following sections, we will explore each kinetic regime in more detail with particular reference to the kinetic factors controlling rates of release of individual elements.

4.3 REGIME I - INSTANTANEOUS RELEASE

Before considering the results from the multi-phase ceramic Synroc C in this regime, it is important to review the evidence (described in Chapter 2) for this kinetic regime applying to the major Synroc phases perovskite, hollandite and zirconolite. For perovskite, an initial loss of Ca from the first 1-2 mono-layers of the surface was observed for all specimens in the first 5 minutes of solution attack (Pham, 1989a; Pham et al, 1990 a,b). Further attack depends on the presence of micro-structural features (e.g. grain boundaries, porosity) or surface roughness and damage. High resolution transmission electron microscopy, using lattice fringe imaging, confirmed that selective calcium extraction by ion exchange did not play a significant role (Pham et al, 1990b). In $Ca_{0.8}Sr_{0.2}TiO_3$, Ca and Sr were released into solution at rates in the same ratio as they occur in the bulk reaching steady values after initial high rates corresponding to 1-2 mono-layers loss. The initial attack on hollandite is closely similar to that on perovskite. Losses to solution in the first 5 minutes correspond to ≤2 mono-layers and selective extraction by ion exchange of Cs^+ and Ba^{2+} does not appear to play a significant role. Preliminary experiments with zirconolite also indicate that initial losses are limited to the first 1-2 mono-layers. Hence, work on the single phase mineral indicates that ions immediately available to solution are those exposed by

termination of the crystal lattices with consequent structural alteration in the first 1-2 unit cells.

In addition to these major phases, represented as separate grains in the multi-phase ceramic, Synroc C has the usual range of other features common to ceramics:- closed porosity; triple points; minor phases (e.g. metal alloys, magnetoplumbite, Ti relict regions from metal additions for redox control); intergranular films between grains of different phase (approximately 2nm wide) (Segall et al, 1983; Smart et al, 1987; Cousens et al, 1985). It is known that these features contribute additional loss (in regime I) to that found from the surface of the grains of minerals of the major phases. Intergranular films and pore surfaces lose Cs, Na, K and Ca immediately on immersion (Cooper et al, 1986; Smart, 1985). Metal alloy phases and the regions surrounding Ti relict regions also leach Mo, Ca and Al very quickly (Segall et al, 1983).

To amplify the description in Section 4.1 above, the instantaneous release into solution of particular elements from the surface of Synroc C is expected to be dependent on the following, often related factors:

- Procedures used to prepare the disc, e.g. cutting and polishing in water compared with the same preparation in iso-propyl alcohol. (Water used in preparation preleaches the surface before testing begins.);
- The extent of surface roughness, e.g. unpolished specimens are expected to show an increase in the instantaneous release of particular elements over those of polished specimens due to;
- The concentration of defects on the surface, e.g. exposed pores, kink sites, adsorbed species, line and planar defect intersections, intergranular film intersections and exposures (e.g. crushed vs. uncrushed samples) and;
- Surface area;
- The concentration of metastable regions, e.g. the surfaces of rutile/magneli phases in Ti-rich relics, triple points at the surface;
- Possibly the chemical nature of the solution, e.g. silicate, bicarbonate,brine;

It should also be noted that the instantaneous release is not expected to be significantly dependent on either pH or temperature of the solution.

The data available for consideration of this regime is limited. In the inactive leach data, the only tests performed for durations less than 1 day were for the fabrication SFG626. No data showing variation of loss rates with temperature, solution type or polishing conditions were available for this regime. The available data from SFG626 i.e. 0-5min at 21.3°C are summarised in Table 4.2. For comparison, this table also includes data from a 1 day leach test following the 5 minute leach test. The leach rates clearly show that there has been a dramatic reduction in loss of barium, cesium, calcium and strontium to solution following the rapid loss rates in the first 5 minutes. (Data for loss rates of other elemental species, e.g. Ti, Zr, were below the limit of detection of the analysis methods used.)

A further experiment in this regime was conducted at Griffith University using Synroc fabrication SFG531 (SA/V = 375cm^{-1}) prepared as a powder (for comparison with disc samples in Table 4.2) for a 1.5g sample in 15ml of doubly distilled deionised water (DDDW). Table 4.3 sets out the results from four successive periods of 10 minutes, a period of 1 day and a period of 4 day leaching successively with solution replacement after

each period. The concentrations are in ppm. The solution temperature was 25°C. The results clearly indicate that loss rates in regime I differ from one element to another, although the concentrations have not been normalised for the content of each element in the bulk Synroc C sample. The duration of loss of this regime is also element-dependent. For Cs, Ba, and Sr, the release of the majority of exposed ions occurs in the first 10 minutes whereas, for Mo, significant release continues over periods of several days. For Ca, the release appears to be dependent on a saturation concentration in solution. This last characteristic has been separately confirmed in experiments for perovskite described in Chapter 2.1.1.

TABLE 4.2: INSTANTANEOUS RELEASE-REGIME I

Inactive leach no. : 2939, Batch SFG/626*
Temperature : 21.3°C
Leachant : Water
Duration of test : 0-5 minutes

Element	Solid wt%	Solution Concentration (mg/L)	Loss Rate ($gm^{-2}d^{-1}$)	Loss %
Ba	4.00	0.0120	8.387	0.00093
Cs	5.92	0.0320	15.1117	0.00168
Ca	6.79	0.0020	7.0777	0.00079
Sr	0.24	≤0.0005	≥5.8243	≤0.00003

Leach test no. : 2944
Duration of test : 24 hours (1 day following 5 minute leach)

Element	Solid wt%	Solution Concentration (mg/L)	Loss Rate ($gm^{-2}d^{-1}$)	Loss %
Ba	4.00	0.038	0.0933	0.00296
Cs	5.92	0.001	≤0.0124	≤0.00039
Ca	6.79	0.024	0.0398	0.00126
Sr	0.24	≤0.0005	≤0.0205	≤0.00065

* It has not been confirmed whether the fabrication for this batch was satisfactory.

Further evidence has also been obtained from Synroc C leached at 25°C in 2 wt% acetic acid (i.e. 1.5g in 18ml of doubly distilled deionised water (DDDW)). Table 4.4 sets out the concentrations of calcium and strontium measured in this experiment using similar solution replacement to that in Table 4.3. The higher concentration of calcium is due to the alteration of pH from the normal Synroc pH (i.e. ~4.5). It is important to note that the powder was not exposed to air during the leachant replacement in this experiment. Exposing the leached Synroc after the final (i.e. 25 min) leach to air and then subsequently leaching for a further 5 minute gave a calcium concentration of 12ppm. The equilibrium ($CaCO_3 = Ca^{2+} + CO_3^{2-}$) for $CaCO_3$ gives a value of 7.5ppm at 25°C for solution saturation.

TABLE 4.3: RELEASE OF ELEMENTS IN REGIME I FOR SYNROC C POWDER

Condition	Ca						Sr					
	10	10	10	10	1d	4d	10	10	10	10	1d	4d
1.5g/15ml 25°C	5.6	5.6	5.6	5.6	5.6	5.7	0.1	.025	.015	.06	.06	0.025

Ba						Mo						Cs					
10	10	10	10	1d	4d	10	10	10	10	1d	4d	10	10	10	10	1d	4d
1.77	.61	.30	.25	1.75	.96	5.25	3.12	1.5	1.5	16.6	4	1.48	.15	.12	<0.12	.61	.35

Notes:

(i) Leachant was replaced after each period

(ii) 10, 1d, 4d, were used to denote after 10 min., after 1d, after 4d.
The first 10 is the 1st 10 min.
The second 10 is the 2nd 10 min. etc.

(iii) Conc. is ppm.

TABLE 4.4: SYNROC LEACHED AT 25°C IN 2wt% CH_3COOH

Ca(ppm)					Sr(ppm)				
5 min	5 min	5 min	5 min	5 min	5 min	5 min	5 min	5 min	5 min
12	12	12	0.05	0.02	0.375	0.125	0.125	≤0.001	≤0.001

Note:

(i) '5 min' is used to denote after 5 min of leaching - the fresh leachant was then replaced and leaching was repeated for further 5 min etc.

(ii) Just Ca and Sr were monitored in this experiment.

(iii) Exposing leached Synroc (after the last 5 min) to air; and then leaching for a further 5 min would give [Ca] = 12ppm.

The equilibrium $CaCO_3 = Ca^{2+} + CO_3^{2-}$ has $[Ca^{2+}] = 7.5$ppm at 25°C.

Hence, we are able to conclude that the calcium concentration in solution is limited by reprecipitation of $CaCO_3$ in these powder experiments. This may also be true, on inspection of the data in Table 4.2, for the disc experiments. The availability of calcium ions at the surface for release in regime I is determined by reaction with ambient water at the surface of the perovskite phase. This has been independently established in single mineral studies described in Chapter 2.1.1.

These data establish that 1-2 monolayer-equivalents of Ca, Sr, Cs, Ba and Mo are released from the surface in the first 5 mins after immersion. Earlier work with fracture faces (Cooper et al, 1986) and crushed samples (Smart et al, 1987; Coles and Bazan, 1982) suggests that some release occurs immediately on contact with the DDDW, i.e. there is little time dependence in this initial release and, hence, little dependance on temperature is expected. The apparent element-dependence is likely to come from reprecipitation of Ca and a slower, continuing reaction reoxidising the dissolving Mo alloy surfaces. Continuing leaching (Table 4.3) depends on other mechanisms (Regimes II and III) and is expected to be dependent on time and solution temperature.

4.4 REGIME II - ION EXCHANGE AND MINOR PHASE DISSOLUTION

Again, before consideration of Synroc C, it is useful to note that the work on single phase minerals of perovskite and hollandite (Chapter 2) does not indicate any ion exchange beyond the second mono-layer, on immersion in DDDW. In particular, there is no evidence for a concentration profile of Ca and Sr with depth into the surface of an intact perovskite lattice or similar profiles of Cs and Ba in the surface of intact hollandite grains. Where concentration profiles of this kind are detected by surface analysis and electron microscopy, they are always associated with base catalysed hydrolysis of the titanate lattices of these minerals (i.e. regime III).

The ceramic Synroc C, however, has other features which may give rise to ion exchange. In particular, the thin intergranular films, of different composition from the adjoining grains of different phase, may allow ion exchange to greater depths than the major phases (Cooper et al, 1986). Material in triple points and exposed pore surfaces can also potentially contribute. In a previous NERDDC report (Smart et al, 1987), it was also reported that the surfaces of alloy phases containing molybdenum oxidise immediately on exposure to air or to solution to produce readily-soluble Mo species. This oxidation/dissolution mechanism accounts for the high loss rates for Mo in Table 4.3 above. The existence of predominant reactions of ion exchange and dissolution of glassy material in this Regime can also be inferred from the high elemental loss rates relative to those in Regime III where base catalysed hydrolysis predominates.

Kinetic control in regime II is expected to be dependent on the following factors:

- Temperature of the solution;
- Concentration of dissolved ions and, consequently, solution type;
- Ion exchange characteristics of particular ions, e.g. Ca^{2+}, Cs^{+}, Ti^{4+};
- Grain size and intergranular film formation;
- Concentration of soluble material in the surface;
- Disorder in surface layers due to cutting, polishing and fabrication conditions.

Table 4.5 is a particular set of results from the new inactive leach rate data from the project comparing loss rates for individual elements determined over the 0-1 day, 0-7 day and 1-7 day periods. Different discs were used, with consequent uncertainties in rates for 0-1 and 0-7 day measurements and the 1-7 day rates obtained by subtraction. It is important

TABLE 4.5: ELEMENTAL LOSS RATES FROM INACTIVE SYNROC BATCH 903 LEACHED AT 70°C AND 150°C IN WATER

Element	Loss rate at 70°C (g m^{-2} d^{-1})			Loss rate at 150°C (g m^{-2} d^{1})		
	0-1 day[a]	0-7 day[b]	1-7day[c]	0-1 day[a]	0-7 day[b]	1-7 day[c]
Mass	0.125	0.0014	≤	0.0334	0.0310	0.0306
Ba	0.0904	0.02233	0.0109	0.3254	0.0549	0.0098
Ca	0.1106	0.0151	≤	0.1618	0.0335	0.01211
Cs	0.1154	0.0265	0.0117	0.3513	0.0689	0.0218
Gd	≤0.0034	≤ 0.0005	≤1.6x10-	0.0034	0.0005	≤
Mo	0.444	0.0904	0.0315	0.9085	0.2045	0.0871
Nd	0.0009	0.0002	≤	0.0064	0.0008	≤
Sr	0.0065	0.01157	0.0124	0.1186	0.0396	0.0264
Y	0.0024	0.0003	≤	0.0081	0.0011	≤
Al	<0.0019	0.00596	0.0066	0.1005	0.018	≤
Ce	0.0024	0.0005	0.0002	0.009	0.001	≤
Na	0.5742	0.1032	0.0247	1.1413	0.2269	0.0075
Ru	0.0212	<0.0038	0.0009	0.0788	0.0111	≤
Te	<0.0092	0.0097	0.0098	0.3336	0.0367	≤

[a, b] - loss rates were recorded for 0-1 and 0-7 days on different disc samples. Hence, variations in microstructure and surface preparation of the discs can introduce variation in loss rates by factors up to ~2.

[c] - values obtained by subtraction i.e. (7b-a)/6. Values with ≤ indicate a 0-1 day loss larger than the total 0-7 day loss (due to disk variation).

to note that both the 0-1 day and 0-7 day loss rates include the instantaneous loss rate of regime I discussed above. The data strongly indicate the major contribution of 0-1 day rates compared to 1-7 day rates for all elements except Sr and Al at 70°C. The predominant location of the elements in Table 4.5 are given in Table 4.6 (from Fielding and White, 1987).

The influence of temperature on the individual elemental loss rates is also clear from Table 4.5. Activation energies, and particularly changes in these values, can indicate the type of reaction mechanisms predominating in the kinetics. Values <20kJmol^{-1} generally indicate diffusion in limited processes (e.g. ion exchange) whilst higher values are normally associated with chemical reactions. The inclusion of the regime I instantaneous releases and variation between discs makes estimation of activation energies in regime II very uncertain but, based on 0-1 day measurements (Table 4.5), Table 4.7 sets out the results of these estimates. These data must be treated with caution, since they are statistically limited being derived from single different discs, but comparison with activation energies at later times is useful. Table 3.3 in Section 3.2.3.2 also gives activation energies derived from 0-7 day data averaged over all specimens in the inactive (903) data base. Comments on these values can be found in that section. The values are consistent with ion exchange and diffusion limited reactions (e.g. oxidation of Mo alloys) for Ba, Ca, Cs, Mo, Y, Ce, Na and Ru. Sr, Nd and

probably Al behave differently with marked dependence on temperature suggesting a chemical reaction (e.g. hydrolysis) mechanism. These rates also give some indication of the relative ion exchange characteristics of particular ions. Ti and Zr are at such low concentrations that estimates of loss rates are not possible.

TABLE 4.6: FROM FIELDING & WHITE (1987), A SUMMARY OF ELEMENTS AND THEIR LOCATIONS IN THE PREDOMINANT PHASES

Element		Predominant Phase Location
Barium	Ba	H
Calcium	Ca	P
Cesium	Cs	H
Gadolinium	Gd	Z
Molybdenum	Mo	M
Neodymium	Nd	Z
Yttrium	Y	Z
Strontium	Sr	P
Cerium	Ce	P
Ruthenium	Ru	M

H - Hollandite, P - Perovskite, Z - Zirconolite, M- Metal alloys

An indication of the dependence of regime II ion exchange characteristics on concentration of dissolved ions and solution type can be seen in Table 4.8 taken from active Synroc data (Reeve et al, 1987) of 0-1 day duration. The dependence for individual elements is not large although there is some indication that the brine solution inhibits loss of Ce, Rh and Nb. There are considerable uncertainties in the brine results due to the observation of extensive corrosion of the stainless steel supports used in reaction vessels during testing. pH variation and the general values of loss rates are within expected ranges but the effect of dissolved cations, altered redox potential and precipitation is not known. The results are included for completeness.

Table 4.8 also indicates differences between polished and unpolished samples relating to disorder in surface layers and surface area differences as well as different solution types. Previous work by Coles and Bazan (1982) and Oversby and Ringwood (1982) has also illustrated the difference between crushed and cored samples and the dependence on temperature in this regime. For comparison, graphs from their work are reproduced as Figures 4.1, 4.2 and 4.3 to illustrate this dependence.

TABLE 4.7: ACTIVATION ENERGIES FOR DIFFERENT ELEMENTS IN REGIME I (0-1 DAY) FROM TABLE 4.5

Element	Activation Energy ($kJmol^{-1}$)
Ba	19.3
Ca	5.7
Cs	16.8
Gd	*
Mo	10.8
Nd	29.6
Sr	43.8
Y	18.3
Al	*
Ce	19.9
Na	10.4
Ru	19.8
Te	*

*estimate not possible due to undetermined rates

TABLE 4.8: LOSS RATES ($g\ m^{-2}\ d^{-1}$) FOR ELEMENTS IN REGIMES I,II, ACTIVE SYNROC 0-1 DAYS, 90°C, AFTER REEVE ET AL (1987)

	Polished	Unpolished	Brine	Silicate	Bicarbonate
Ce(HA4)	0.0038	0.16	0.0012	0.0038	ND
Cs(HA4)	0.15	0.91	0.089	0.15	0.10
Ru(HA4)	0.011	0.38	0.022	0.012	0.0097
Nb(HA4)	ND	0.047	0.00045	0.0024	0.0012
Ba(HA4)	0.51	3.4	0.082	0.52	0.49

ND - not determined

There are qualifications relating to the crushed samples particularly in respect of the presentation of residues of intergranular films on the fracture faces of the crushed particles. Previous work (Cooper et al, 1986) has shown that Synroc C fractures along the thin intergranular films between grains of different phase. The majority of the film tends to adhere to one surface leaving 1 or 2 mono-layers of the film on the opposite face. Hence, the composition of the surface of crushed samples represents the composition of the intergranular films. These have been found (Cooper et al, 1986; Smart, 1985; Myhra et al, (1985) to contain increased concentrations of Cs, Si, Al, Mo and impurity alkali metal cations, e.g. Na relative to the bulk concentration of the sample. The ion exchangeable cations are released to solution from these film residues immediately after contact with the solution. This is clearly evident in Figures 4.1, 4.2 and 4.3 where relatively high initial rates

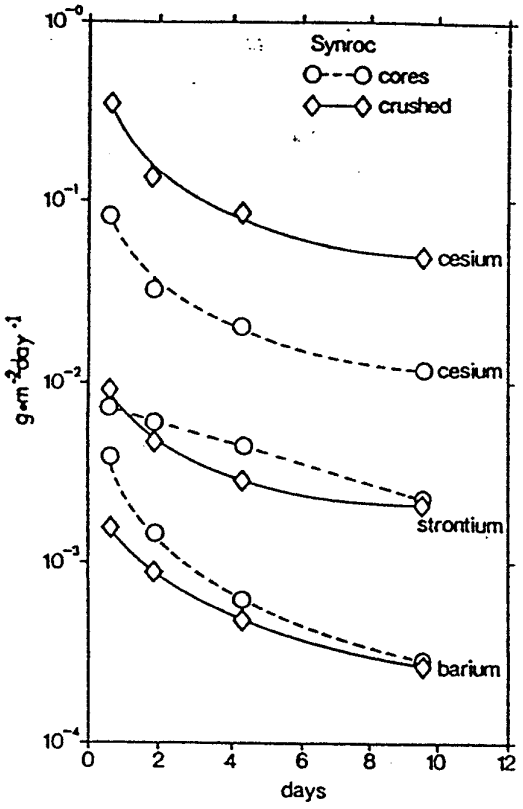

Figure 4.1
Leach data for cored and crushed Synroc C of low density (≈95% of theoretical); adapted from Coles and Bazan (1982).

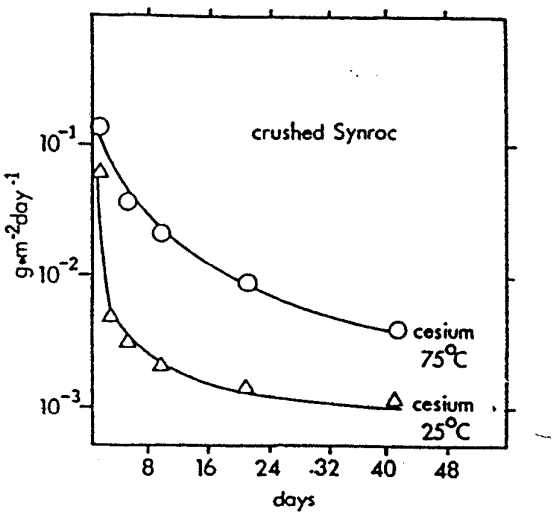

Figure 4.2
Temperature dependence of cesium leach rates in porous Synroc C; adapted from Coles and Bazan (1982).

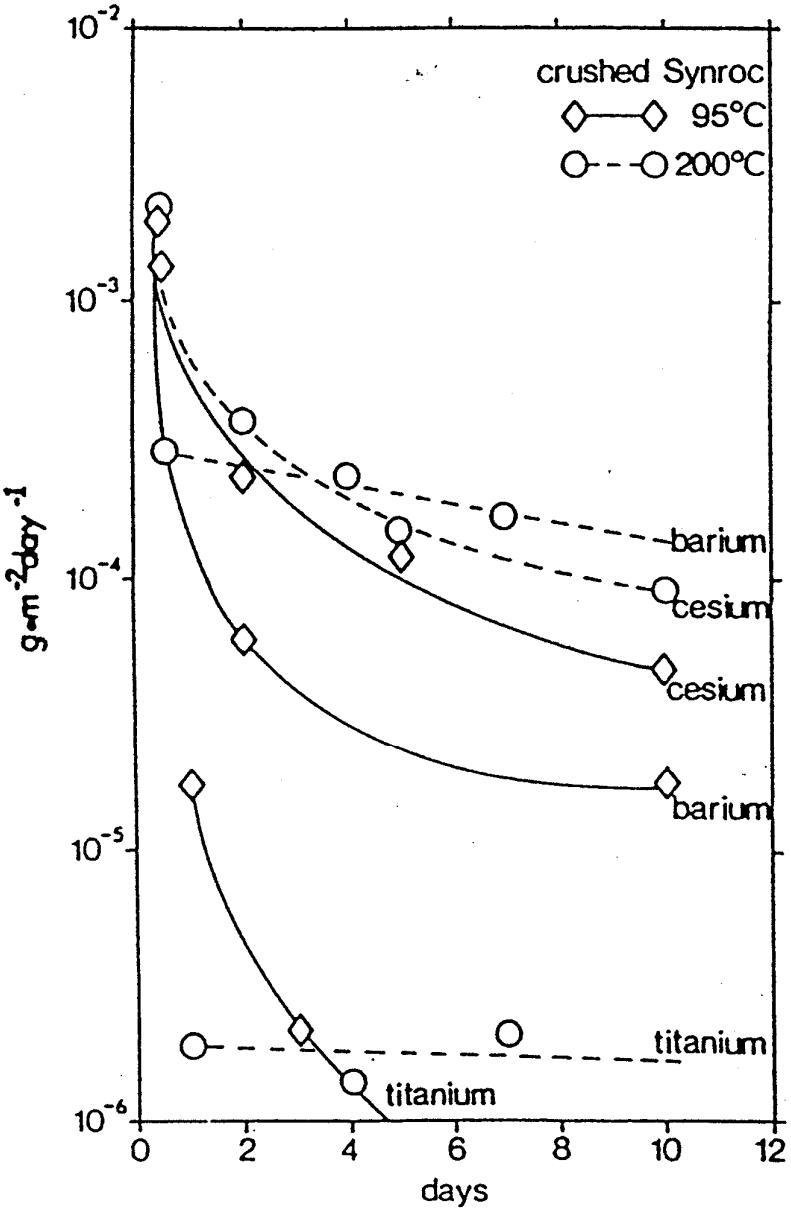

Figure 4.3
Leach data for fully dense Synroc C at 95°C; adapted from Oversby and Ringwood (1982).

are measured for crushed Synroc at times ≤1 day. It is also evident that this initial release of cesium is relatively independent of temperature as found for ion exchange of Cs^+ in these film residues (Cooper et al, 1986). Over longer time periods, i.e. ≥ 2 days, the effect of temperature giving increased loss rates for cesium is apparent from Figures 4.2 and 4.3. Similar increased rates of loss can be seen for barium in Figure 4.3. It is not possible to conclude with certainty whether the increases in rate with temperature are due to increased diffusion and ion exchange of these ions in intergranular films, defects, minor phases or to the appearance of a kinetic dependence of the base catalysed hydrolysis reaction discussed in regime III.

4.5 REGIME III - BASE CATALYSED HYDROLYSIS REACTION

The base catalysed hydrolysis reaction, leading to disruption of the titanate lattice of perovskite and hollandite, has been described above (section 4.1) and in Chapter 2. The rate of this reaction varies considerably with the particular phase, the temperature of the solution and the pH. The nature of the reaction products, i.e. a coherent, hydrolysed $Ti(OH)_x^{4-x+}$ layer at epithermal temperatures or recrystallised TiO_2 in-situ, at hydrothermal temperatures, is determined by the solution temperature. Continued attack at hydrothermal temperatures results in the loss of all surface-exposed perovskite grains and the formation of crystalline TiO_2 precipitates in the perovskite "pores" (Kastrissios et al, 1988). TiO_2 crystallites were also observed on the hollandite phase but at lower numbers per unit area (Pham et al, 1989b). Zirconolite grains appear to be the most durable; there were no effects of attack resolvable on this phase in SEM of disc surfaces or TEM of thinned sections after treatments at temperatures ≤250°C (Pham, 1989).

Other evidence for the reaction is found in:-

- SIMS spectra of $TiOH^+$ and $CaOH^+$ species in reacted surface layers of perovskite (Pham et al, 1990b) and hollandite (Pham et al, 1989b) with depth profiles showing their concentrations across the reaction layer;
- XPS spectra of altered Ti(3p) signals after reaction corresponding to hydrolysed TiO_2 layers (Myhra et al, 1984a, b);
- scanning Auger surface analyses showing extensive reaction of perovskite grains, less reaction of hollandite and no discernible reaction of zirconolite (Myhra et al, 1988; this report);
- observation of amorphous titanaceous films in TEM images of reacted surfaces at <90°C (Kastrissios et al, 1988);
- release of cations previously incorporated into crystal lattice sites of the minerals.

To extend the consideration of regime III, we will consider the period of attack from 7-100 days in which it is expected that the base catalysed hydrolysis reaction will dominate the kinetic rate control. We will also consider data relating to hydrolysis from the earlier (0-7 day) period and from different time periods within the 7-100 days. As with the previous regimes, it is possible to set out the parameters likely to control the kinetics in this regime, namely:

- the temperature of the solution;
- the pH of the solution;

- the extent of surface roughness since defect and/or kink sites are likely to be preferred positions for enhanced rates of hydrolysis;
- grain size and intergranular film formation which will also give preferred sites of attack;
- concentration of dissolved ions and, hence, solution type, e.g. silicate, brine, bicarbonate.

An indication of the effect of temperature on hydrolysis can be seen in the data of Table 4.5 where elemental leach rates in the 1-7 day period are compared. Figures 4.1, 4.2 and 4.3 also contain relevant data comparing the effects of temperature in this period. Loss rates from the original inactive data base for a standard Synroc C (10%HLW) reacted in DDW at 90°C in the time period 7-14 days are set out in Table 4.9 (Myhra et al, 1988).

It is now possible to consider additional data generated from the new inactive leach rate data base, i.e. new testing of inactive Synroc C specimens produced in this project, and data from the active (fission products and actinides) leach testing.

TABLE 4.9: LOSS RATES (g m^{-2} d^{-1}) FOR A STANDARD SYNROC (10% HLW) REACTED IN DDW AT 90°C (AFTER MYHRA ET AL., 1988)

	0-1d	0-7d	7-14d
Mass	0.036	0.018	0.008
Al	≤0.27	≤0.03	≤0.01
Ba	0.792	0.092	0.015
Ca	0.080	0.019	0.007
Cs	0.850	0.079	0.018
Mo	1.677	0.335	≤0.031
Sr	0.192	0.026	≤0.005
Ti	≤0.001	≤0.0001	≤0.0001
Zr	≤0.017	≤0.0023	≤0.0013

Figures 4.4 and 4.5 illustrate representative samples of the data from the new inactive leach rate data base at different temperatures, i.e. 40°C and 90°C respectively. Table 4.10 gives some estimates of elemental loss rates in regime III (i.e. 10-120 days) for Synroc batches SFG325 and SFG326 from the original inactive data base. By comparison with the data in Table 4.5 (i.e. regime II), it is clear that the loss rates are generally lower in this regime. The very small differences between successive cumulative amounts leached makes estimation of activation energies unreliable particularly when due account is taken of experimental errors introduced between different batches. The results in Table 4.10 tend to indicate that there are not major differences in loss rates between 40°C (SFG325) and 90°C (SFG326).

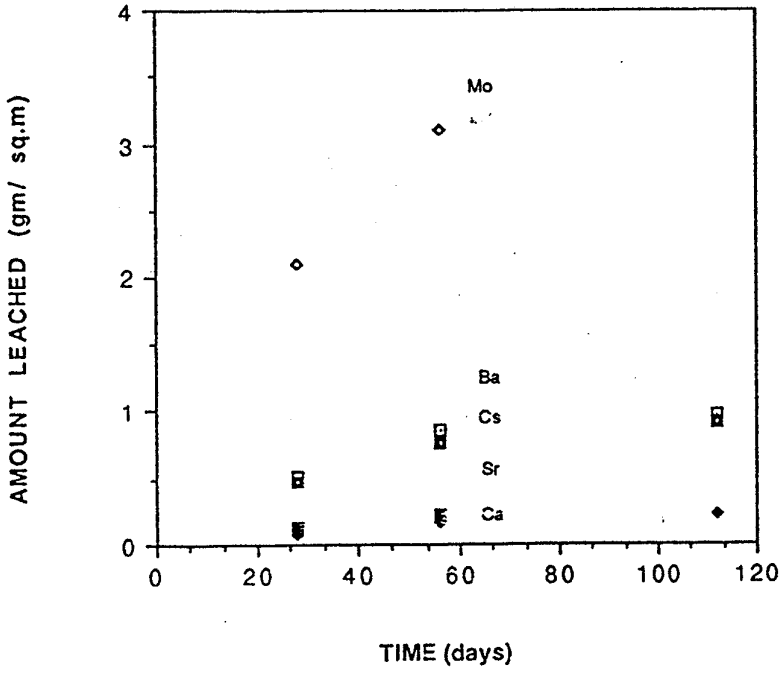

Figure 4.4
Cumulative amount leached with time for elements as marked from inactive Synroc C (SFG 325) at 40°C in DDW.

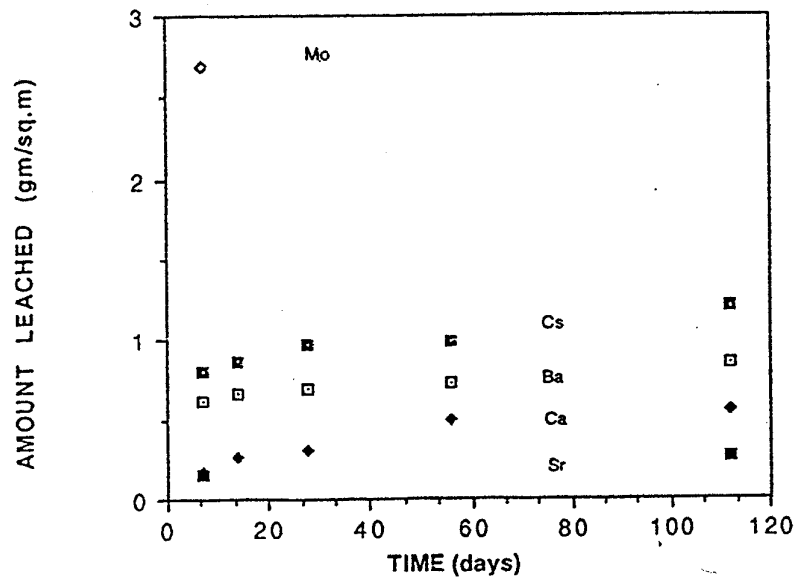

Figure 4.5
Cumulative amount leached with time for elements as marked from inactive Synroc C (SFG 326) at 90°C in DDW.

TABLE 4.10: ESTIMATED ELEMENTAL LOSS RATES (g m^{-2} d^{-1}) IN REGIME III (10-120 DAYS) FOR INACTIVE SYNROC BATCHES SFG325 AND SFG326 AT DIFFERENT TEMPERATURES

Element	SFG325, 40°C	SFG326, 90°C
Cs	4×10^{-3}	4.5×10^{-3}
Ba	4×10^{-3}	3.5×10^{-3}
Ca	2×10^{-3}	3×10^{-3}
Sr	2×10^{-3}	2×10^{-3}
Mo*	3.6×10^{-2}	-

* incomplete data

Selected data from the new inactive leach testing conducted in this project, i.e. Synroc SFG903 described in Chapter 3.2, is illustrated in the graphs of particular elements (as shown) in Figures 4.6-4.18. In regime III, estimates of loss rates for individual elements for a variety of specimens taken from this fabrication are presented in Table 4.11 (70°C) and 4.12 (150°C). The rate estimates were made in the time periods 7-14 days and 84-112 (70°C) or 84-105 (150°C) days using data derived directly from solution measurements in these time periods. The tables exemplify the variation in loss rates between different samples. Nevertheless, there is a consistent trend showing reduction in loss rates for each element across this period in which base catalysed hydrolysis is expected to predominate. Between the two periods of the estimates, the rates reduce by factors between 4 and 23 for the data at 70°C and by factors between 1.6 and 115 for the data at 150°C. Activation energies, averaged for each element for each of the two time periods, are calculated in Table 4.13. Much of the data for the 84-112 (105) day period, and hence the activation energies in this period, must be regarded with caution because the analyses for dissolved species are close to detection limits and precipitation on the Synroc surface is a major complication. Also, the single mineral studies have shown that different mechanisms (or at least kinetics) of TiO_2 recrystallisation occur at 70°C and 150°C. With these qualifications, comparing these results with activation energies from regime II (Tables 4.7 and 3.3), suggests the following conclusions:

- that activation energies for all elements increase significantly between 0-7 day and 7-14 day periods suggesting a change in predominant mechanism to the base catalysed hydrolysis reaction;
- that, specifically, activation energies for calcium release roughly double between regimes II and III suggesting change-over from a diffusion-based mechanism to base catalysed hydrolysis of initially the perovskite phase and possibly later the zirconolite phase;
- that strontium activation energies are relatively high compared to other elements through regime II and the first stages of regime III, eventually reducing to ~14kJmol^{-1}, suggesting that base catalysed hydrolysis of perovskite is the primary mechanism for release of this element even in regime II but after perovskite loss, diffusion becomes important in further reaction;

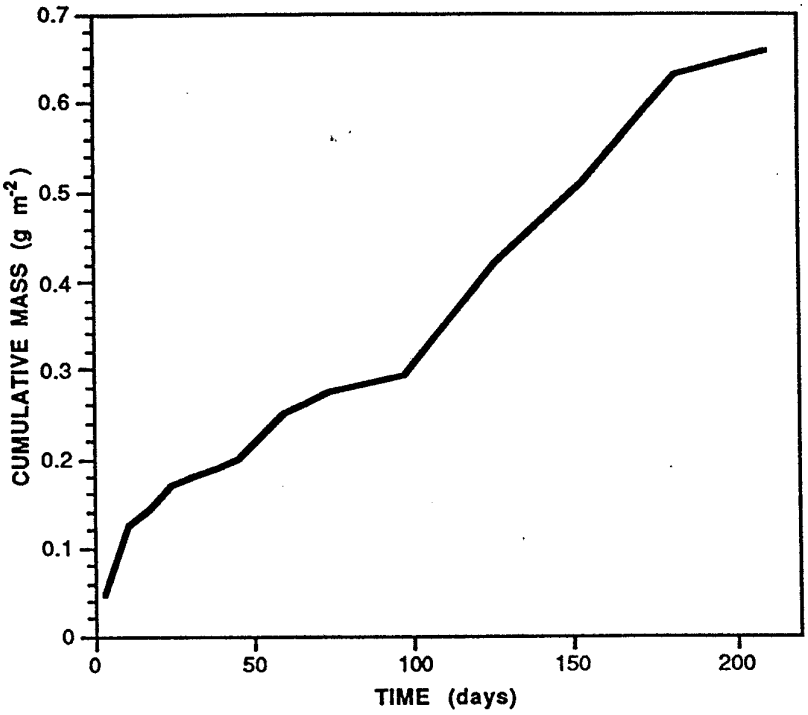

Figure 4.6 Cumulative amount of Ca leached from sample 16 (inactive Synroc 903) exposed to DDW at 70°C.

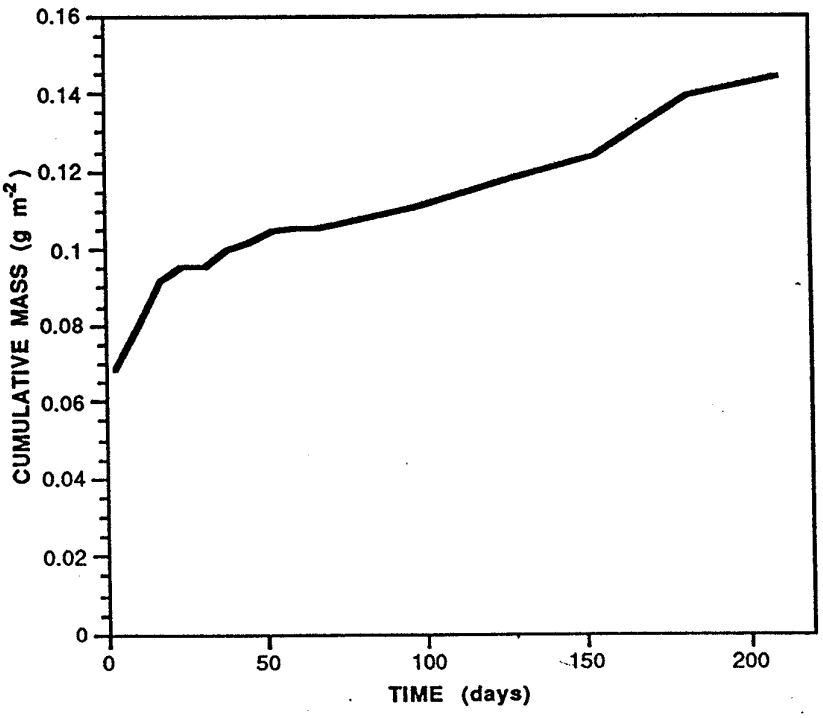

Figure 4.7 Cumulative amount of Sr leached from sample 18 (inactive Synroc 903) exposed to DDW at 70°C.

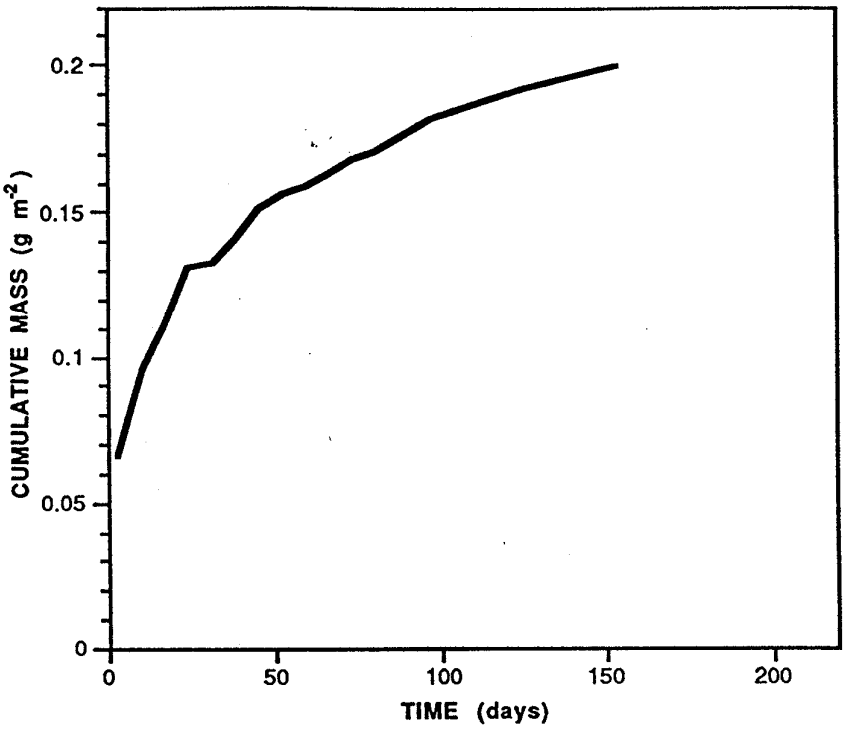

Figure 4.8 Cumulative amount of Cs leached from sample 15 (inactive Synroc 903) exposed to DDW at 70°C.

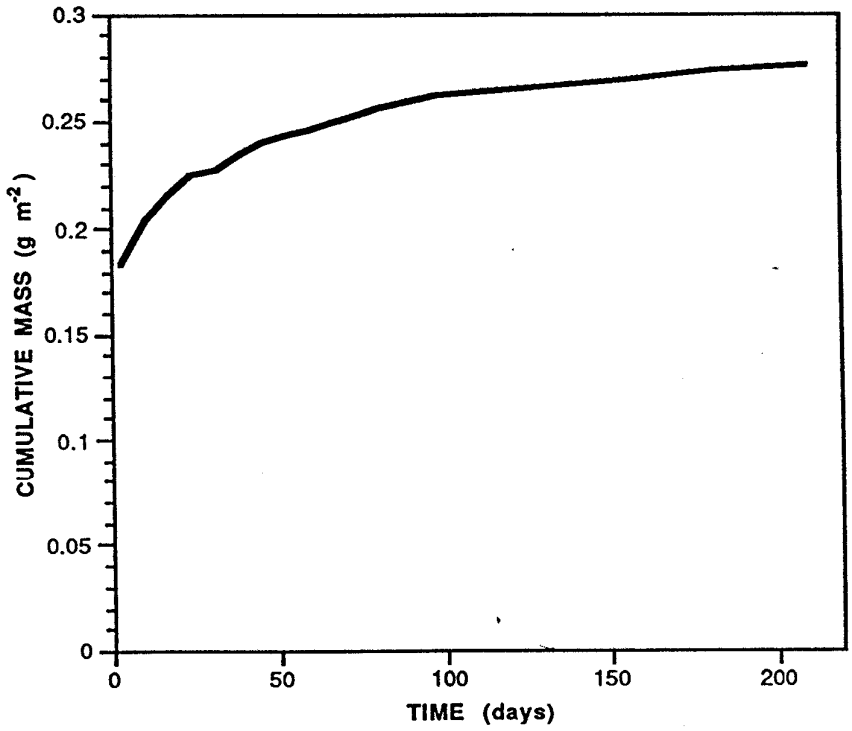

Figure 4.9 Cumulative amount of Cs leached from sample 18 (inactive Synroc 903) exposed to DDW at 70°C.

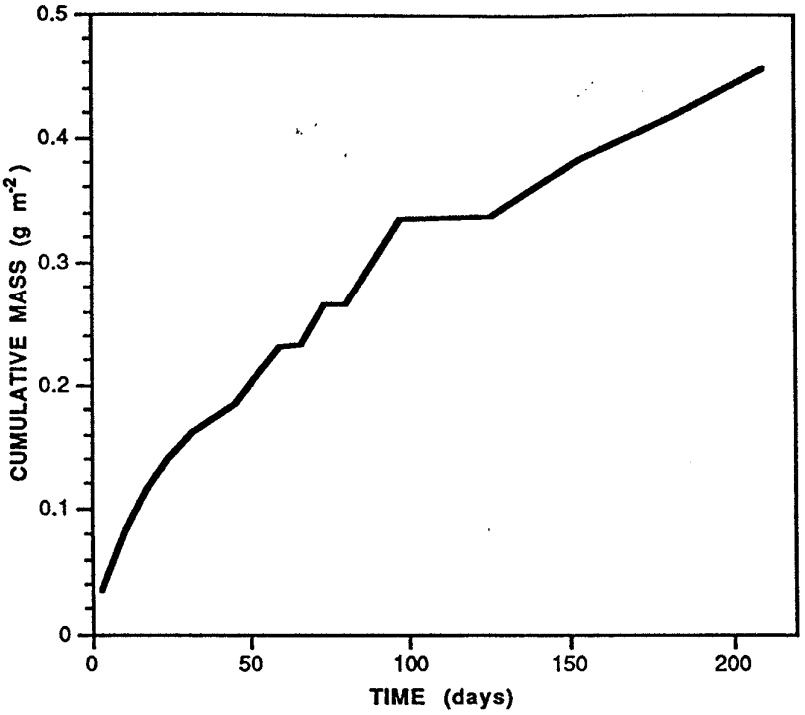

Figure 4.10 Cumulative amount of Al leached from sample 19 (inactive Synroc 903) exposed to DDW at 70°C.

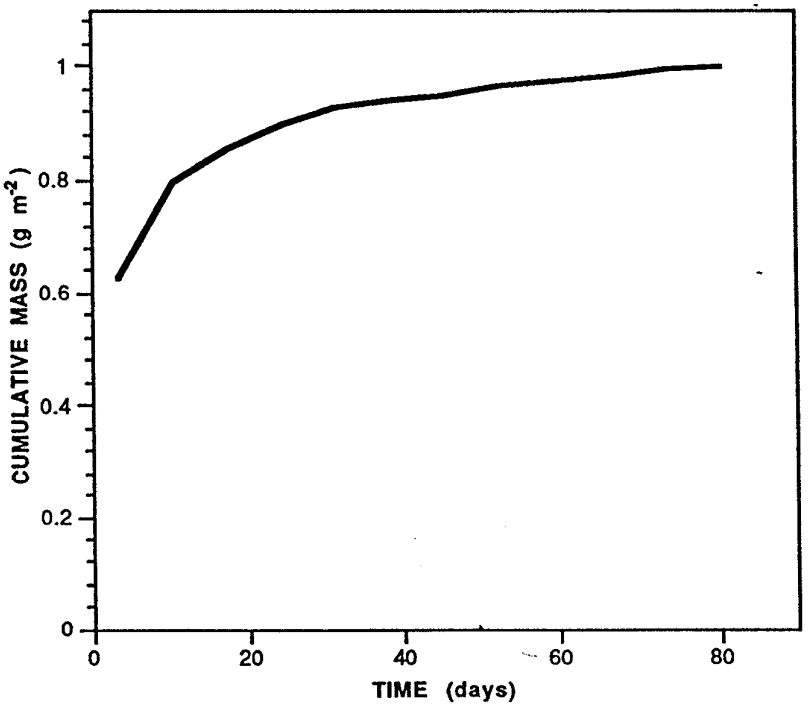

Figure 4.11 Cumulative amount of Mo leached from sample 14 (inactive Synroc 903) exposed to DDW at 70°C.

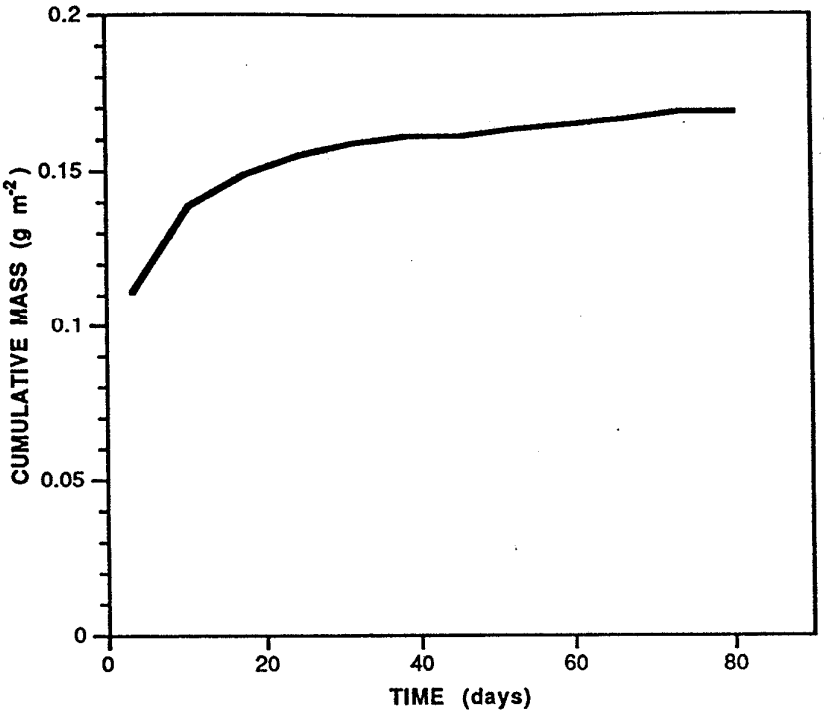

Figure 4.12 Cumulative amount of Ba leached from sample 14 (inactive Synroc 903) exposed to DDW at 70°C.

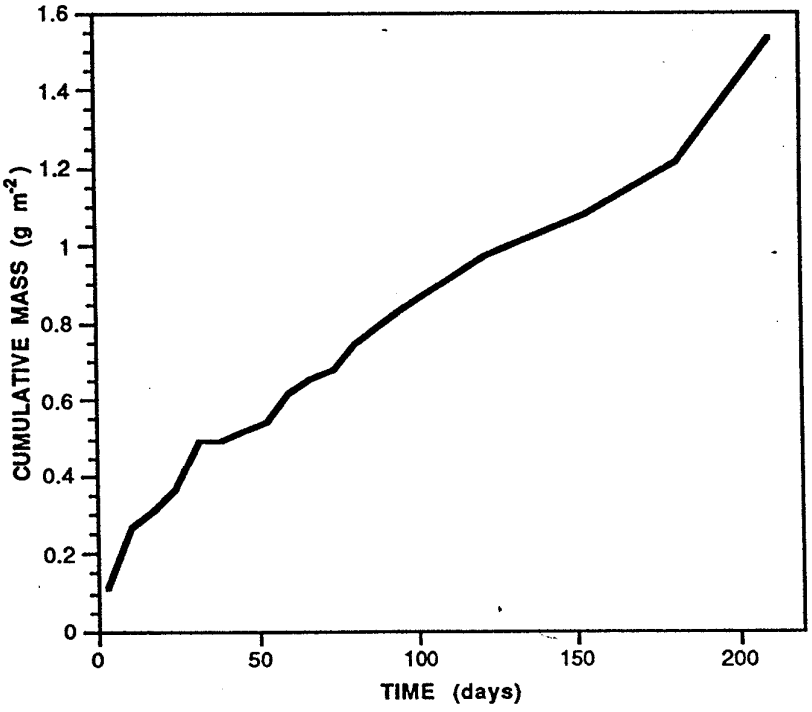

Figure 4.13 Cumulative amount of Ca leached from sample 9 (inactive Synroc 903) exposed to DDW at 150°C.

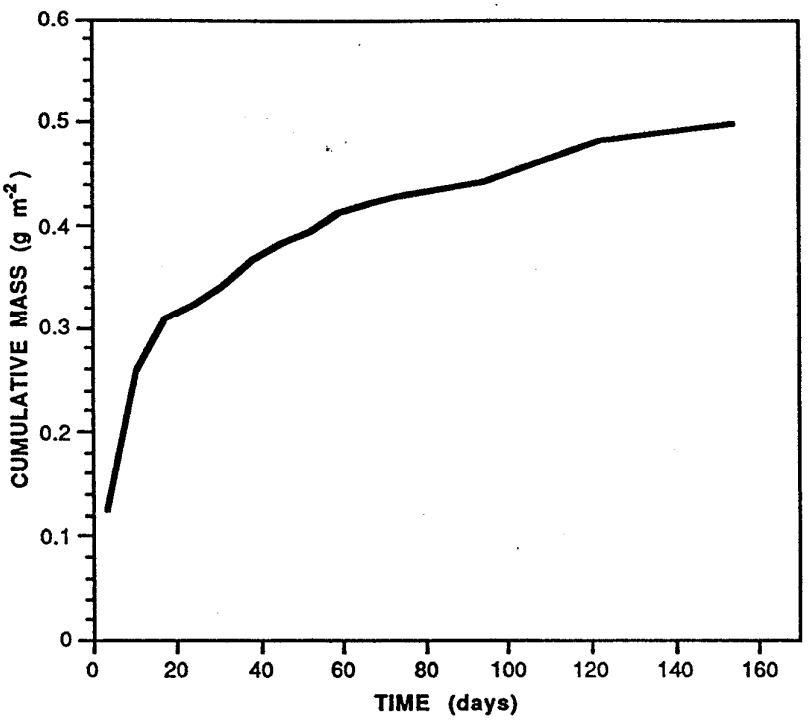

Figure 4.14 Cumulative amount of Sr leached from sample 8 (inactive Synroc 903) exposed to DDW at 150°C.

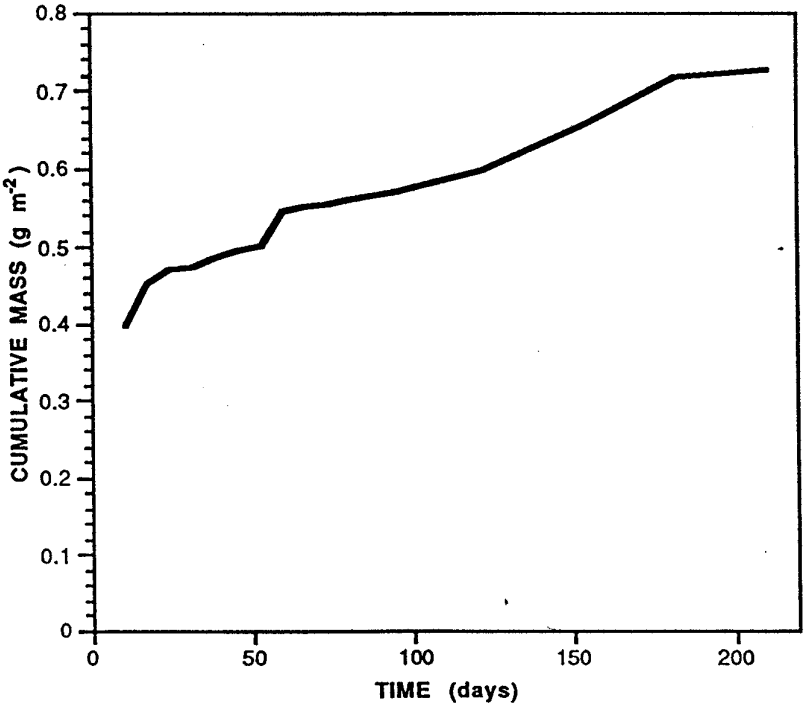

Figure 4.15 Cumulative amount of Cs leached from sample 10 (inactive Synroc 903) exposed to DDW at 150°C.

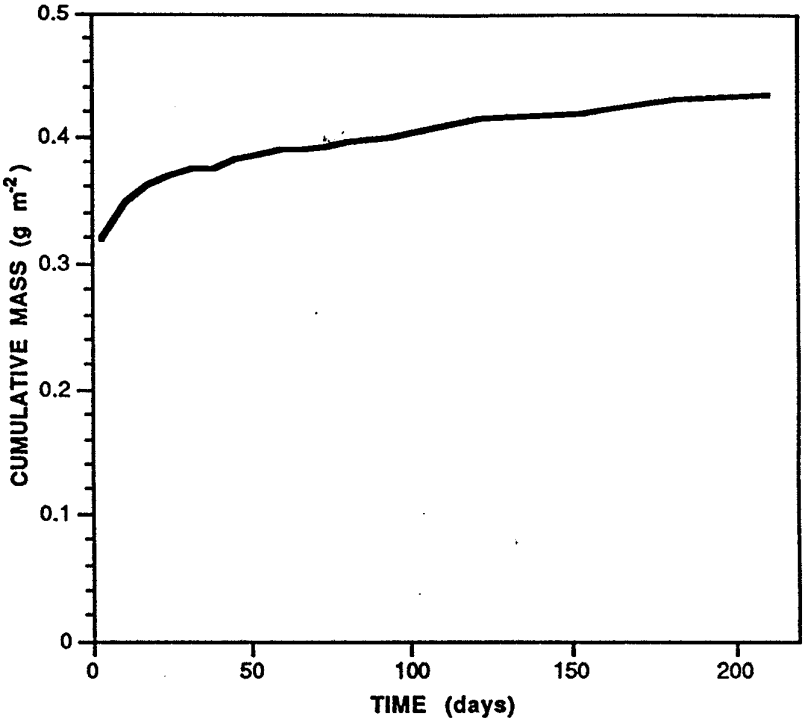

Figure 4.16 Cumulative amount of Ba leached from sample 9 (inactive Synroc 903) exposed to DDW at 150°C.

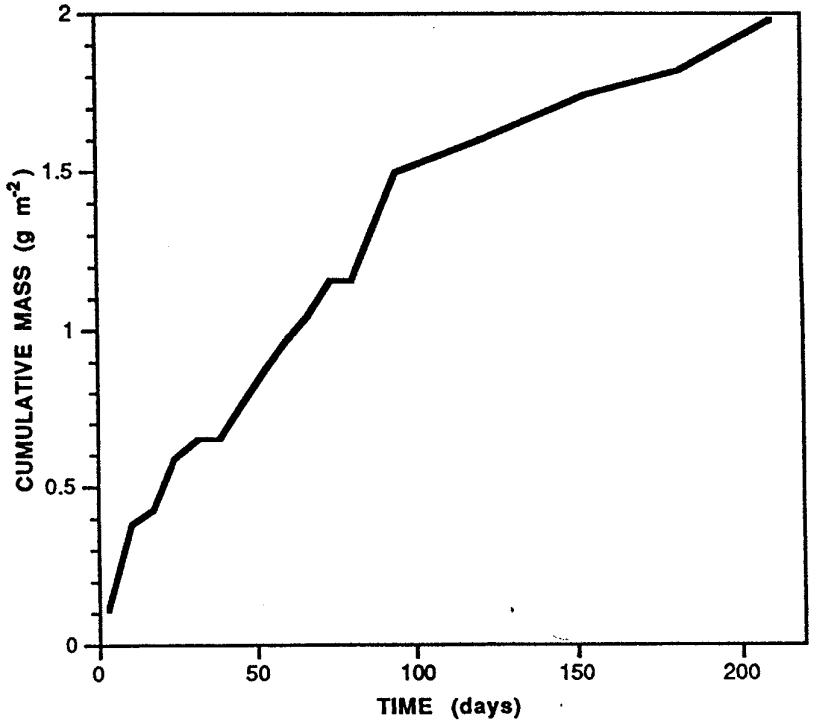

Figure 4.17 Cumulative amount of Al leached from sample 9 (inactive Synroc 903) exposed to DDW at 150°C.

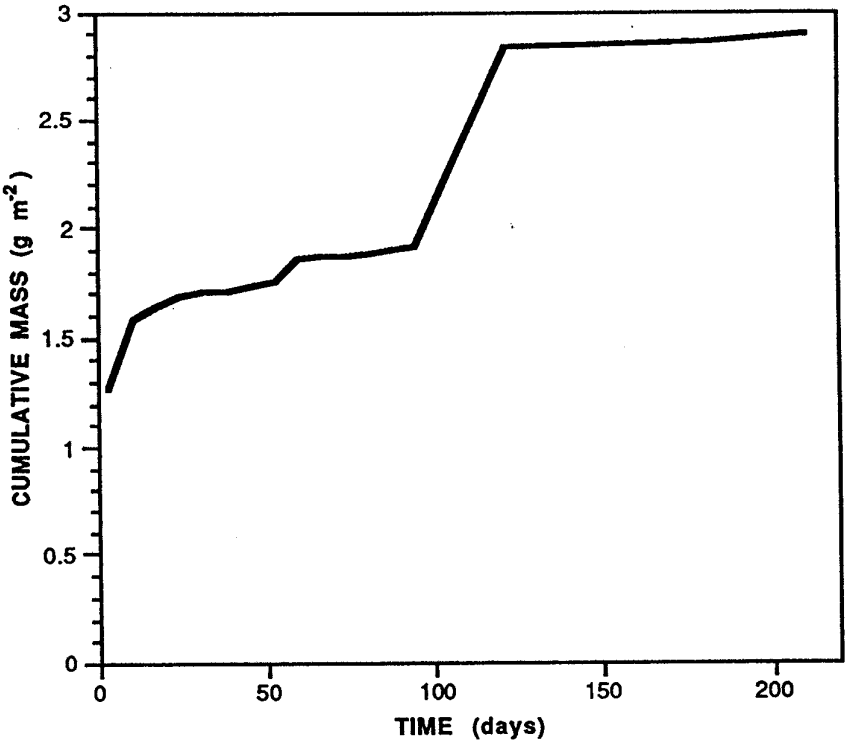

Figure 4.18 Cumulative amount of Mo leached from sample 9 (inactive Synroc 903) exposed to DDW at 150°C.

TABLE 4.11: KINETIC REGIMES III, IV, V RATES ($g\ m^{-2}\ d^{-1}$) OF ELEMENTAL RELEASE FOR SYNROC C (SFG903) IN DDDW AT 70°C

Element/Sample	7-14 days	84-112* days
Ca/15	6.3×10^{-3}	6×10^{-4}
Ca/16	1.14×10^{-2}	5×10^{-4}
Ca/17	1.11×10^{-2}	5×10^{-4}
Ca/18	1.55×10^{-2}	6×10^{-4}
Ca/19	1.18×10^{-2}	6×10^{-4}
Ca/20	5.2×10^{-3}	1.0×10^{-3}
Sr/15	1.0×10^{-3}	2.4×10^{-4}
Sr/16	1.8×10^{-3}	1.8×10^{-4}
Sr/17	1.4×10^{-3}	2.1×10^{-4}
Sr/18	1.7×10^{-3}	1.2×10^{-4}
Sr/19	3.9×10^{-3}	2.0×10^{-3}†
Sr/20	1.4×10^{-3}	2.3×10^{-4}
Cs/15	4.2×10^{-3}	4×10^{-4}
Cs/16	4.5×10^{-3}	3×10^{-4}
Cs/17	4.3×10^{-3}	2×10^{-4}
Cs/18	3.0×10^{-3}	2×10^{-4}
Cs/19	2.9×10^{-3}	2×10^{-4}
Cs/20	2.8×10^{-3}	4×10^{-4}
Ba/15	2.3×10^{-3}	1.0×10^{-4}
Ba/16	3.0×10^{-3}	1.5×10^{-4}
Ba/17	3.3×10^{-3}	1.7×10^{-4}
Ba/18	3.1×10^{-3}	1.8×10^{-4}
Ba/19	5.7×10^{-3}	1.1×10^{-4}
Ba/20	2.1×10^{-3}	1.1×10^{-4}
Al/15	2.2×10^{-3}	6.6×10^{-4}
Al/16	4×10^{-3}	6.3×10^{-4}
Al/17	2.4×10^{-3}	1.33×10^{-3}
Al/18	3.6×10^{-3}	8.5×10^{-4}
Al/19	7.1×10^{-3}	2.5×10^{-3}
Al/20	$7.1x\ 10^{-3}$	8.5×10^{-4}
Mo/15	1.2×10^{-2}	8.1×10^{-4}
Mo/16	1.3×10^{-2}	7.1×10^{-4}
Mo/17	7.4×10^{-3}	7.3×10^{-4}
Mo/18	1.36×10^{-2}	6.6×10^{-4}
Mo/19	9.3×10^{-3}	4×10^{-4}
Mo/20	1.6×10^{-2}	4.5×10^{-4}

* solution analyses close to detection limits. Data has large errors.
† erratic result - neglected

- that activation energies for cesium suggest a predominant sequence of diffusion, in regimes I and II, reaction in the early stages of regime III, i.e. hydrolysis of hollandite, and diffusion in later periods presumably due to reaction layers and microencapsulation;
- that activation energies for barium release are similar to cesium across the two regimes;
- that apparent activation energies for molybdenum release vary widely apparently through regimes of oxidation/diffusion, reaction and diffusion (i.e. microencapsulation) at later times;
- that loss rates for aluminium are relatively high in Table 4.12, particularly at 150°C, and the activation energy increases with time again suggesting a primary mechanism of reaction for release of this element from the zirconolite phase, c.f. activation energy for Ca at 84-105 days.

TABLE 4.12: KINETIC REGIMES III, IV, V RATES (g m^{-2} d^{-1}) OF ELEMENTAL RELEASE FOR SYNROC C (SFG903) IN DDDW AT 150°C

Element/Sample	7-14 days	84-105 days
Ca/8	4.9×10^{-2}	1.8×10^{-3}
Ca/9	2.2×10^{-2}	4.0×10^{-3}
Ca/10	5.1×10^{-2}	1.9×10^{-3}
Sr/8	1.9×10^{-2}	4.3×10^{-4}
Sr/9	6.3×10^{-3}	5.2×10^{-4}
Sr/10	2.8×10^{-2}	5.8×10^{-4}
Cs/8	2.2×10^{-2}	5×10^{-4}
Cs/9	7×10^{-3}	3×10^{-4}
Cs/10	5.6×10^{-2}	5×10^{-4}
Ba/8	2.2×10^{-3}	2.1×10^{-4}
Ba/9	4.1×10^{-3}	1.8×10^{-4}
Ba/10	5.0×10^{-2}	2.2×10^{-4}
Al/8	1.3×10^{-2}	1.4×10^{-2}
Al/9	3.8×10^{-2}	1.6×10^{-2}
Al/10	1.4×10^{-2}	1.3×10^{-2}
Mo/8	4.5×10^{-2}	1.4×10^{-4}
Mo/9	4.3×10^{-2}	1.5×10^{-3}
Mo/10	1.57×10^{-1}	4.9×10^{-4}

TABLE 4.13: AVERAGE RATES (g m^{-2} d^{-1}) AND ACTIVATION ENERGIES Ea (kJ mol^{-1}) FOR EACH ELEMENT FROM TABLES 4.11,4.12

	7-14 days			84-112 (105) days		
	70°C	150°C	Ea	70°C	150°C	Ea
Ca	1.0×10^{-2}	4.1×10^{-2}	21.0	6.2×10^{-4}	2.6×10^{-3}	21.4
Sr	1.87×10^{-3}	1.8×10^{-2}	34.1	2.0×10^{-4}	5.1×10^{-4}	14.1
Cs	3.6×10^{-3}	2.8×10^{-2}	30.9	2.8×10^{-4}	4.3×10^{-4}	6.5
Ba	3.2×10^{-3}	1.9×10^{-2}	26.9	1.4×10^{-4}	2.0×10^{-4}	5.4
Al	4.4×10^{-3}	2.2×10^{-2}	24.3	1.1×10^{-3}	1.4×10^{-2}	38.4
Mo	11.8×10^{-3}	8.2×10^{-2}	29.2	6.3×10^{-4}	7.1×10^{-4}	1.8

The more general conclusion from these results is that activation energies for all elements across this temperature range is still relatively low compared with activation energies found for borosilicate glasses with values typically ≥ 70 kJ mol^{-1}. The low rates of release combined with the relatively low activation energies suggest that, even after 100 days, one of two possible mechanisms is dominating the kinetics, namely: base catalysed hydrolysis with relatively small dependence on temperature of reaction or; diffusion of the products of the hydrolysis limited by a reacted over-layer of titanaceous, hydrogen-bonded surface structure. The former mechanism is consistent with observations for the single-mineral phases at 150°C where recrystallisation in-situ is observed for perovskite and hollandite and the latter mechanism is consistent with observations at 70°C where the amorphous, titanaceous layer has been observed.

The active leach results, (Reeve et al, 1987), provide additional evidence in regime III for the effects of change-over to the base catalysed hydrolysis mechanism; surface roughness and defects; and reaction in different solution types, i.e. brine, silicate, bicarbonate compared with DDW. Analysis of data from this data base completed in this project is presented in the following figures. Figure 4.19 compares cesium loss from active batch HA4 (at 70°C) for an unpolished cut disc and polished discs leached in DDW, brine, silicate and bicarbonate solutions. Work on fission products and the actinide release rates from this sample was previously reported (Reeve et al, 1987). The presentation in this figure shows clearly that the major effect of the roughened surface of the unpolished disc is in the earliest stages of release, ie.$\leq$ 1 day. The remainder of the loss rate curve for the unpolished disc can be transposed onto the polished discs by moving the initial point down to values comparable with the initial points for the polished discs. The rates of release for the unpolished disc beyond 20 days are slightly increased (by a factor of approximately 2) relative to the rate in DDW for a polished disc. Electron microscopy on single-mineral samples has suggested that this is likely to be due to preferential attack at damaged and defective regions which show enhanced rates relative to a polished surface. On the polished discs, there is relatively little variation in loss rates for the period 20-100 days between attack in bicarbonate, silicate, DDDW and brine. The loss rate for DDDW in this region is approximately 2×10^{-3}g m^{-2} d^{-1}. The loss rates in brine and silicate are slightly higher, i.e. a factor of 2, closely similar to the rate observed for the unpolished disc.

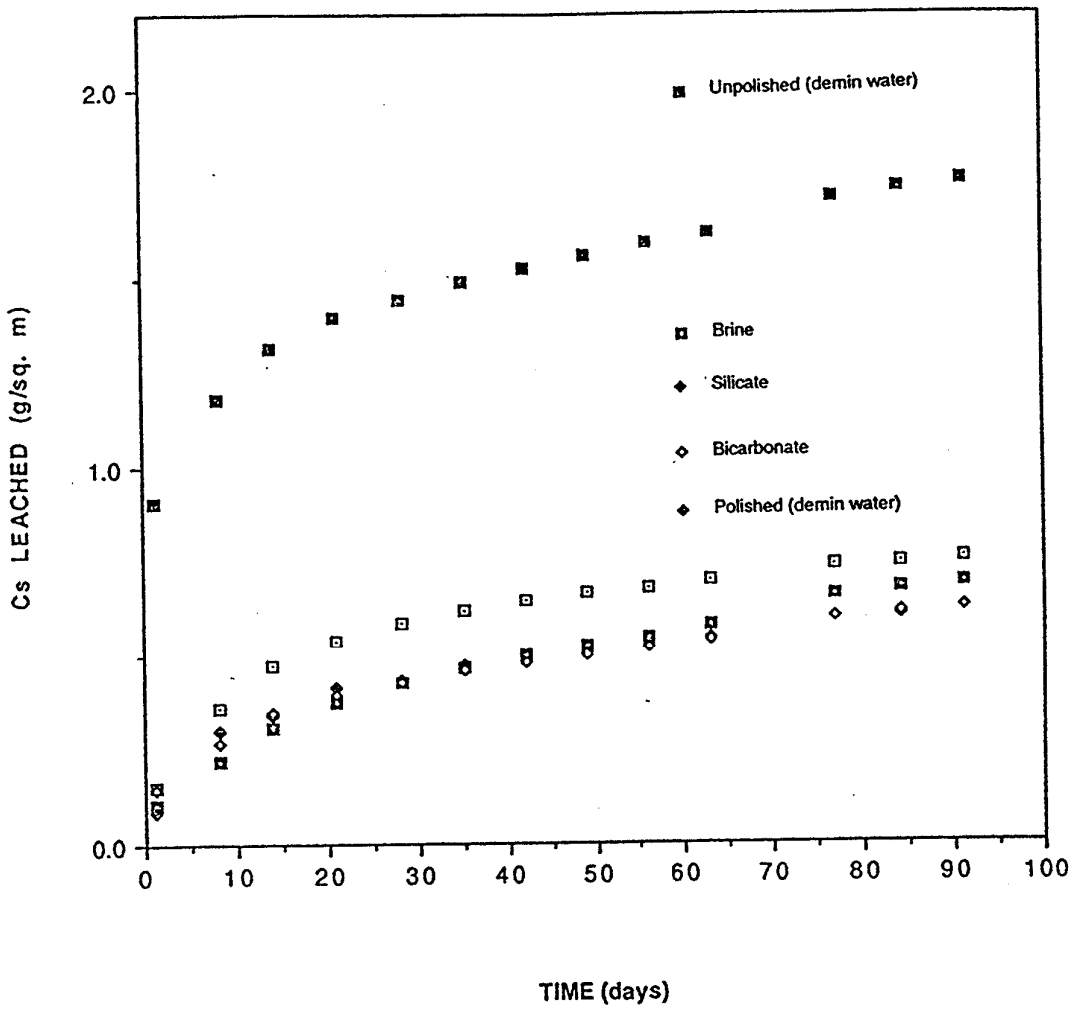

Figure 4.19
Effect of polishing and leach solution type on kinetics of cumulative Cs leached at 70°C in DDW from active Synroc C (HA4).

Figure 4.20 compares barium loss rates for the same set of experiments as described in the previous figure. There are difficulties with the early stages of leaching of the unpolished disc due to values of Ba leached in the time period 0-10 days apparently exceeding the subsequent values. The early values, for this reason, have not been plotted in figure 4.20. This also introduces uncertainty in the relationship between the unpolished and polished discs. It is likely that the correct values of initial points should have shown the same early release of Ba as was found for Cs but this data is not available. Nevertheless, the loss rate for barium from the unpolished disc in the 20-100 day period is considerably higher, i.e. $\sim 1.3 \times 10^{-3}$ g m^{-2} d^{-1} compared with that for the polished disc in DDW, i.e. 2×10^{-3}g m^{-2} d^{-1}. Polished discs in silicate, bicarbonate and brine solutions give slightly higher rates than those found for DDW, i.e. $3\text{-}5 \times 10^{-3}$g m^{-2} d^{-1}. Loss rates for Cs and Ba in DDW for polished discs are closely comparable over this time period.

Figure 4.21 shows a similar set of experiments from the active data for loss of ruthenium from batch HA4. A similar initial rapid loss in the first day is noted for the unpolished disc with the loss rate in the 20-80 day period becoming comparable with loss rates from the polished discs, i.e. $\sim 1 \times 10^{-3}$g m^{-2} d^{-1}. For the polished discs, there is a suggestion that the release rate in brine solution is faster than that in silicate, bicarbonate or DDW and is comparable in magnitude to that of the unpolished disc in the 20-80 day period. Rates in silicate, DDW and bicarbonate are considerably lower in the range $2\text{-}4 \times 10^{-4}$g m^{-2} d^{-1}. There is a suggestion that, in the later leaching, i.e. 60-80 day period, for DDW and bicarbonate solutions, the rate is becoming immeasurably small.

Release of the rare earth elements is also exemplified in figure 4.22 where loss rates for cerium are plotted from the same set of experiments. Again, there is a sharp initial loss for the unpolished disc with more advanced rates becoming closely similar to those for the polished samples. In fact, the loss rate for the unpolished disc in the 20-120 day period is extremely small, i.e. $\leq 2 \times 10^{-5}$g m^{-2} d^{-1}. Similar rates are measured across this time period for Ce loss in brine, DDW and silicate for polished discs. The loss profile for Ce in bicarbonate solution suggests an initial process lasting approximately 60 days in which the loss rates are depressed relative to the other solutions. After this period, the loss rates become of comparable magnitude, i.e. $\leq 2 \times 10^{-5}$g m^{-2} d^{-1}. It is noted that $CeCO_3$ and $RuCO_3$ are insoluble at very low concentrations of the dissolved cation. With the very low release rates for these elements, it is possible that this period of time represents a period of reprecipitation of the carbonates before a stable equilibrium is established.

An alternative method of analysis that is also useful for the comparison of the effects of different solution compositions is consideration of the relative amounts leached for the different elements at 80 days as compared with the amount leached for that element in DDW at the same time. For instance, the effect of surface roughness can be compared by noting that the unpolished disc compared with the polished disc in DDW has increased loss factors of 2-2.5 for Ba, 2.5-3 for Cs, 12 for Ru and 12 for Ce. The previous NERDDC report on the active leaching (Reeve et al, 1987) has noted that Ru and Ce are shed from the surface as colloids in some cases contributing to the additional concentration in solution. The comparability of the Ba and Cs results is consistent with their availability on the roughened, unpolished surface. As explained previously, the results from brine solutions are suspect due to support corrosion but they are discussed here for completness. The effect of brine relative to water for the polished discs can be seen in the close correspondence of Cs and Ce lost but increase of Ru by a factor of ~2.5 and reduction of Ba by a factor of 0.62. Ru forms strong complexes with Cl^- which would explain increased loss rates for this element in brine. The reason for the reduction in loss of Ba is not obvious from these results.

The effect of silicate solution relative to water on the polished discs is very small. All four elements give similar losses presumably due to similar complexation effects in the

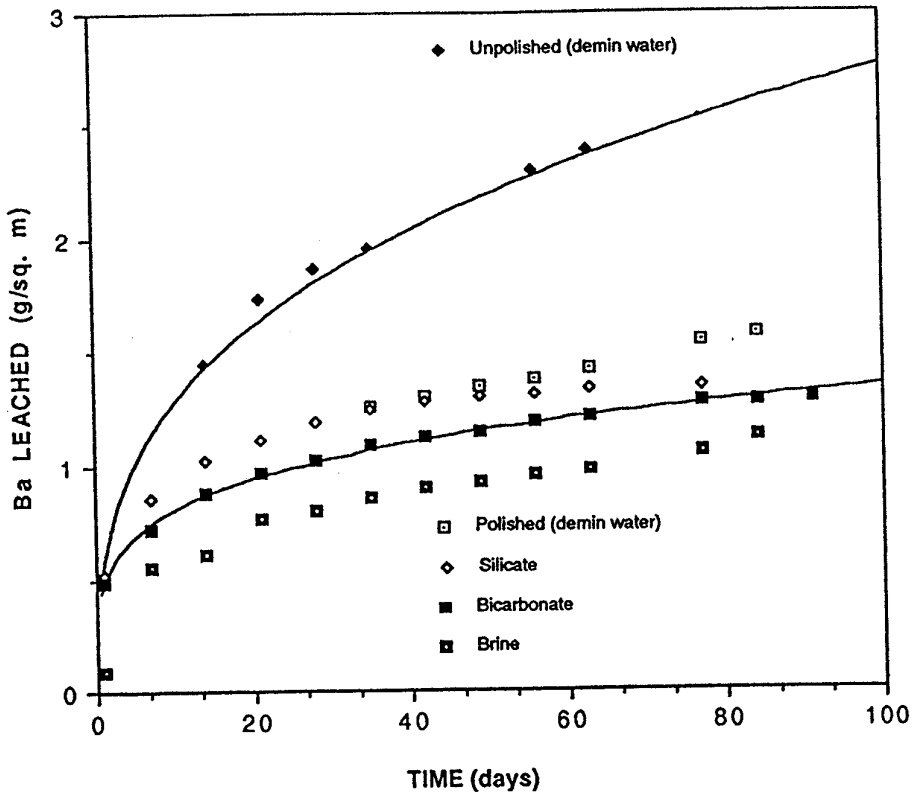

Figure 4.20
Effect of polishing and leach solution type on kinetics of cumulative Ba leached at 70°C in DDW from active Synroc C (HA4).

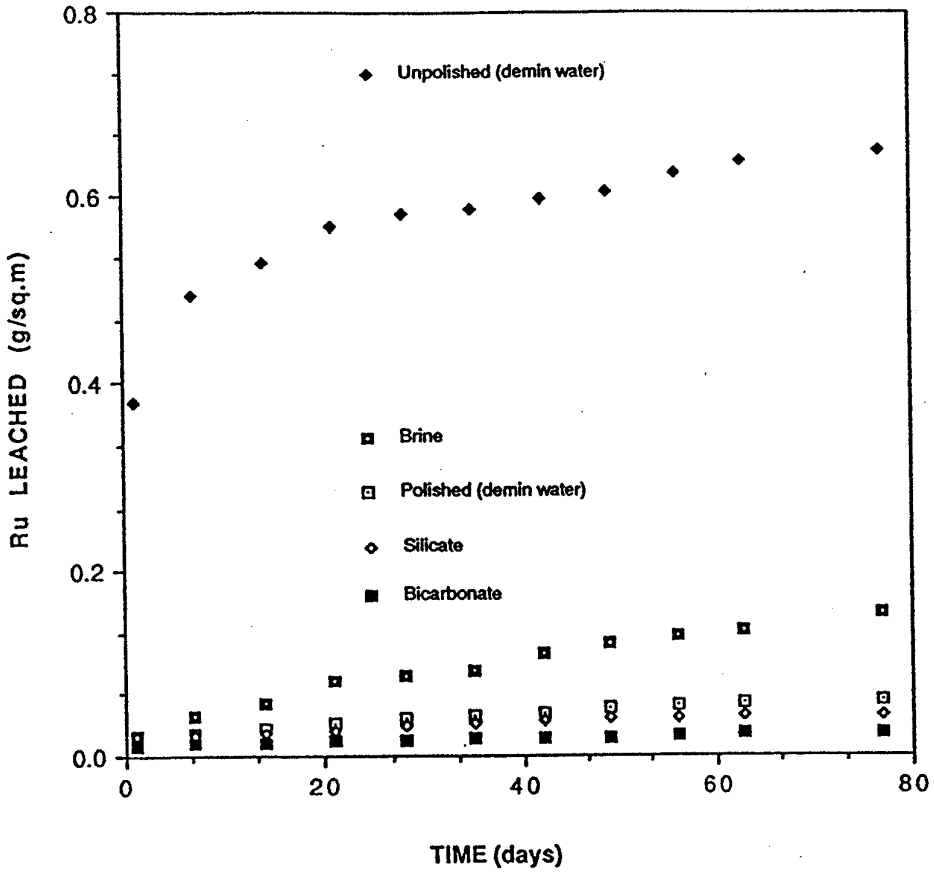

Figure 4.21
Effect of polishing and leach solution type on kinetics of cumulative Ru leached at 70°C in DDW from active Synroc C (HA4).

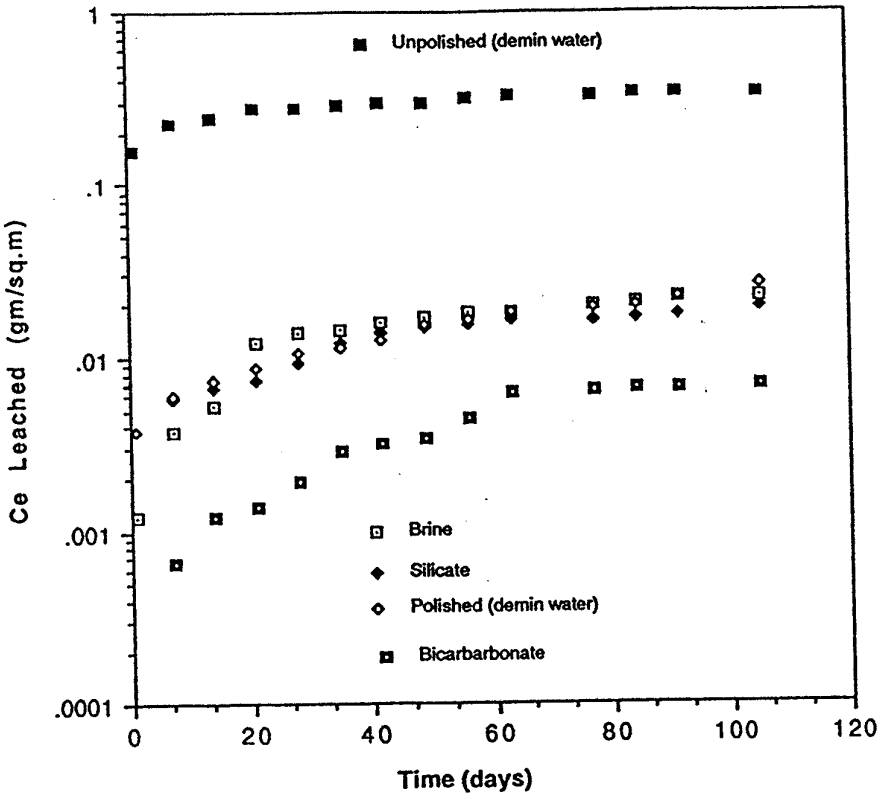

Figure 4.22
Effect of polishing and leach solution type on kinetics of cumulative Ce leached at 70°C in DDW from active Synroc C (HA4).

solution. Secondary silicate phases are observed in regimes IV and V. The effect of bicarbonate on all four elements was considerable. Cs is increased by a factor of 1.4, Ba is decreased by 0.83, Ru by 0.50 and Ce by 0.25. The reason for the increase in the Cs concentration is not clear although there may be some association in the stronger bicarbonate solution between these ions tending to increase the solubility of the Cs^+ ions. The other three elements all form insoluble carbonates so that the reason for their reduction relative to DDW is likely to be due to reprecipitation and the establishment of equilibria with these precipitates in the solution.

In summary, regime III is characterised by decreases in loss rates for all elements as the base catalysed hydrolysis reaction becomes the rate determining step. The rates tend to become relatively constant at both 70°C and 150°C across the 60-120 day period for all major elements of the matrix phases. Activation energies for these elements are also relatively low showing that the effect of temperature in increasing loss rates is quite small. For the transition metal elements and rare earth elements, the loss rates are in this regime become very small, i.e. $\leq 2 \times 10^{-5}$g m^{-2} d^{-1}.

4.6 REGIMES IV & V - DIFFUSION, PRECIPITATION & RECRYSTALLISATION

In the curtailed one year project, the analysis of data for this regime is substantially incomplete. The inactive leach rate data base did not provide any reliable long-term loss rates worthy of further analysis. Previous work at Griffith University (e.g. Myhra et al, 1984a, b; Myhra et al, 1987b; Myhra et al, 1988; Smart et al, 1988; Smart et al, 1989) with samples from the inactive fabrication program has, however, clearly identified precipitated phases of Ca and Sr bearing carbonates, molybdate, sulphates, Ti and Zr oxides and Al oxides/hydroxides. The new inactive leach test (Synroc batch SFG903) has provided SEM and TEM results in these regimes described in Sections 3.4 and 3.5. The active leach rate data base (Reeve et al, 1987) also provides some limited data relevant to these regimes.

The SEM and TEM results from the inactive samples from this project have verified precipitation of similar phases to those found previously. In particular, molybdates, carbonates and oxides of Ti, Al and Nd/Al/Zr are present after 28 days even at 70°C in DDDW. Mo, Ru and Pd-rich precipitates appear in the same time after silicate and carbonate solution attack. At 150°C, oxides of Ti, Al and Fe are found after 28 days.

Hence, it is clear that precipitation and recrystallisation begin relatively early in the sequence of reaction and that they substantially overlap with regime III with inevitable effects on (lower) solution concentrations of particular elements, reduction of surface area and activation energies. Some of these phases are metastable, detaching from the surface or redissolving, as seen in excursions of increased elemental concentrations in particular runs (see Fig 4.18 for example).

In the longer term, via microencapsulation, it is the stability of the zirconolite phase, and particularly the Ti and Zr in its lattice, that is critical to Synroc durability.

Figure 4.23 is loss rate data for the matrix element zirconium in the period 0-400 days. Since this element is located in the most durable of the matrix phases, i.e. zirconolite, it is expected that loss rates to solution would be very small. The data showed that this is evidently true with loss rates, even in regime III (20-100 days), $\leq 2 \times 10^{-5}$g m^{-2} d^{-1}. The data again illustrate the effect of a roughened, unpolished surface on initial loss. Close correspondence of loss rates for polished discs between bicarbonate, silicate and DDW is found across the period of the test. The loss rates for brine are generally lower than for the other three solutions and the reason for this effect is not obvious. In the period 100-300

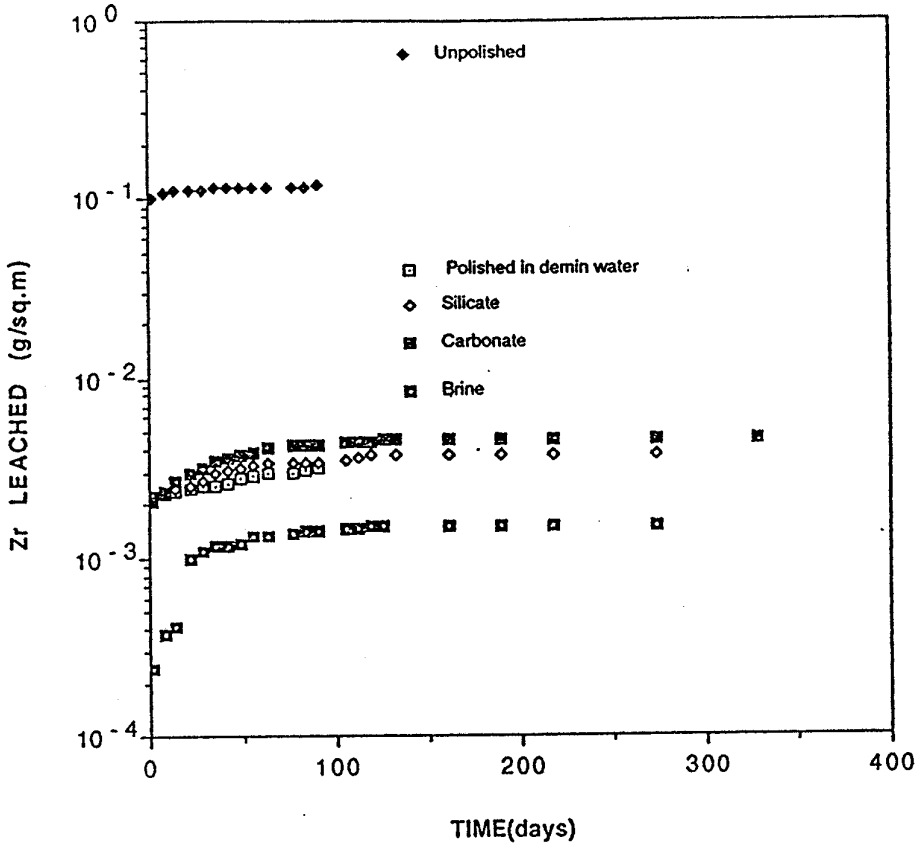

Figure 4.23
Effect of polishing and leach solution type on kinetics of cumulative Zr leached at 70°C in DDW from active Synroc C (HA4).

days, the loss rates for all four solutions are of the order of 10^{-6}g m^{-2} d^{-1} or lower. It is possible, as with the immeasurably small loss rates for Ti discussed in Chapter 1.4, that Zr is effectively not dissolving into the solution but is recrystallising in-situ with equilibration of the ZrO_2 crystallites with the solution.

Figure 4.24 presents results from a specific analysis for Cs from the active batch HA2 up to 1200 days. In this case, three discs are compared showing reasonable comparability of leach rates in the period beyond 300 days, i.e. ~$5.5x10^{-5}$g m^{-2} d^{-1}. The rates appear to have become relatively constant in these regimes. Considering all of the evidence from electron microscopy and surface analysis of single mineral phases, the probably explanation for the constancy of rate is that base catalysed hydrolysis reaction continues at the reaction front beneath the surface of the minerals whilst there is also continuing loss either to solution or by in-situ recystallisation of reacted species at the solution interface. This would have the effect of maintaining a diffusion layer of similar thickness across the whole of this regime. This thickness is likely to be maintained by the ability of reactants to cross the diffusion layer producing further hydrolysis of the titanate lattices at the reaction front. Since Cs does not readily form insoluble precipitates or complex strongly with dissolved species, this element is a good indicator of the mechanism prevailing in this regime.

The work of D.K. Pham (1989) with powdered samples of standard Synroc C is also relevant to consideration of kinetic factors in Regimes IV and V. A series of experiments at high surface area/volume ratios (SA/V) has been conducted to accelerate the approach to and to saturation conditions in the solution. For instance, the SA/V ratio for these powders is of the order of 375cm^{-1} compared with a usual SA/V ratio for polished discs of 0.1-0.3cm^{-1}. Hence, in terms of approach to saturation, a 14 hour run using a powdered sample is equivalent to ~1100 days dissolution for a disc under the same conditions. To set against this advantage, it has been explained above that powdered samples show different surface characteristics when compared with polished discs due to the preferential exposure of intergranular films, defects introduced by crushing and selective attack on small crystallites. Nevertheless, it is useful to consider the results in summary form for comparison with disc samples since they do throw some light on mechanisms applying to advanced kinetics and saturation conditions.

The approach to saturation for a particular element can, in general, involve several stages exemplified in the diagram in Figure 4.25. This illustrates the change in concentration of an element in solution as a function of time (Pham, 1989). The time interval T_1 represents the early stage of the dissolution process during which the solution is under-saturated with respect to the element concerned. As the dissolution proceeds, the dissolution rate decreases due to a decrease in the chemical potential difference of the element between the solid and solution phases. In the second stage, T_2, the concentration can become time-invariant. This does not necessarily imply that the dissolution reaction has ceased but that the rate of release of the element from the waste form is balanced by its rate of precipitation as a secondary phase. This secondary phase may be initially metastable eventually transforming to a stable form through a series of intermediate steady-states. The solubility of the metastable solid phases decreases as the reaction progresses (19). The precipitation of a more stable phase is shown in Figure 4.25 by the approach to a new steady-state condition in the interval T_3.

The Synroc sample used in these powder studies (Pham, 1989) was SFG531 containing 10 wt. % of simulated waste PW-4b-D according to standard methods of fabrication used at ANSTO. The samples were examined using a combination of solution analysis, SEM/EDS and surface analysis.

The effect of SA/V will be considered first before examining the detailed solution concentration -vs- time curves for individual elements. Loss rates for mass and particular

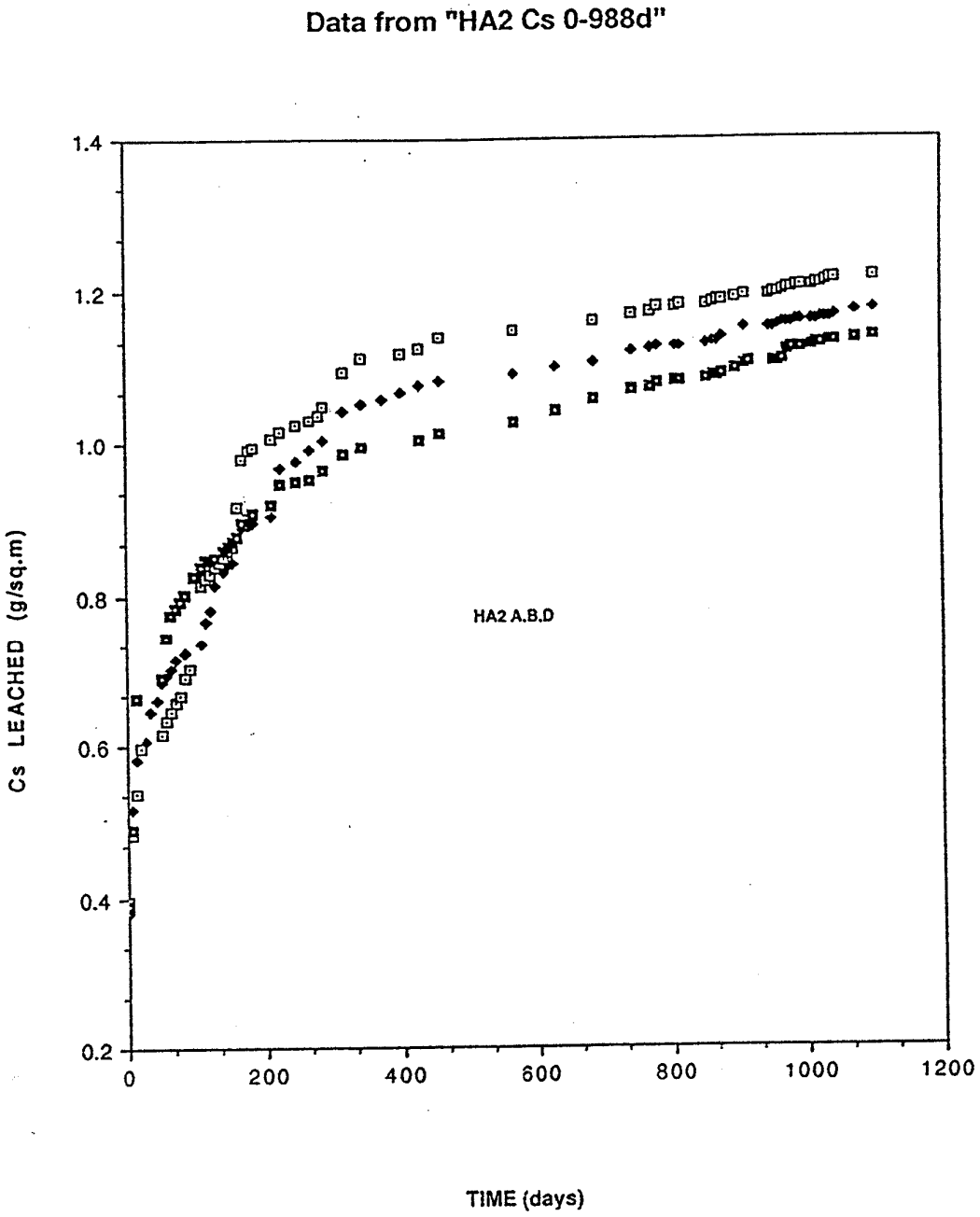

Figure 4.24
Triplicate determination (samples A,B,D) of cumulative amount of Cs leached at 70°C in DDW to >1000 days from inactive Synroc (HA2).

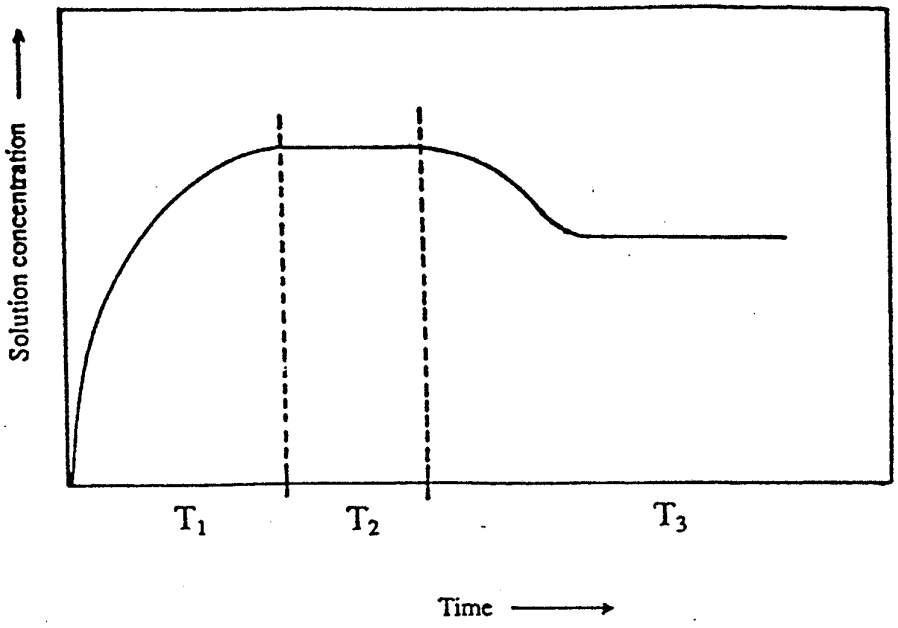

Figure 4.25
A schematic diagram showing the concentration of an element released from a metastable waste form as a function of time (after Savage [19]).

elements in low SA/V runs have already been presented in previous Tables 4.5, 4.9, 4.10, 4.12 describing the dissolution of polished disc samples. The effect of high SA/V can be seen in Figures 4.26 and 4.27 where the concentrations of Ca, Ba, Mo, Sr, and Cs in solution are plotted as functions of SA/V after hydrothermal treatment at 150°C for 14 hours. The concentration of Cs increases monotonically with SA/V. For all other elements, steady values are reached after particular values of SA/V. Ca gives a steady value of ~5ppm even at the lowest values of SA/V. Ba levels at ~6.5ppm for SA/V $\leq 118 cm^{-1}$. Mo levels at ~14ppm at SA/V $\leq 220 cm^{-1}$. Sr gave increased concentration to a maximum of ~0.3ppm before levelling at ~0.2ppm for SA/V $\leq 220 cm^{-1}$.

The results suggest that Cs does not reach a saturation limit, within the parameters of this experiment, at any value of SA/V but that the other four elements are precipitating from solution above particular values of SA/V for each element. This latter observation results from concentrations which become independent of the SA/V parameter once the system approaches the saturation limit. In the case of Sr, it appears that a metastable intermediate phase may first precipitate before a final more stable preciptate is formed. In observations described below, these results will be correlated with direct SEM/EDS observations of the relevant precipitate phases. Under the conditions of this experiment, with approximate equivalence for powders of SA/V=$375 cm^{-1}$ to 1100 days for a disc sample, it is expected that Regimes III, IV and V overlap but that the onset of precipitation is accelerated by the high SA/V.

The concentrations of particular dissolved elements in solution as functions of the duration of attack can now be compared with the generalised curve in Figure 4.25. In these experiments a SA/V of $375 cm^{-1}$ was used at three different temperatures of 90°C, 150°C and 190°C. Based on SA/V differences alone, a duration of one day for the powder sample would correspond to ~1875 days attack for a disc sample. This estimate obviously applies only to the amount of each dissolved species in solution and not to the depth or extent of hydrolysis of the solid surface. Nevertheless, it allows us to examine the forms of precipitates resulting from saturation of the solution in practical time periods.

Figure 4.28 shows the concentrations of Ca in solution as a function of duration of chemical attack at three different temperatures. At 90°C, the Ca concentration was ~6ppm, within the scatter of the measurements, across the time period of 100 days. At 150°C and 190°C, the concentration initially increased up to 22 days and 4 days respectively before decreasing and levelling at ~2.8ppm for both temperatures. The forms of these two curves are similar to those of the general curve in Figure 4.25 but the appearance of the metastable and final stable phases varies with the temperature. Examination by SEM/EDS of powder specimens attacked at 90°C did not show any distinct precipitates in secondary electron or back-scattered imaging. Computer simulation using the EQ3/6 program described in Chapter 5.2 below indicated that the solutions were saturated or super-saturated with calcium carbonate or calcium molybdate phases at this temperature. It is therefore likely that the calcium concentration (i.e. ~6ppm) at 90°C is controlled by precipitation of a relatively uniform layer of these phases across the surface. At 150°C and 190°C, distinct preciptates were observed. Details of the composition of these precipitates will be given in the SEM/EDS discussion below. As the duration of attack at 150°C increased barium-calcium molybdate and then calcium molybdate phases were observed. The majority of precipitates after attack at 190°C were calcium molybdate crystals detected after periods as short as 3 hours of chemical attack. Barium-calcium molybdate phases were also found occasionally at this temperature.

Figure 4.29 shows the concentration of Ba as a function of duration of chemical attack. The curves are of similar form to those for Ca but, at 90°C, the Ba concentration increases with time beyond 30 days possibly indicating further dissolution of a metastable phase. Concentration peaks occur after 25 days at 150°C and 10 days at 190°C. These

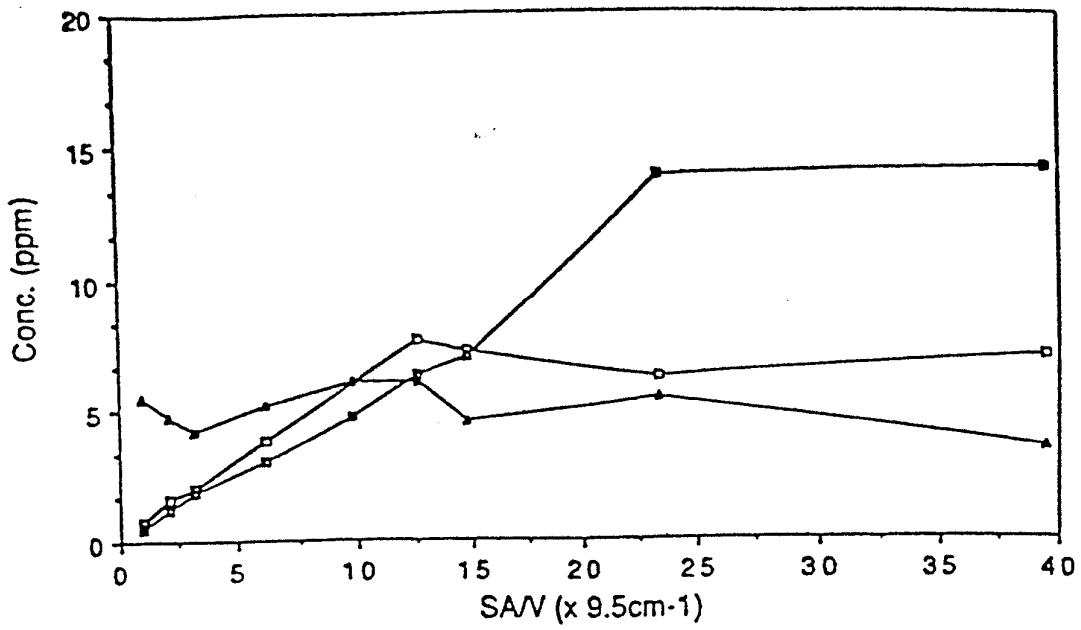

Figure 4.26
Concentrations of Ca (▲), Ba (⧈) and Mo (⧈) in solution as functions of SA/V ratio after hydrothermal treatment at 150°C for 14hr (R2).

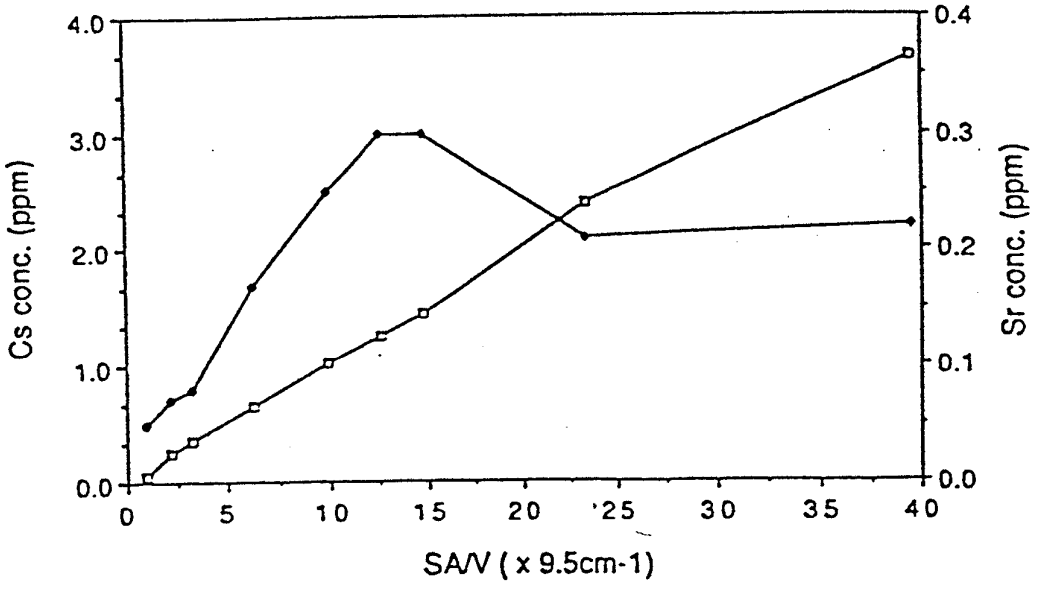

Figure 4.27
Concentrations of Cs (⧈) and Sr (◆) in solution as functions of SA/V ratio after hydrothermal treatment at 150°C for 14hr (R2).

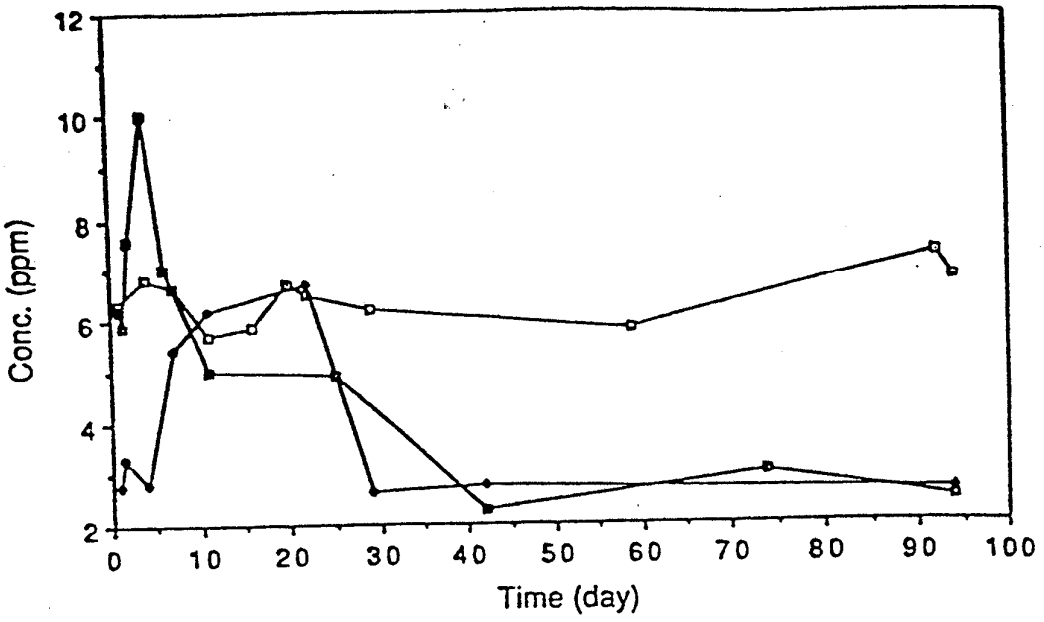

Figure 4.28
Concentrations of Ca in solution as functions of duration of chemical attack.
(▫ = 90°C, ◆ =150°C, ◘ = 190°C).

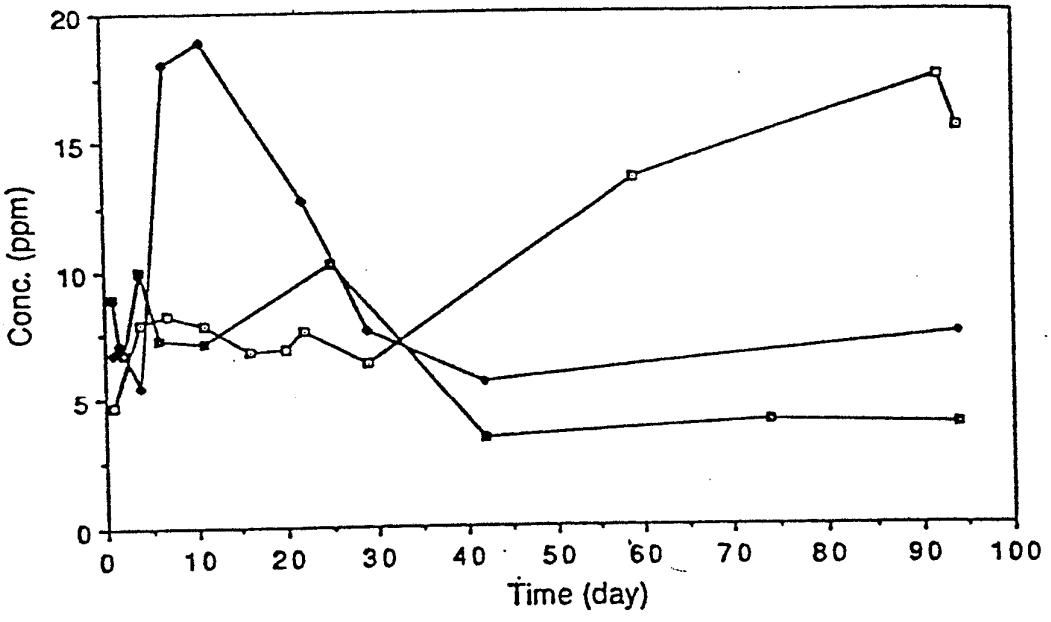

Figure 4.29
Concentrations of Ba in solution as functions of duration of chemical attack.
(▫ = 90°C, ◆ =150°C, ◘ = 190°C).

observations are again consistent with SEM/EDS observations showing no distinct precipitates at 90°C, precipitation of barium molybdate after 4 days at 150°C (with barium-calcium molybdate at later times) and both barium calcium molybdate and barium molybdate phases at 190°C.

For Mo, the concentration -vs- time curves are similar in form to those for Ba although the concentration values are different. At 90°C, the concentration is initially steady to ~30 days but increases monotonically beyond this time from ~12ppm to 18ppm. At 150°C, a broad maximum of concentration (ie ~60ppm) is reached after 23 days following which the concentration declines to a steady value beyond 40 days of ~15ppm. At 190°C, a sharp maximum (ie ~60ppm) is reached at 4 days with a steady value of ~12ppm beyond 15 days. Observations using SEM/EDS are similar to those for the previous two elements. At 90°C, no distinct precipitates are observed although it is likely that there is some equilibration with a thin, continuous calcium-barium molybdate precipitated layer. The observations of the molybdates described above account for the behaviour of the two curves at 150°C and 190°C.

For Sr, again the form of the curve is similar to that for Ba with a steady concentration (i.e. 0.3ppm) at 90°C up to 30 days and a monotonic increase beyond this time to 0.7ppm at 100 days. For 150°C and 190°C, concentration peaks are found at 12 days and 5 days respectively declining to steady concentrations of 0.25ppm and 0.08ppm respectively after 40 days. Computer simulation using EQ3/6 (Chapter 5.2) suggests that strontium carbonate and molybdate should also saturate at 90°C although no SEM/EDS evidence for this precipitation is found. It is again assumed that kinetic constraints govern the recrystallisation of a thin, reprecipitated, possibly amorphous layer of these phases. At 150°C and 190°C, crystallites containing strontium-calcium molybdates, strontium-barium molybdates and (apparently) strontium carbonate are observed in isolated cases.

For Al, the general features of the concentration -vs- time curve are again similar to the Ba and Sr cases. At 90°C, the initial steady concentration of 0.5ppm increases monotonically beyond 30 days to 0.7ppm at 150°C, a broad concentration peak at ~2.5ppm extends to 25 days but, beyond this time, the concentration levels out at ~1ppm. At 190°C, a sharp concentration peak, i.e. 2.5ppm, occurs at 4 days with a steady value of ~0.5ppm beyond 10 days. The characteristics of precipitation are similar to those in the previous two cases. Computer simulation of saturation (see Chapter 5.2) suggests that the solutions are saturated with respect to Al O(OH), Al $(OH)_3$ and Al_2O_3 for attack at 150°C and 190°C. These theoretical predications were supported by the detection of crystals showing only the Al peak in EDS spectra. Other SAM examinations of surfaces have detected aluminium oxide phases (Myhra et al, 1984a, b). The results suggest that the long term concentration of Al in solution is controlled by precipitation of oxides or hydroxides. It is also noteworthy that SAM and SEM in combination have detected the formation of these phases on the hollandite phase after hydrothermal attack at low SA/V conditions (Smart et al 1987; Myhra et al 1989).

Concentrations of Si in solution as functions of duration of chemical attack give different forms of curves to those discussed above as shown in Figure 4.30. At 90°C, the Si concentration increases for the first 60 days and then appears to reach steady values at ~0.55ppm. At 150°C and 190°C, steady values were obtained after ~40 days and 4 days respectively of attack. The final concentration of Si is ~0.8ppm in these cases. For Si, the saturation index data suggests that the solution should be saturated with respect to SiO_2 phases in most cases. The very low concentration of Si (as an impurity) in Synroc C precludes observation of these separate crystallites in SEM or SAM observations. Results discussed in the previous NERDDC Report No. EG89/809(Smart et al, 1989) have clearly illustrated the formation of silicate and alumino-silicate phases during dissolution testing of Synroc C in silica-saturated water and simulated ground water solutions.

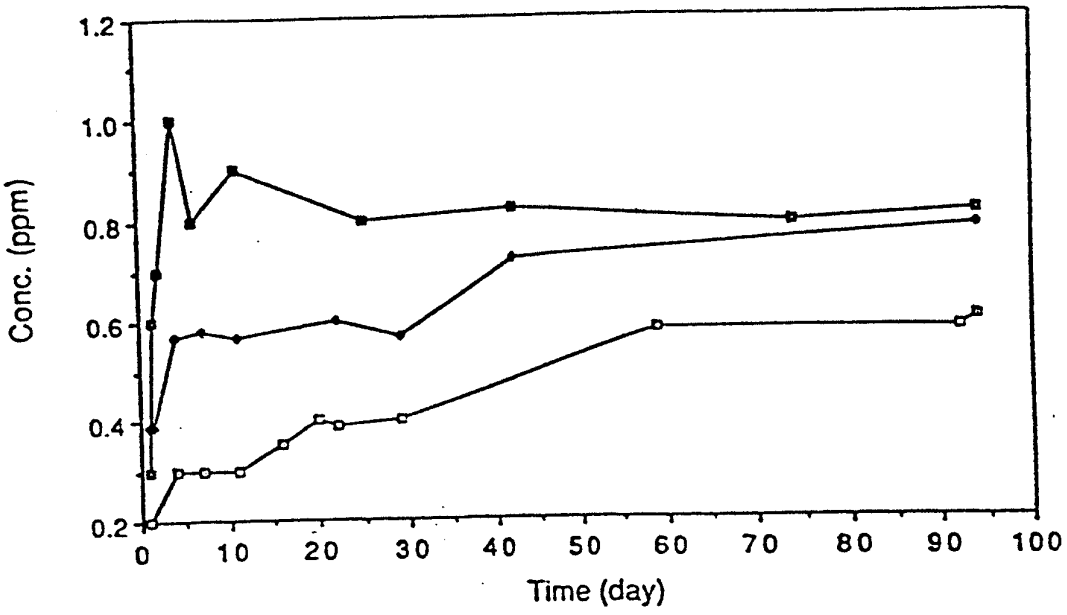

Figure 4.30
Concentrations of Si in solution as functions of duration of chemical attack.
(⧈ = 90°C, ◆ =150°C, ◘ = 190°C).

Generally, Cs and Na concentrations in solution appear to increase steadily with duration of attack and with temperature (Figure 4.31). The curves for Na dissolution are closely similar to those for cesium. The experimental data suggests that Cs and Na remain under-saturated in solution and this is confirmed by the saturation index data from EQ3/6. No evidence of Cs precipitation has been found with any of the electron microscopy or surface techniques.

Concentrations of Ti, Zr, Ni and total inorganic carbon have also been monitored but the concentrations are so low as to be essentially uninterpretable (see Chapter 2.1.2).

Some comments have been included on the SEM/EDS observations with the solution analysis above but further clarification of these results can be provided to illustrate the nature of these observations. It has been noted that, at 90°C, no distinct precipitates are formed although there is some evidence from SAM results, ie very surface-specific analyses, that a surface layer of calcium and barium carbonates and molybdates is formed on the Synroc surface. At 150°C, after 4 days of chemical attack, the majority of precipitates were barium molybdate phases. As the duration of attack increased, barium-calcium molybdate and then calcium molybdate phases started to form. Minor phases were also observed on these surfaces as oxides, carbonates or hydroxides of iron, calcium, barium, titanium, aluminium and zirconium. These minor phases were more scattered amongst the predominant molybdate phases. At 190°C, the majority of precipitates were calcium molybdate detected after only 3 hours of chemical attack. Barium-calcium molybdate and barium molybdate phases were also found amongst the predominant calcium molybdate. The minor phases identified above were also represented and, in some cases, Zr-Al containing precipitates were observed.

It is important to point out that the distribution of these precipitated products varies widely from one Synroc particle to to another even within samples treated under the same conditions at the same temperature. Figure 4.32 illustrates a Synroc particle treated at 150°C for 11 days with sparsely distributed barium molybdate and barium calcium molybdate particles on its surface. In contrast, Figure 4.33 is a secondary electron image from a Synroc surface treated at 190°C for 4 days showing a much higher concentration of precipitated particles. It is possible to find Synroc particles at 190°C with coverage as sparse as that in Figure 4.32 and, conversely, at 150°C, particles as heavily covered as that in Figure 4.33.

The data clearly demonstrates the importance of saturation of elements in solution and precipitation of secondary solid phases in the kinetics of Synroc durability. These phases will, to some extent, determine the extent of near-field retardation of radionuclides in solution as opposed to migration into the far-field regions around the repository core.

4.7 SUMMARY

Evidence has been summarised for seven major mechanisms controlling leaching and dissolution of Synroc, namely:- instantaneous dissolution of surface-exposed ions; ion exchange and diffusion/oxidation of minor (e.g. metal alloy) phases; base catalysed hydrolysis of the major titanate phases; precipitation from solution, in-situ recrystallisation (e.g. TiO_2, ZrO_2) and diffusion-limited release (i.e. microencapsulation). Correlation of results from solution analyses, surface analysis and analytical electron microscopy provides the basis for definition of these mechanisms. The kinetics of Synroc leaching and dissolution has been divided into 5 regimes in which particular mechanisms or combinations of mechanisms are predominant. There is substantial overlap between regimes but this subdivision provides a basis for relating the kinetics to the mechanisms.

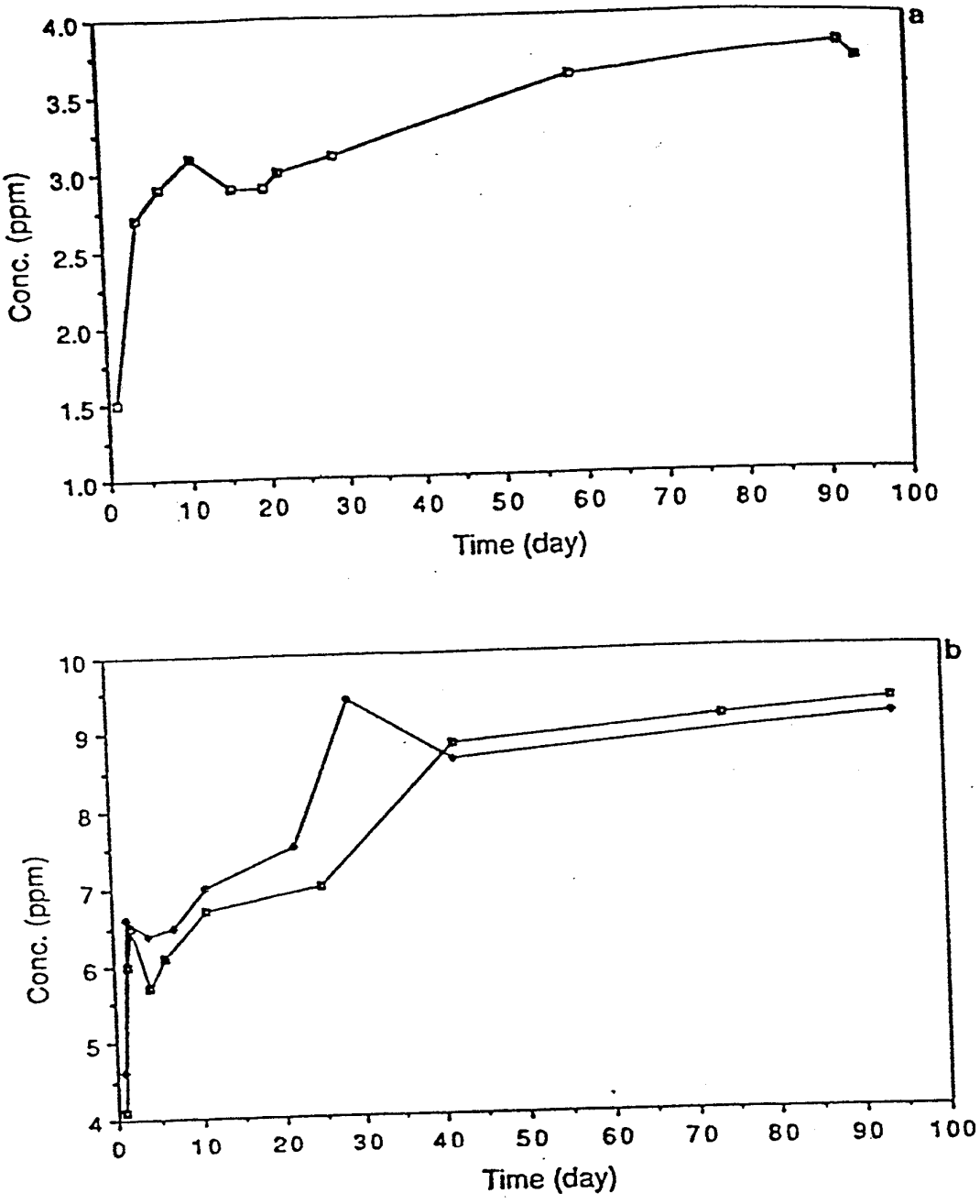

Figure 4.31 a & b
Concentrations of Cs in solution as functions of duration of chemical attack.
(▫ = 90°C, ◆ =150°C, ◘ = 190°C).

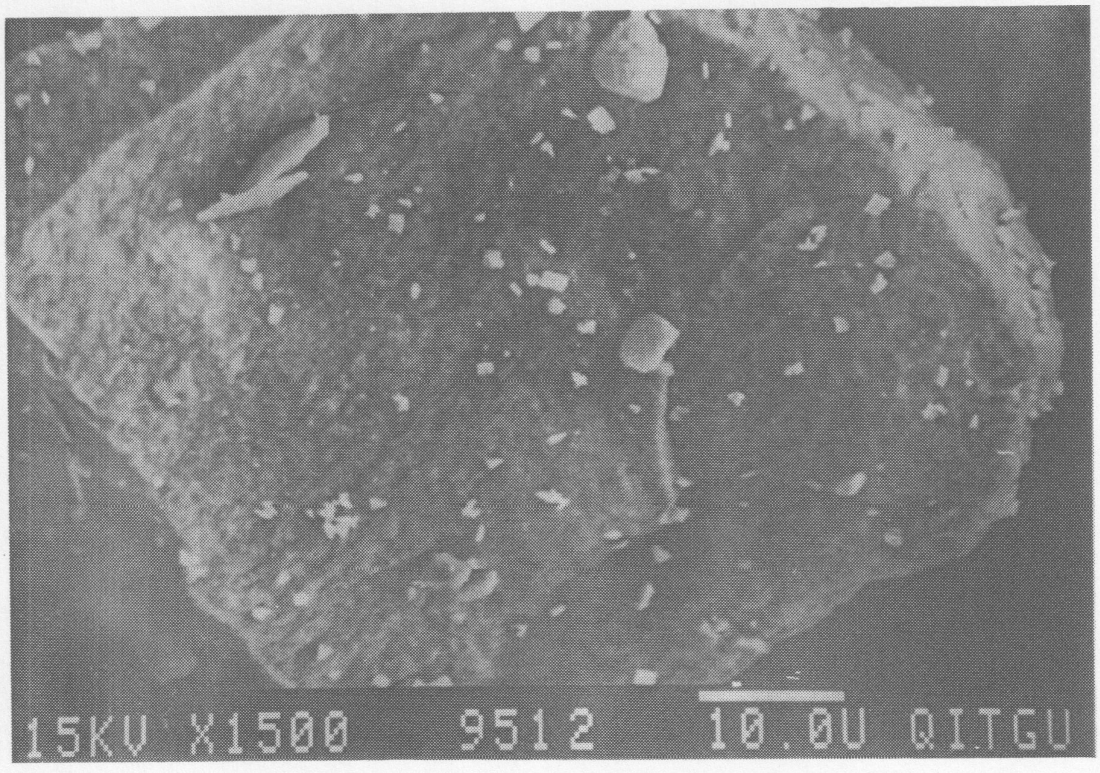
15KV X1500 9512 10.0U QITGU

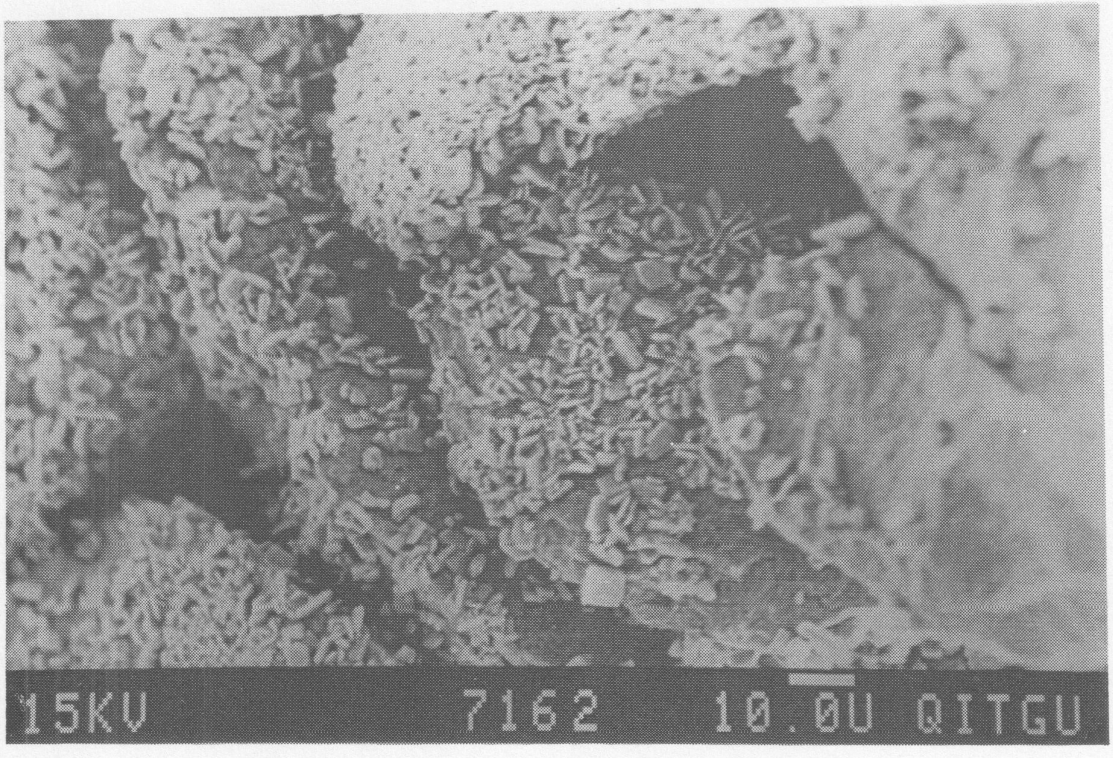
15KV 7162 10.0U QITGU

In regime I - instantaneous dissolution of exposed ions - the effects of prior treatment, ambient reaction, surface disorder and surface area on particular elements are important. In regime II - ion exchange and minor phase reactions - the effects of surface disorder, ceramic microstructure (intergranular films, pores, Ti-relict regions) and minor metal alloy phases are demonstrated. In regime III - titanate hydrolysis - the different reaction rates of perovskite>hollandite>zirconolite, microencapsulation, alterations in the structure of surface-reacted layers at different temperatures, and distribution of elements between phases determine elemental release rates. Regimes IV and V - precipitation, recrystallisation and diffusion - are evident relatively early in the reaction process altering solution concentrations of particular elements and limiting release through hydrolysed layers.

The combination of these mechanisms suggests that long-term kinetics are dominated by:- continuing diffusion - limited hydrolysis of zirconolite; release of particular elements from metastable precipitates; recrystallisation of hydrolysed $Ti(OH)_x^{(4-x)+}$ species to TiO_2 (and probably equivalent ZrO_2 and Al oxide/hydroxide reactions); and consequent surface coverage by precipitates and recrystallised solutions.

4.8 RECOMMENDATIONS

In regime I, there is a need to distinguish between elements released immediately after immersion and those released more slowly via ion exchange, i.e. the time period for release requires further study.

1. It is recommended that standard Synroc disc samples, cut and polished in appropriate non-aqueous solvents, be tested for instantaneous (i.e. <10 sec) release of particular elements.

2. Further work on ambient reaction of perovskite, metal alloy and other surfaces to define the reasons for continuing availability of Ca, Mo and other elements is required.

It is recommended that surface Auger analysis of particular phases reacting in air as a function of time be completed.

3. In regime II, a lack of understanding of the effects of microstructural features such as intergranular films, pores and amorphous triple points on diffusion has limited quantitative correlation with solution analyses. It is recommended that specific studies of diffusion in these microstructural features be continued.

4. In regime III, the nature and extent of reaction, and the structure of the altered surface layer, on zirconolite grains requires definition for long term prediction of stability from microencapsulation.

It is recommended that single-mineral and Synroc studies of zirconolite be continued for this purpose.

5. In regime IV, generally, there is a good agreement between the theoretical model concerning the predicted products and the experimental results throughout this study. However, it is recommended that further work to determine the actual structures of the precipitated phases be continued.

6. A lack of understanding of the effects of solution chemistry on the reactivity of the titanate phases and of microstructural features such as intergranular films, pores and "glassy" triple points has hindered further interpretation of the experimental data and

limited the correlation with results from low SA/V conditions. Lack of knowledge concerning precipitation/crystallisation kinetics of various secondary solid phases has introduced further uncertainities. These are the more important aspects that have to be resolved for a more complete picture. It is recommended that work be continued on these aspects of the long-term stability of Synroc.

7. Another factor that has complicated the interpretation is the presence of CO_2 in solution. Atmospheric CO_2 might be absorbed into the starting solution, or adsorbed onto Synroc powder surfaces (as CO_3^{2-} and HCO_3^-) before commencement of the experiments. Definition of the effects of CO_2 is therefore essential, not only for the concerns of this study but it is also relevant to realistic repository conditions, where ground water is expected to contain a substantial amount of dissolved CO_2. Within this context it is recommended that the effects of silica and the interactions between Synroc and repository rock minerals should be investigated, so that these factors can be incorporated into long term extrapolation models. Experiments at higher temperatures (in the range 250-350°C) should also be conducted since these temperatures may occur in "fresh" waste disposal strategies and could alter reaction paths in the system.

8. In parallel with the complex experiments described above, studies to investigate the temperature-pressure characteristics of solid precipitates should be carried out. This is important in reliable long term extrapolation, and may be achieved by experimental work on simple systems and by consideration of the geological occurences or "natural analogues" of the solids. More thermodynamic data for species and minerals relevant to Synroc (eg Ti, Zr, Ni) should be added to the database of EQ3NR.

9. Finally, in relation to the ultimate question as to which chemical forms dominate the very long term durability of Synroc, some observations can be made at this time but further testing remains critical. Microencapsulation of the less durable perovskite, hollandite and minor phases by zirconolite provides the structural stability of the Synroc matrix. However, a substantial (i.e. micrometers thick) reacted layer develops on the Synroc surface even after 500 days (Smart et al, 1988, 1989). In Chapter 2.1.2, the equation for loss rates of particular elements with time incorporates a term describing the saturation concentration for that element in the ultimate, equilibrated solution surrounding the Synroc surface. The loss rate is then determined by the factor derived from multiplying this saturation concentration with the flow rate through the repository. Using 1,000-day data, it has been previously estimated (Reeve et al, 1988) that the titanium concentration in solution equilibrates to ~0.007gm^{-3}. This estimate is based on actual data from samples that were generated in the actinide testing program. In previous NERDDC Reports (Smart et al, 1988; Smart et al, 1989), discussion of the surface structure and composition of 1,000-day leached samples led to the conclusion that precipitated and/or recrystallised TiO_2 dominated the surface of the ceramic. However, "holes" or pores were still apparent in an almost-continuous layer of TiO_2 suggesting that diffusion of dissolving species was still able to occur through these outlets. In the context of long term rates, 1,000 days is still a relatively short period. It is clearly critical to know whether, eventually, the surface forms a continuous layer of TiO_2 or whether these holes remain in the structure due to kinetic requirements of elemental release. If the former is true, then the concentration to be incorporated in the final rate term is that associated with the equilibration of TiO_2 with the solution whereas, if the latter is true, the present estimate of 0.007g m^{-3} is more correct. The presence of other precipitates of the type discussed in this section is likely only to obscure part of the available surface thereby lowering the available surface area for dissolution. It is unlikely that they will constitute a coherent overlayer inhibiting further reaction. The importance of

understanding the precipitation reactions lies mainly in the ability to interpret solution analysis data correctly.

It is recommended that more extensive study of the structure of this long-term reacted layer be undertaken to provide evidence on the chemical form likely to control these kinetics.

5.0 SOLUBILITY LIMITS AND PRECIPITATION FROM SOLUTION OF ELEMENTAL SPECIES LIBERATED DURING SYNROC DISSOLUTION

5.1 LITERATURE SEARCH

In order to extend the current data base of information regarding the thermodynamic and kinetic constraints of TiO_2 dissolution, a thorough literature search was undertaken.The search was performed on-line to the American Chemical Societies' chemical abstract service in the USA.

The list of keywords used in various permutations in the computer search is as follows:

thermodynamics, kinetics, dissolution, titanium dioxide, perovskite, anatase, rutile, titanate, solubility.

From this initial search two hundred and four titles of scientific reports from journals, conference proceedings, patents etc were obtained.These ranged from reports describing the thermodynamics of titanate mineral phase formation to the chemistry of paint and polymer applications of TiO_2. From this list of titles, twenty five abstracts (summaries), relating to solubility and thermodynamics were procured and examined in further detail.

Eight papers were finally obtained from examination of the abstracts, their references are as follows:

1. Wiese, G.R.et al .,"Solubility Effects in Al_2O_3 and TiO_2 Colloidal Dispersions," Journal of Colloid and Interface Science, 52 , 452 (1975).

2. Berube, Y.G.et al.,"Adsorption at the Rutile-Solution Interface," Journal of Colloid and Interface Science, 27 , 305 (1968).

3. Nesbitt, H.W. et al.,"Thermodynamic stability and kinetics of perovskite dissolution," Nature , 289 ,358 (1981).

4. Yang, H,Y.,"Stability of ilmenite and titanomagnetite in the presence of carbon dioxide," Contrib. Mineral. Petrol., 95 , 202 (1987).

5. Hunt, J.A.,"The stability of sphene," Geochimica et Cosmochimica Acta, 41 , 279 (1977).
6. Banon, S.et al.,"Free energy of mixing in $CaTiO_3$-Ti_2O_3-TiO_2 melts by mass spectrometry," Can.Metall.Q., 20 , 79 (1981).

7. Pogorelov, V.I. et al.,"Some questions of thermodynamics in the interaction between iron and titanium minerals with acids," Deposited Doc., VINITI, 1447 (1974).

8. Sinha, H.N.,"Solubility of titanium minerals in acids,"(Minerals Research Labs, CSIRO, Aust), Int Conf Adv.Chem Metall.,2,16,India (1979).

The final references obtained provided no significant data on the solubility and dissolution kinetics of TiO_2, or titanate phases, beyond that which has been previously cited in this and other NERDDP Synroc reports.The results of this extensive literature search indicate that the worldwide database on TiO_2, and titanates is extremely limited.

It is recommended that limited studies of the solubility of TiO_2 phases and selected relatively insoluble titanates be undertaken to extend this database.

5.2 SOLUBILITY LIMITS AND PRECIPITATION FROM SOLUTION

5.2.1 Introduction

This section reports on a preliminary study concerning the saturation of species in solution and precipitation of secondary phases as a result of chemical attack on Synroc. Some of the material in this section overlaps with that of section 4, but in the interest of coherence we have not sought to eliminate that overlap.

The essence of the approach used to describe the behaviour of a HLW disposal material is shown in Fig. 4.25, illustrating the change in the concentration of species in solution with time for the cases where solution saturation effects are important. The time interval T_1 represents the early stage of the dissolution process, during which the fluid phase is undersaturated with respect to the element concerned. The dissolution rate is described by the tangent to the concentration curve. As the dissolution progresses, the dissolution rate decreases as a result of the decrease in the chemical potential difference of the element between solid and fluid phases [Apted et al., 1982]. Eventually, at some stage T_2, the concentration is essentially time-invariant [Savage, 1984]. However, this does not necessarily mean that the dissolution stops, but that the rate of release of the element from the waste form is balanced by its rate of precipitation as a secondary phase. The overall reaction may take place via a series of these intermediate steady-states [Fyfe and Verhoogen, 1958]. As pointed out Savage, [1984], the solubility of metastable solid phases decreases as the reaction progresses. The precipitation of a more stable intermediate phase is shown in Fig. 4.25 by the approach to a new steady-state condition in the interval T_3.

This approach thus concentrates on the elements once they are released from the solid. It is essential that the evolution of the total system - the fluid phase, the waste form, and the secondary solid phases - be fully characterised in order that experimental results be interpretable in terms of overall reaction paths, and be predictable in the long term.

In this chapter, some fundamental and relevant aspects concerning the microstructure and surface reactivity of Synroc are introduced. Most previous studies on the chemical durability of Synroc were carried out in the regime where solubility constraints in the fluid phase were not important. This knowledge is useful in defining the intrinsic chemical durability of Synroc and, in some cases, essential for the understanding of the experimental results obtained in this study. Also discussed here are the methodology employed, and details of experiments carried out, in order to obtain the steady state conditions for various elements and to characterise the system from its initial to its final state.

5.2.2 Methodology and Experimental Details

5.2.2.1 Methodology

In order to compress the long term effects of saturation and precipitation to the timescale of laboratory experiments, it is necessary to accelerate the reaction kinetics. This was achieved by increasing the SA/V ratio and the temperature of attack. Synroc monoliths were therefore powdered by crushing and milling in order to increase the area of the solid surface. The use of powders to increase the SA/V ratio has been advocated as a legitimate means of accelerating the approach to solubility limits of monoliths [Macedo et al., 1982].It should be noted, however, that high temperature may change the reaction path (or rate-determining step) of the system, making extrapolation to lower temperature of doubtful validity [Cousens et al., 1981].

A method similar to the MCC-3 type leach test was employed. In the present case, the reaction vessels were Teflon liners incorporated in "Parr" bombs. As a result, the highest temperature that could be used in the chemical durability runs was 190°C. At temperatures above approximately 200°C, Teflon is sufficiently permeable to water vapor so that significant changes in the solution volume may occur during periods as short as a week .

Although the sudden quenching of the system introduces the possibility of modification of solid and liquid products during quenching process, these techniques are widely applied in hydrothermal work and will not, in most cases, invalidate the results. In general, the overall trends of geochemical reactions are preserved by this method. In the present study, the effect on the solution composition of cooling from 90°C to room temperature was investigated by analysing samples taken at temperature and after cooling. Also, the properties of the fluid products can be used to justify the quench-type technique employed (see section 5.2.4.1).

The starting solution used in all experiments was DDW. Understanding of this relatively simple case is essential if more complex systems (such as synthetic or natural ground water) are to be unravelled.

The regime in which the effects of saturation and precipitation are prominent was determined by varying the SA/V ratio. The evolution of the system in that regime was then investigated by systematically changing the duration of attack which, for practical reasons, ranged from 1 to 100d, while other relevant parameters such as temperature and SA/V were kept constant. Experiments were conducted at 90, 150 and 190°C to examine the effects of temperature. Monolithic specimens were also included in a few selected runs for purposes of carrying out surface analysis.

The evolution of the total system was characterised not only by solution analyses but also by SEM/EDS and XPS for powdered and monolithic specimens, respectively. The use of surface sensitive techniques served the main purpose of detecting secondary solid phases when they appeared either as discrete crystallites or as surface layers. XRD was not effective for the identification of precipitate phases, probably due to their low concentration and small particle size.

An important feature of the methodology employed in this study is that the characterisation of the solutions (such as the aqueous speciation and secondary solid phase chemistry) was complemented by use of the sophisticated computer code EQ3NR [Wolery, 1979]. This code is essentially a geochemical aqueous speciation - solubility program for modelling the thermodynamic chemical state of an aqueous solution by calculating the distribution of aqueous species (single ions, ion-pairs, and aqueous complexes). The input to the code is the chemical composition of a solution and various user-defined parameters (e.g. temperature, alkalinity balance, charge balance, etc.). These inputs represent the total values for concentrations of dissolved species, as determined by bulk analyses, which do not distinguish between contributions from single ions, ion-pairs or aqueous complexes. The speciation calculation is based on thermodynamic equilibrium constants, which are included in the database. The output of EQ3NR contains the aqueous species distribution in solution (concentrations and thermodynamic activities). It also includes the saturation indices (SI= log Q/K, where Q is the activity product, and K is the equilibrium constant for a dissolution reaction) and the thermodynamic affinities (A= 2.303RT x SI, where R is the gas constant, T is the Kelvin temperature and SI is the saturation index) of precipitation reactions of minerals. Both SI and A are positive for supersaturation, zero for saturation, and negative for undersaturation with respect to a particular mineral.

The main short-coming of this code is that its database did not include several important species and minerals relevant to Synroc (e.g. Ti, Zr or Mo species and minerals).

Some thermodynamic data for these species and minerals are available and were added by the the Griffith University Synroc Group. However, full implementation of the code requires further expansion of the database.

5.2.2.2 Experimental Details

5.2.2.2.1 Materials and Sample Preparation

The Synroc specimen material used in this study (code SFG-531) was fabricated by ANSTO. The material contained 10 wt% of simulated waste PW-4b-D and was fabricated according to the preparative route developed by Dosch and his colleagues [Dosch and Lynch, 1981; Dosch et al., 1983] at the Sandia National Laboratory.

The material was supplied as monoliths which had dimensions of about 4.0cm diameter and 1.5cm thickness. The samples were prepared by cutting these monoliths into smaller pieces with a diamond saw. These pieces were then crushed , ground and sieved to powders of size fraction 50 - 100μm, using a tungsten - carbide mortar and pestle.

Ultrafine particles were removed by ultrasonic agitation in distilled ethanol. The specific surface area of the powders was measured to be 0.25 m^2g^{-1} (using the BET method with N_2 as the adsorbate). The geometric surface area was calculated as 0.02 m^2g^{-1}, assuming cubic particles. Monolithic specimens of dimensions 2x3x1mm^3 were also prepared, with one large face polished to 1μm diamond paste finish, for SEM/EDS and XPS characterisations.

5.2.2.2.2 Chemical Durability Runs

The experiments were carried out in accordance with the methodology described above. The details are summarised in Table 5.2.2.1. The choice of using the measured SA/V rather than the geometric value, for runs with powders in Table 5.2.2.1, is rather arbitrary.

A number of runs of experiments (R4, R5, and R6) with critical values of solution concentrations were repeated in order to confirm the validity of the results. The quenching from hydrothermal conditions to ambient took approximately 30min for all runs.

5.2.2.2.3 Analysis

Measurements of pH and analyses for a range of elements were carried out for all solutions after chemical attack. For most runs, analyses were carried out for the following elements with ICP: Ca, Ba, Mo, Sr, Al, Si, Ti, Zr, Ni. However, Cs was analysed by AA. Only Ca, Ba, Mo, Sr and Cs were analysed for the R1 runs. After chemical attack at 150°C for 4d (R5/4d), Fe, Ru, Ce, Nd, Pd, Gd, U, Y, Cr, Ag, Cd and Te were also analysed by ICP. All relevant solution analytical data, except those for Ti, Zr, and Ni, were used as input to the code EQ3NR for theoretical prediction of aqueous species and secondary solid phases. Limits of detection for the various elements are presented in Table 5.2.2.2.

TABLE 5.2.2.1: Details of Chemical Durability Runs.

Experiment	Specimen	Temp (^{0}C)	Duration	Measured SA/V (cm^{-1})	Note
RO	Blank	150	10d	0	Blank solution.
R1	Monolith	150	1, 7d	0.1 (geometric)	To measure loss rates for comparison with other standard Synroc
R2	Powder	150	14hr	9.5 - 375	Solutions were extracted at temperature and after cooling
R3	Powder	90	87d	375	
R4	Powder	90	1 - 100d	375	Monolith was included for 22d run for XPS analyses
R5	Powder	150	1 - 100d	375	
R6	Powder	190	1 - 100d	375	Monolith was included for 7d run for XPS analyses
R7	Monolith	190	7d	0.1 (geometric)	For XPS analyses.

TABLE 5.2.2.2: Limits of Detection of Elements

Element	Detection Limit (ppm)	Element	Detection Limit (ppm)
Ca	0.00005	Ru	0.02
Ba	0.0003	Nd	0.05
Mo	0.004	Pd	0.05
Sr	0.001	Gd	0.01
Al	0.01	Y	0.0005
Si	0.008	Cr	0.003
Ti	0.002	Ag	0.02
Zr	0.003	Cd	0.003
Ni	0.001	Te	0.04
Cs	0.017	Fe	0.002

The total inorganic carbon in solution was measured for all the R4, R5 and R6 runs using a carbon analyser (Beckman Industrial Tocamaster, Model No. 915/B) with a detection limit of 1ppm.

SEM/EDS was used to examine powders after all the R4, R5, R6 runs, and to establish initial surface conditions of unattacked monoliths and powders. Quantitative XPS

analyses of the surfaces (after about 1nm has been removed by Ar^+ ion sputtering) of monoliths before and after aqueous attack were confined to Ti, Ca, Ba, Zr, Al and Mo. Instrumental parameters and other relevant technical details were the same as those for other sections (e.g., 2.2) of this report, except that examinations by SEM/EDS were carried out at 30kV in some cases.

5.2.3 Results

5.2.3.1 Material Characterisation

Unlike the borosilicate glass waste forms designed for HLW disposal, (e.g.,the standard PNL 76-78 formulation), Synroc is not a single, homogeneous entity. Variations in composition and fabrication conditions have led to a range of results being reported for phase relationships and microstructures, as well as the chemical durability. In particular, it has been found [Woolfrey et al., 1987] that many properties of Synroc are strongly dependent on the extent of pre-calcination mixing (i.e., homogeneity) and hot pressing conditions (i.e. pressure and temperature). Formulations with < 94% theoretical density do not have acceptable properties for comparison with other waste forms. The fabrication of Synroc with > 99% theoretical density is now routine. Detailed description of these "standard" formulations has been fully reported elsewhere [Woolfrey et al., 1987]. The Synroc material used in this study was fabricated according to the standard preparation conditions. SEM/EDS characterisation of the unattacked polished surface revealed that this material had identical microstructures to those found for other standard specimens. We note here the following important and relevant features:

(i). Back-scattered electron (BSE) images showed that the distribution of contrast areas was uniform, indicating good mixing procedures and resulting homogeneity.

(ii). The alloy phases appeared to lie in two size ranges, < 0.5μm and 1-3μm, and were distributed uniformly throughout the matrix. EDS analyses of these regions revealed that the larger areas (1 - 3μm) were predominantly Ru and Mo with some Fe, while the smaller areas (< 0.5μm) usually contained Pd and Te.

5.2.3.2 Solution Analysis

5.2.3.2.1 Low SA/V (run R1)

Loss rates for mass and some representative elements were measured (R1). The results are presented in Table 5.2.3.1. These results were in good agreement with those previously obtained for other standard Synroc specimens.

5.2.3.2.2 Variable SA/V (run R2)

The concentrations of Ca, Ba, Mo, Sr, and Cs in solution as functions of SA/V are shown in Fig. 5.2.3.1 and 5.2.3.2. It can be seen that Ca exhibited steady values at around 5ppm, irrespective of the value of SA/V. Ba and Sr concentrations increased initially with SA/V. For SA/V values larger than $118cm^{-1}$, Ba leveled out at around 6.5ppm, while Sr decreased to about 0.2ppm. Mo had a concentration of about 14ppm at SA/V ≈ $218cm^{-1}$. It appeared to remain at that value for larger SA/V ratio.The concentration of Cs increased monotonically with SA/V. Fig. 5.2.3.3 shows a rise in the final pH up to 5.5 as SA/V was increased to $223cm^{-1}$. This value of pH was maintained up to SA/V of $375cm^{-1}$.

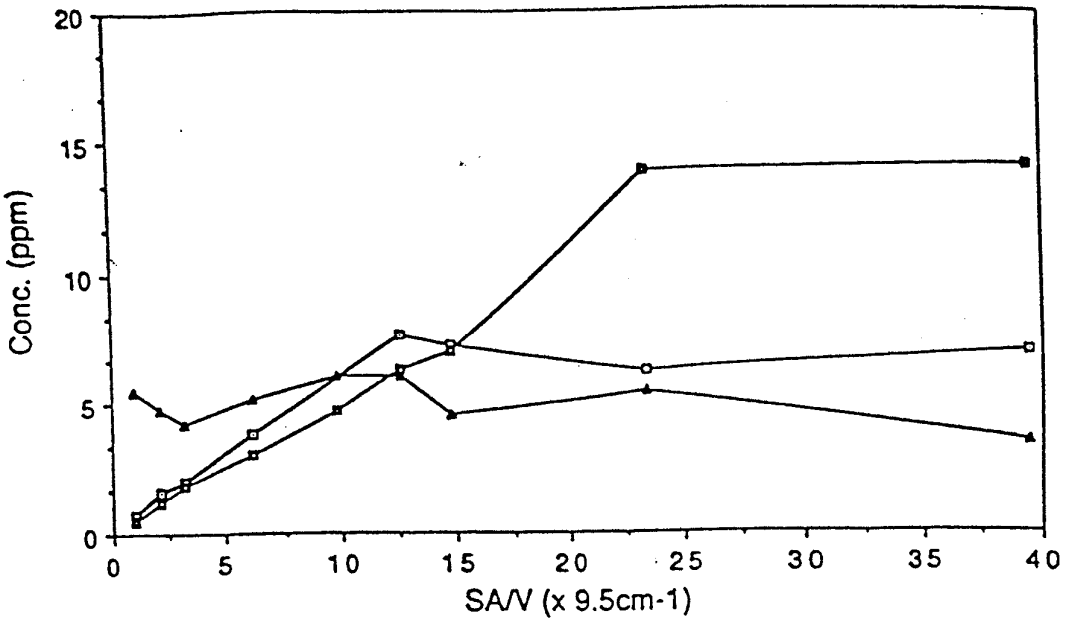

Figure 5.2.3.1
Concentrations of Ca (▲), Ba (⊡) and Mo (■) in solution as functions of SA/V ratio after hydrothermal treatment at 150°C for 14hr (R2).

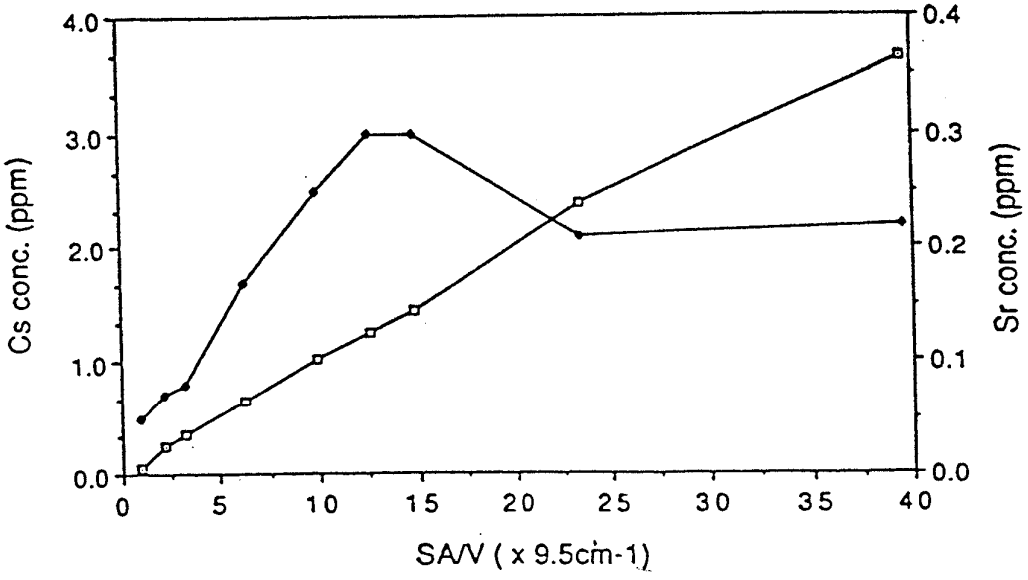

Figure 5.2.3.2
Concentrations of Cs (⊡), and Sr (◆) in solution as functions of SA/V ratio after hydrothermal treatment at 150°C for 14hr (R2).

TABLE 5.2.3.1: Loss Rates ($gm^{-2}d^{-1}$) for Representative Elements as Measured from run R1 (150°C).		
	0-1d	0-7d
Mass	0.520	0.38
Al	0.15	<0.03
Ba	0.280	0.009
Ca	0.262	0.095
Cs	0.565	0.020
Mo	1.620	0.065
Sr	0.490	0.040
Ti	<0.005	<0.005
Zr	<0.025	<0.005
pH(final)	5.1	5.0

5.2.3.2.3 The Effects of Quenching from 90°C (run R3)

Results of analyses of solutions taken at temperature and after cooling are given in Table 5.2.3.2.

TABLE 5.2.3.2: Concentrations of Elements in Solutions (after 87d at 90C, R3) Taken at Temperature (A) and after Cooling (B)							
	Element (ppm)						
Solution	Ca	Ba	Mo	Sr	Al	Ti	Zr
A	6.13	16.51	18.12	0.62	0.66	*	*
B	6.10	16.25	18.20	0.65	0.70	*	*

* Below limits of detection

It can be seen that the values of pH and concentrations of elements in solution are similar, irrespective of whether sampling was done at temperature or after quenching. There is no apparent effect of precipitation or speciation changes on cooling to room temperature.

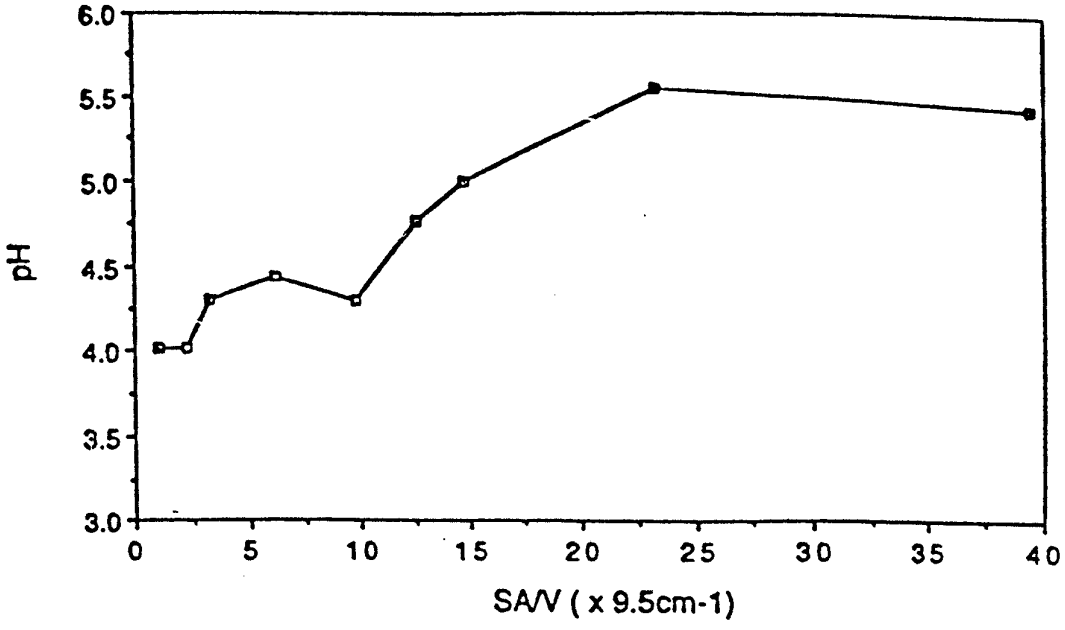

Figure 5.2.3.3
pH of solution as functions of SA/V ratio after hydrothermal treatment at 150°C for 14hr (R2).

5.2.3.2.4 Runs at 90, 150, 190°C with Duration of Attack as Variable (runs R4, R5, R6)

A general feature of the results obtained from solution analyses for runs R4, R5 and R6 was that the solution concentrations as functions of duration of attack for various relevant elements exhibited particular trends. In the case of attack at 90°C, the concentrations of most elements exhibited a steady increase with duration of attack, while the general trends for 150 and 190°C runs were that these concentrations first increased to reach maximum values, followed by a decrease and then the attainment of steady values. In addition to these overall trends, there were considerable scatter in the "fine" structure of the data. These random scatter are likely to be due a variety of factors associated with the experimental and data-acquisition processes, and are not representative of the overall evolution of the system. Critical values and trends were confirmed by repeated runs. In this and later sections, the discussion will be limited to the main trends exhibited by the results for the concentrations of elements in solution.

Calcium (Fig. 5.2.3.4)

The concentration of Ca in solution for all runs at 90°C was about 6ppm. For the runs at 150 and 190°C, Ca concentration appeared to increase with duration of attack up to 22 and 4d, respectively; they decreased thereafter and leveled out at around 2.8ppm for both temperatures.

Barium (Fig. 5.2.3.5)

For runs at 90°C, the Ba concentrations in solution were steady at around 7ppm during the first 30d of chemical attack. They started to rise progressively with duration of attack thereafter, and reached a value of about 16ppm after 95d. Hydrothermal runs at 150°C resulted in an increase of Ba concentrations in solution after 4d of chemical attack, and reached a maximum value at around 18ppm after 12d. They decreased and leveled out in the neighbourhood of 7ppm for longer duration of attack. For runs at 190°C, Ba concentrations appeared to fluctuate around the 7.5ppm value for duration of attack less than 30d. They decreased slightly down to about 3.5ppm for longer duration of attack.

Molybdenum (Fig.5.2.3.6 a and b)

For runs at 90°C, concentrations of Mo in solution increased slightly from 10.5ppm after 1d to about 14ppm after 4d of attack. These values were maintained for the next 30d, and started to increase thereafter. The Mo concentration was 17ppm after 60d of chemical attack, and appeared to rise up to about 18ppm towards 94d. For runs at 150 and 190°C, Mo concentration had maximum values at about 60ppm after 22d and 4d of chemical attack, respectively. They each reached a steady value of around 15ppm after about 40d of attack.

Strontium (Fig. 5.2.3.7)

For runs at 90°C, the Sr concentrations increased slightly from 0.17ppm after 1d to 0.27ppm after 4d of attack, and appeared to remain at that value for duration of attack less than 30d. They started to increase progressively thereafter, and reach a value of about 0.65ppm after 95d. For runs at 150 aand 190°C, the Sr concentrations reached maximum values at 0.74ppm and 0.50ppm, respectively. They started to decrease thereafter, and appeared to attain steady levels at around 0.25ppm and 0.10ppm for 150 and 190°C, respectively.

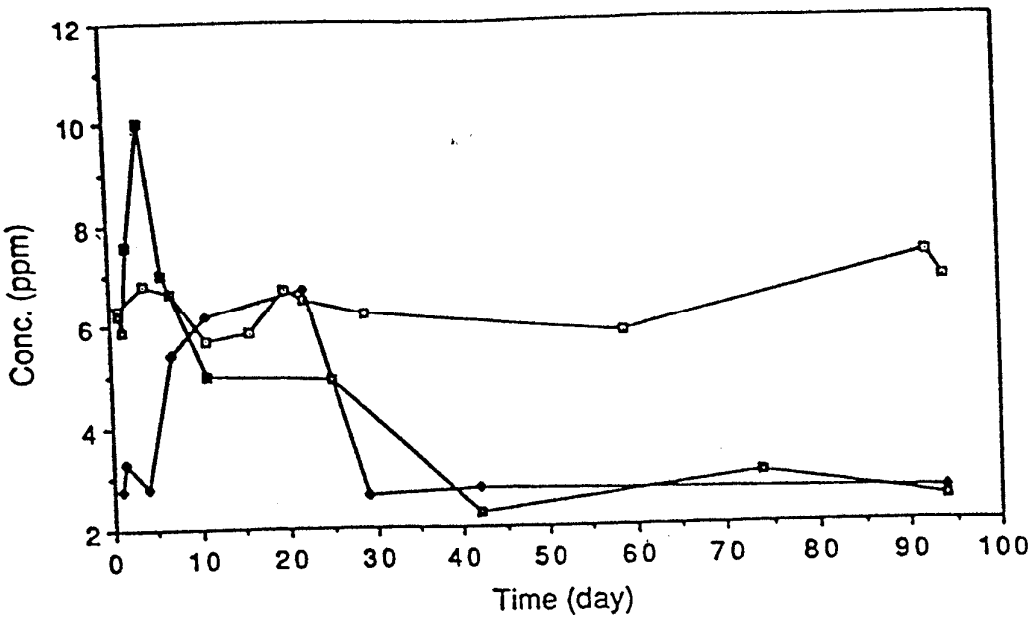

Figure 5.2.3.4
Concentrations of Ca in solution as functions of duration of chemical attack.
(⊡ = 90°C, ◆ = 150°C, ◘ = 190°C).

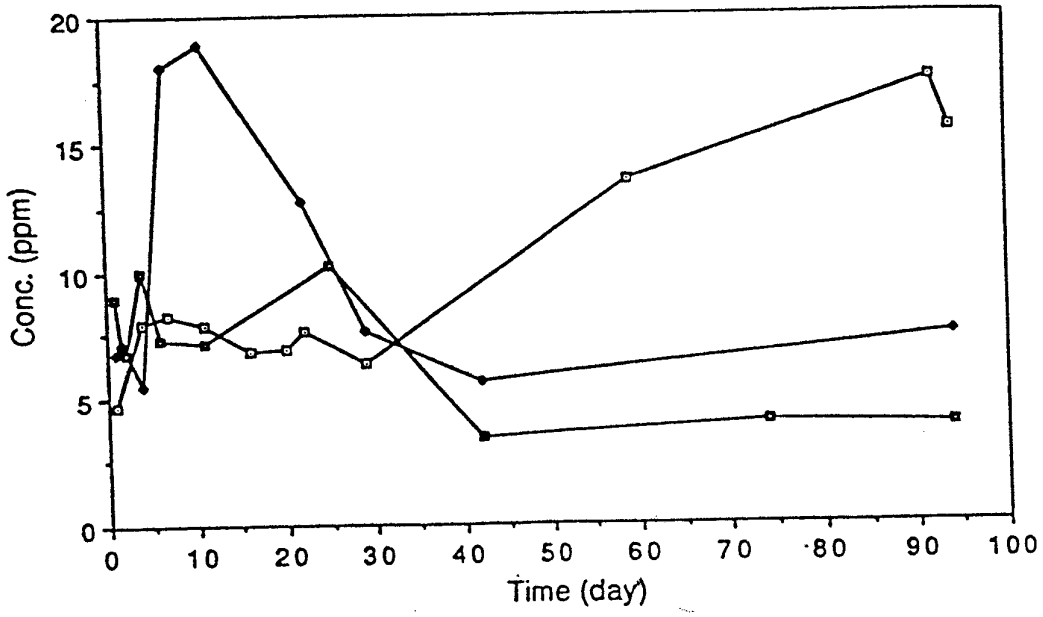

Figure 5.2.3.5
Concentrations of Ba in solution as functions of duration of chemical attack.
(⊡ = 90°C, ◆ = 150°C, ◘ = 190°C).

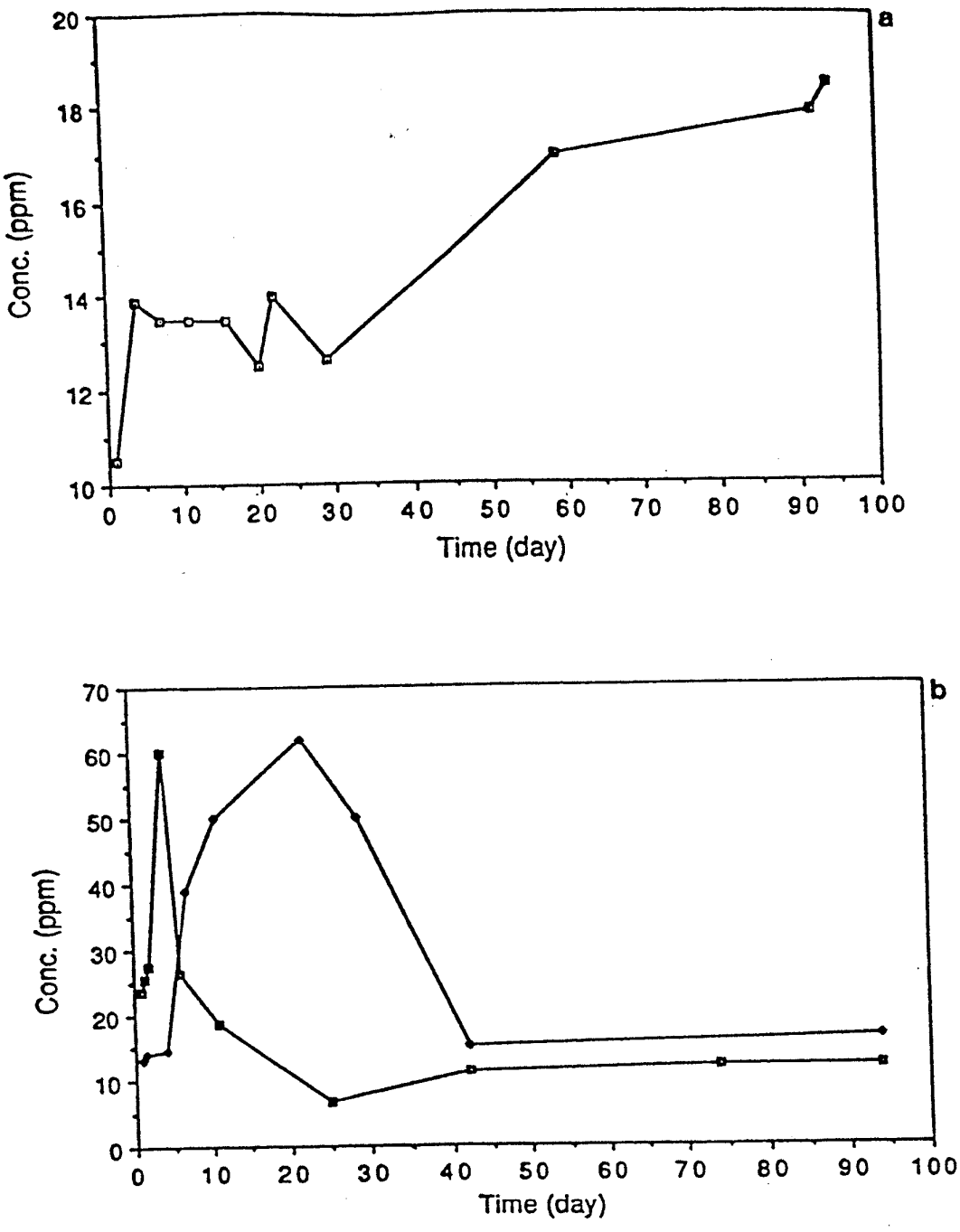

Figure 5.2.3.6 a and b
Concentrations of Mo in solution as functions of duration of chemical attack.
(⊡ = 90°C, ◆ = 150°C, ◘ = 190°C).

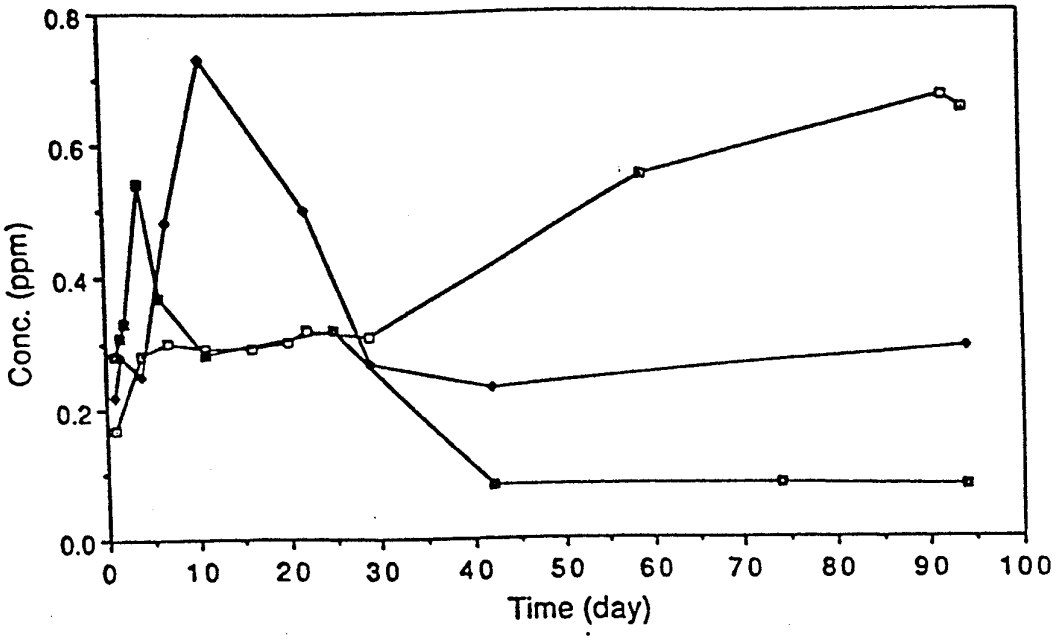

Figure 5.2.3.7
Concentrations of Sr in solution as functions of duration of chemical attack.
(⧈ = 90°C, ◆ = 150°C, ◘ = 190°C).

Aluminium (Fig. 5.2.3.8 a and b)

The general features of Al concentration in solutions after chemical attack at 90, 150 and 190°C were similar to those of Mo. The steady state values were around 0.70ppm for all temperatures.

Silicon (Fig. 5.2.3.9)

For runs at 90°C, the Si concentrations increased with duration of attack for the first 60d. They appeared to reach steady state values at around 0.55ppm for longer durations. For runs at 150 and 190°C, steady values were attained after about 4d of attack. Steady values of Si appeared to be in the order of 90 < 150 < 190°C.
Cesium and Sodium (Fig. 5.2.3.10 (a and b) and 5.2.3.11 (a and b))

Generally, Cs and Na concentrations in solution appeared to increase steadily with duration of attack and with temperature.

pH (Fig. 5.2.3.12)

For runs at 90 and 150°C, pH values of the solutions appeared to rise slightly during the first 10d; then decrease progressively for longer durations of attack. After 95d, the pH of the solutions had a value around 4.7 for both tempertures. Solutions after hydrothermal attack at 190°C generally had pH values lower than those after attack at 90 and 150°C. During the first 10d, the pH's appeared to reach steady values at about 4.3; they increased thereafter and had a value of 5.2 after 94d of chemical attack.

Titanium, Zirconium, Nickel & Total Inorganic Carbon (Tables 5.2.3.3, 5.2.3.4, 5.2.3.5)

Ti, Zr and Ni exhibited irregular and low concentrations in solution. Results for these elements are presented for completeness. Results for these elements are essentially uninterpretable due to the limited database of EQ3NR.

Levels of HCO_3^- in solution did not exhibit any particular pattern. For the three temperatures, the highest and lowest values for the HCO_3^- concentrations were 30 and 5ppm, respectively. Concentrations of the elements Fe, Ru, Ce, Nd, Pd, Gd, U, Y, Cr, Ag, Cd and Te in solution after 4d at 150°C (R5/4d) were below their respective limits of detection.

5.2.3.3 Computer Simulation (EQ3NR)

Analytical data from each run were used as sets of input to the software package EQ3NR. A summary of the major aqueous species, identified by this code at 90, 150 and 190°C, is presented in Table 5.2.3.6 and Table 5.2.3.7 shows representative outputs of the saturation indices for various minerals, contained within the database of EQ3NR, as calculated from the chemistry of the solutions.

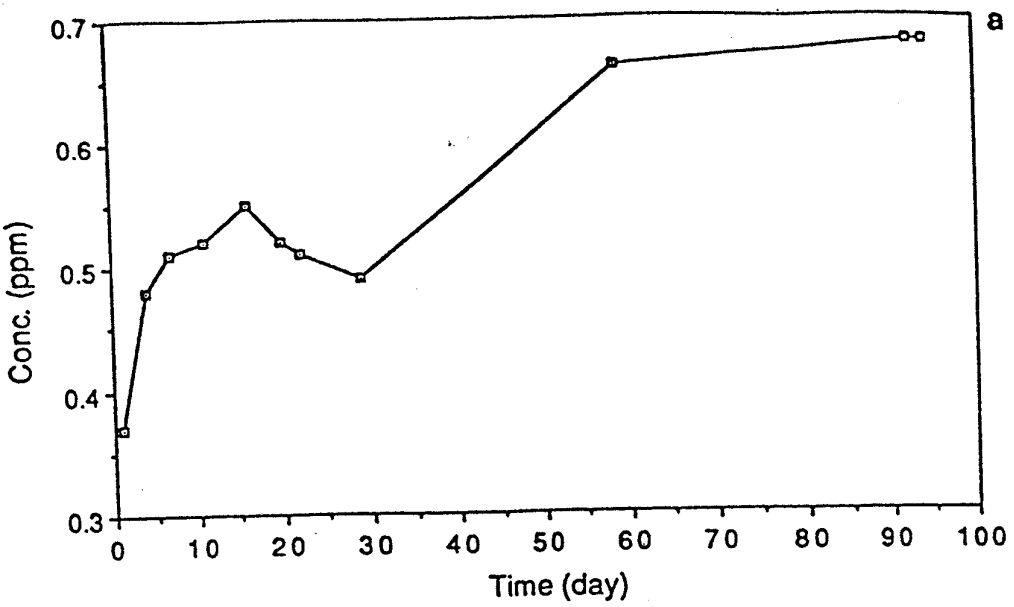

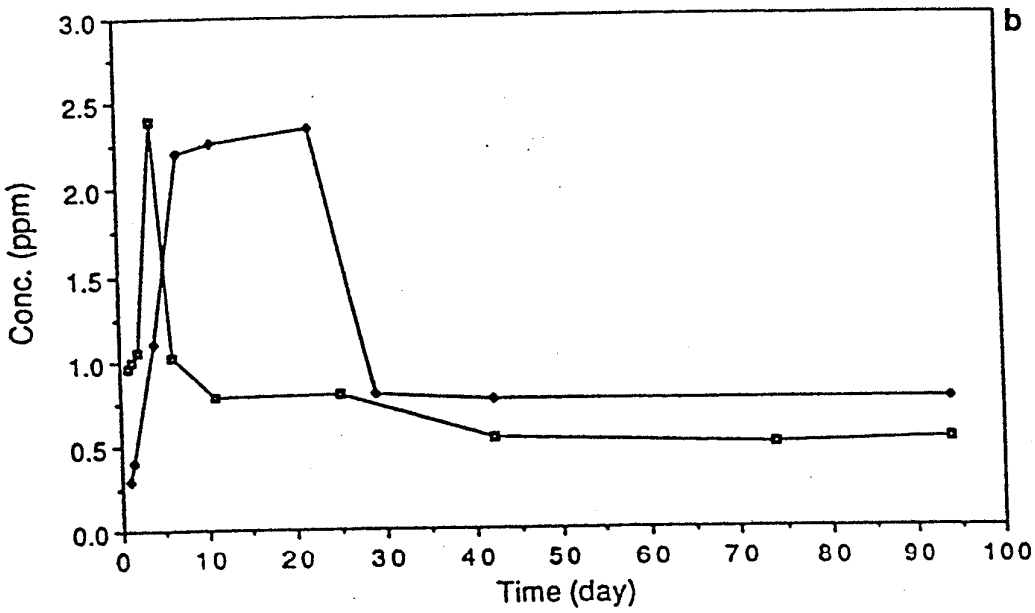

Figure 5.2.3.8 a and b
Concentrations of Al in solution as functions of duration of chemical attack.
(⊡ = 90°C, ◆ = 150°C, ◘ = 190°C).

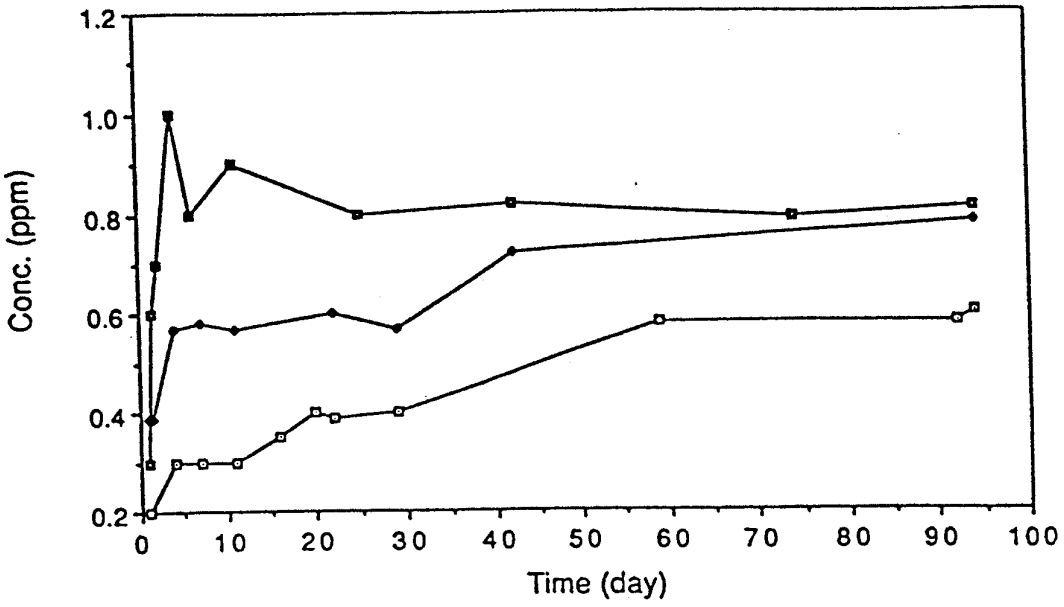

Figure 5.2.3.9
Concentrations of Si in solution as functions of duration of chemical attack.
(⊡ = 90°C, ◆ = 150°C, ◘ = 190°C).

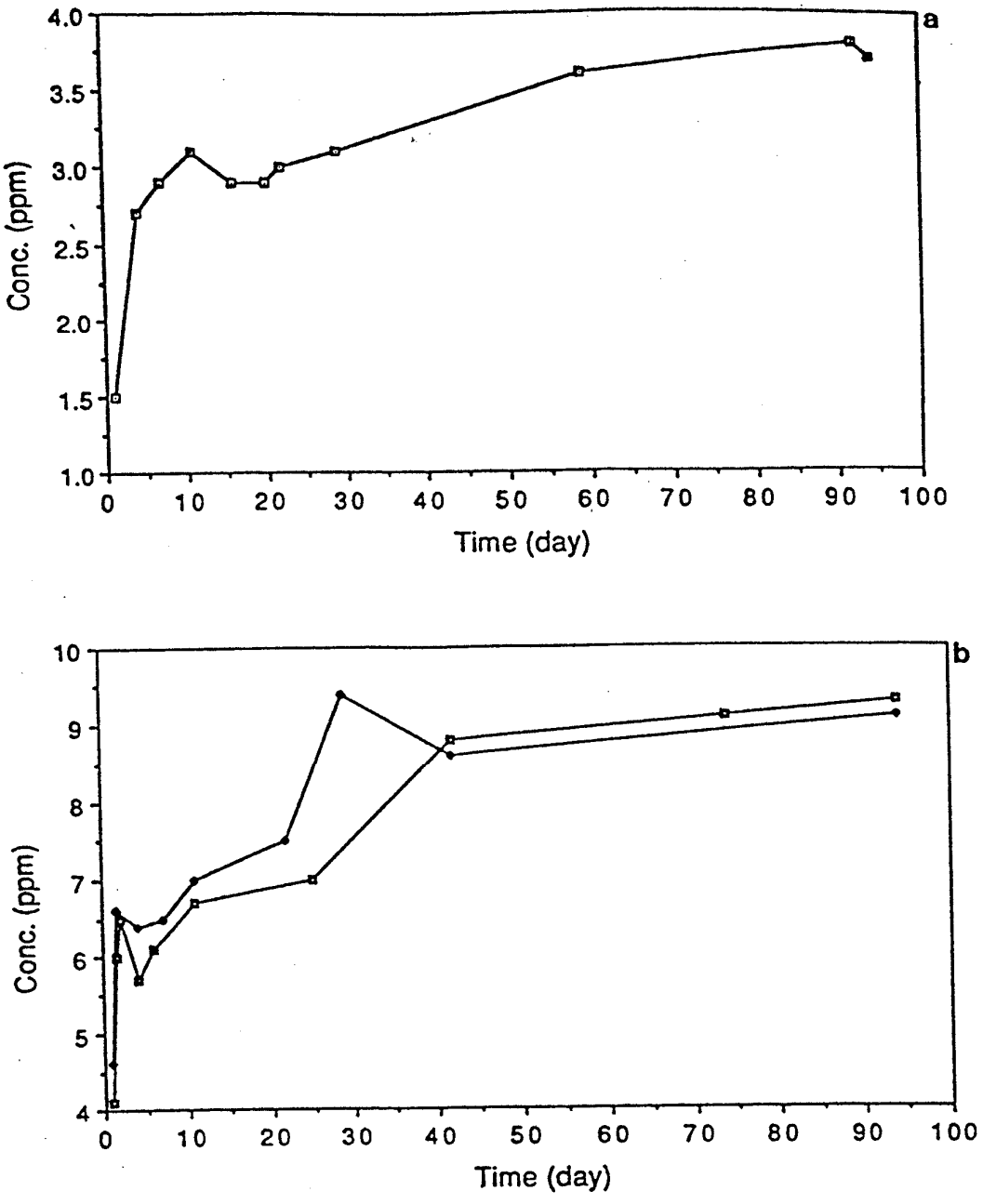

Figure 5.2.3.10 a and b

Concentrations of Cs in solution as functions of duration of chemical attack.

(⊡ = 90°C, ◆ = 150°C, ◘ = 190°C).

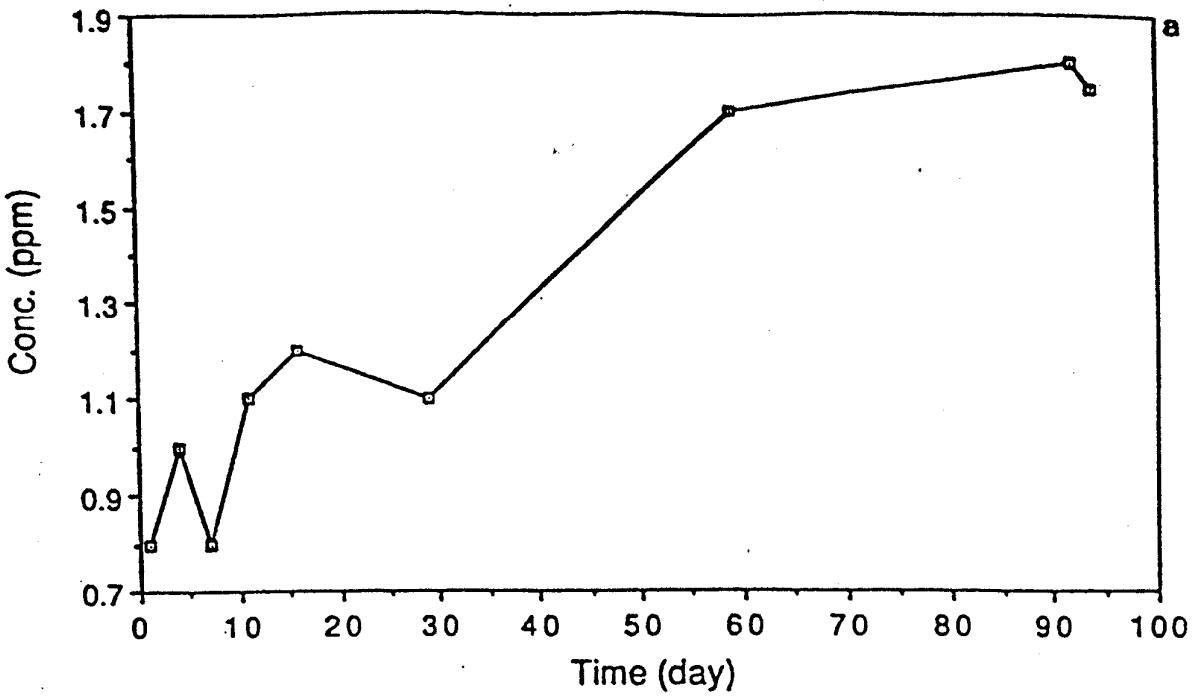

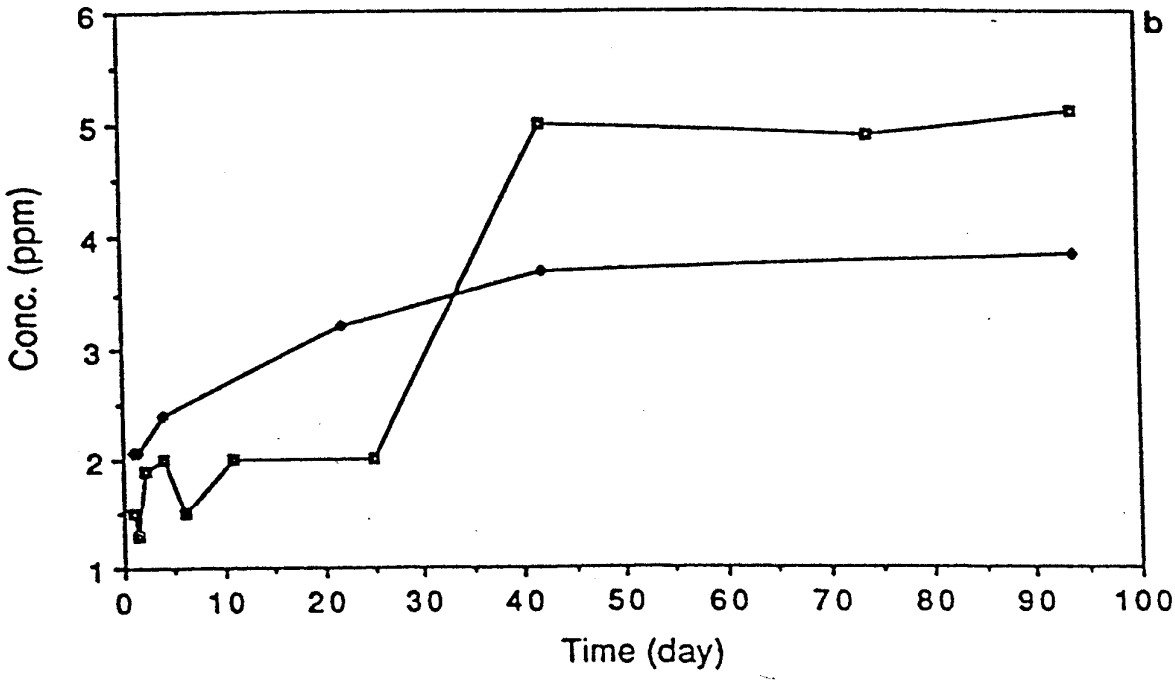

Figure 5.2.3.11 a and b

Concentrations of Na in solution as functions of duration of chemical attack.

(⊡ = 90°C, ◆ = 150°C, ◘ = 190°C).

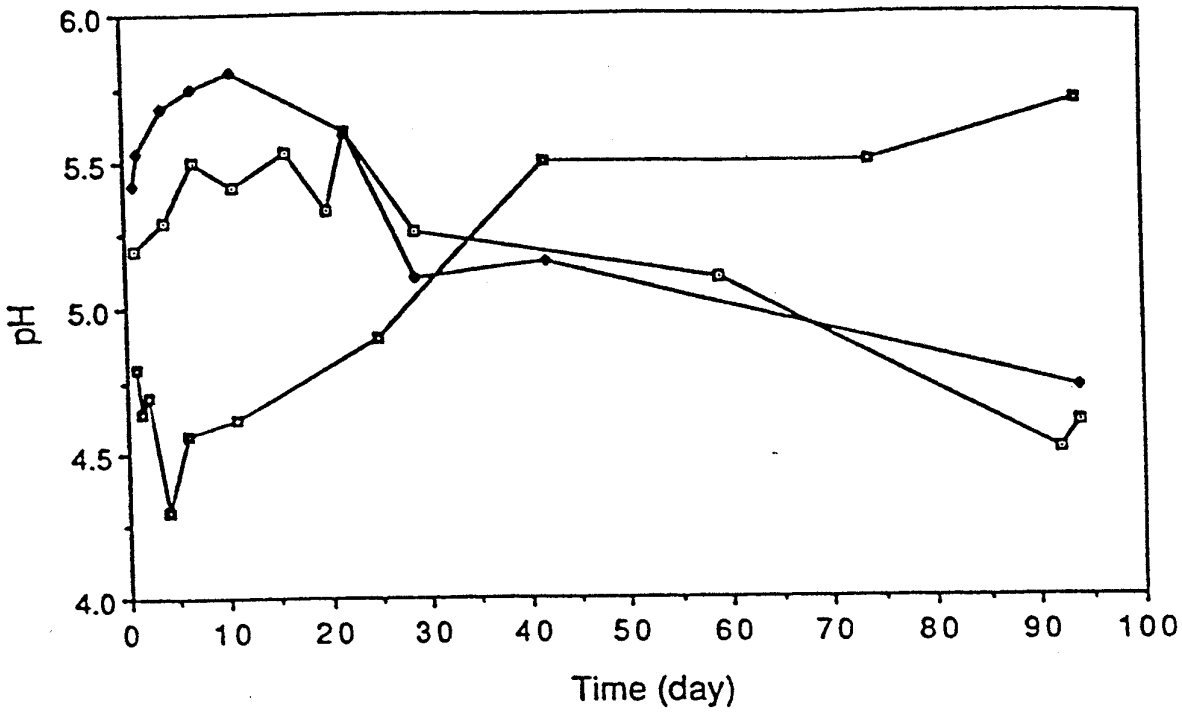

Figure 5.2.3.12
pH's of solution as functions of duration of chemical attack.
(⊡ = 90°C, ◆ = 150°C, ◘ = 190°C).

TABLE 5.2.3.3: Concentrations of Ti, Zr, Ni and HCO_3^- as Functions of Duration of Attack at 90°C (R4).

Duration(d)	Element (ppm)			
	Ti	Zr	Ni	HCO_3^-
1	*	*	*	21.20
4	*	*	0.09	12.12
7	*	*	0.09	29.30
11	*	*	0.56	5.64
16	*	*	0.14	8.65
20	*	*	0.74	29.56
22	*	*	0.12	20.50
29	*	*	0.50	28.49
59	0.10	*	0.09	11.30
92	*	*	0.50	23.47
94	0.39	*	0.84	16.83

* Below limits of detection

TABLE 5.2.3.4: Concentrations of Ti, Zr, Ni and HCO_3^- as Functions of Duration of Attack at 150°C (R5).

Duration (d)	Element (ppm)			
	Ti	Zr	Ni	HCO_3^-
1	*	*	0.18	29.20
2	0.02	*	0.18	6.15
4	0.11	0.02	0.23	6.21
7	*	*	0.08	11.14
11	0.10	*	1.30	9.53
22	*	*	0.35	8.64
29	0.04	*	0.10	17.32
42	0.02	0.08	0.40	21.16
94	0.40	*	0.38	12.50

* Below limits of detection

TABLE 5.2.3.5: Concentrations of Ti, Zr, Ni and HCO_3^- as Functions of Duration of Attack at 190°C (R6).

Duration (d)	Element (ppm)			
	Ti	Zr	Ni	HCO_3^-
1	0.21	0.03	0.20	5.25
2	0.26	0.03	0.10	6.36
4	0.19	*	0.11	11.21
6	0.08	0.03	1.10	10.11
11	0.23	*	0.08	7.63
25	*	*	0.98	8.17
42	*	*	*	12.36
74	0.40	*	*	11.62
94	0.26	*	0.09	5.00

* Below limits of detection

TABLE 5.2.3.6: Major Aqueous Species Identified by EQ3NR.

Element	90°C	150°C	190°C
Ca	Ca^{2+}, $CaCO_3$	Ca^{2+}, $CaCO_3$	Ca^{2+}, $CaOH^+$
Ba	Ba^{2+}	Ba^{2+}	Ba^{2+}
Mo	$HMoO_4^-$	$HMoO_4^-$	$HMoO_4^-$
Sr	Sr^{2+}	Sr^{2+}	Sr^{2+}
Al	$Al(OH)_4^-$	$Al(OH)_4^-$	$Al(OH)_4^-$
Si	SiO_2, $H_3SiO_4^-$	SiO_2, $H_3SiO_4^-$	SiO_2, $H_3SiO_4^-$
Na	Na^+	Na^+	Na^+
Cs	Cs^+	Cs^+	Cs^+
C	HCO_3^-, H_2CO_3	HCO_3^-, H_2CO_3	HCO_3^-, H_2CO_3

TABLE 5.2.3.7: Saturation Indices of Secondary Solid Phases Identified by EQ3NR.

	90°C			150°C			190°C		
	1d	20d	90d	1d	20d	90d	1d	4d	90d
Powellite $CaMoO_4$	2.171	3.117	3.600	0.615	0.694	1.103	0.563	0.522	0.378
$BaMoO_4$	-0.887	0.229	1.007	-1.814	-1.1714	-1.198	-2.001	*	*
$SrMoO_4$	1.235	2.314	3.310	0.119	0.026	1.211	-0.138	-0.212	-0.485
Diaspore AlO(OH)	-0.170	-0.672	-1.082	-0.210	1.507	-0.067	0.350	1.395	-0.468
Boehmite AlO(OH)	-0.740	-1.243	-1.652	-0.602	1.115	-0.459	0.051	1.097	-0.767
Gibbsite $Al(OH)_3$	0.110	-0.393	-.802	-0.312	1.405	-0.169	0.033	1.078	-0.785
Corundum Al_2O_3	*	*	*	*	1.144	-2.005	0.722		1.370
Calcite $CaCO_3$	-0.878	-0.107	0.310	-1.062	*	-0.589	-0.196	-0.989	0.156

5.2.3.4 SEM / EDS

Examination by SEM / EDS of powder specimens, chemically attacked at 90°C did not show any distinct precipitates. After 4d of chemical attack at 150°C, the majority of precipitates were Ba - Mo containing crystals. As the duration of attack was increased, Ba - Ca - Mo and then Ca - Mo containing phases started to form. The majority of precipitates after chemical attack at 190°C were Ca - Mo containing crystals. They could be detected after only 3hr of chemical attack. At this temperature, Ba - Ca - Mo and Ba - Mo phases were also found occasionally. The distribution of these precipitated products varied widely from one Synroc particle to another. In some cases, the surfaces of these particles appeared to be "covered" with precipitated crystals, as can be seen from Fig. 5.2.3.13. In other cases, these crystals were scattered sparsely. This is shown in Fig. 5.2.3.14. For both 150 and 190°C, other types of precipitates were also detected, but to a much lesser extent. Analyses by SEM/EDS of individual precipitate crystals which indicated a single element are assumed to be representative of oxides, carbonates or hydroxides of Fe, Ca, Ba, Ti, Al, and Zr (note that the EDS technique is not sensitive to O, C or lighter elements). In addition, precipitates containing Ba-Sr-Mo, Ca-Sr-Mo, Ba-Sr-Al-Mo, and Al-Zr were also observed. Fig. 5.2.3.15 shows some representative EDS spectra of the precipitated crystals.

5.2.3.5 XPS

Table 5.2.3.8 shows the Ca/Ti, Ba/Ti, Zr/Ti, Al/Ti and Mo/Ti ratios on the surfaces of monolithic disks which had undergone various chemical treatments. Also included in this table are the ratios for an "as-received" polished disc. It can be seen that the ratios of Zr/Ti, Al/Ti and Mo/Ti on the surfaces of disks attacked under high SA/V conditions (with powders) were higher, as compared to those on the "as-received" surface, or on the surface attacked under low SA/V condition (without powders). On the other hand, Ca/Ti and Ba/Ti ratios in the case of high SA/V condition were comparable to those in the case of the "as-received" surface, whereas the surface in the case of low SA/V condition had smaller values for the Ca/Ti and Ba/Ti ratios.

TABLE 5.2.3.8: Comparison of Elemental Ratios from XPS Data of Synroc Surfaces after Various Hydrothermal Treaments.

Surface Treament	Ca/Ti	Ba/Ti	Zr/Ti	Al/Ti	Mo/Ti
"as-received"	0.14	0.08	0.047	0.08	0.00
190°C-7d (R6, high SA/V)	0.15	0.08	0.060	0.21	0.02
190°C-7d (R7, low SA/V)	0.09	0.05	0.050	0.10	0.00
150°C-22d (R5, high SA/V)	0.14	0.09	0.064	0.14	0.05

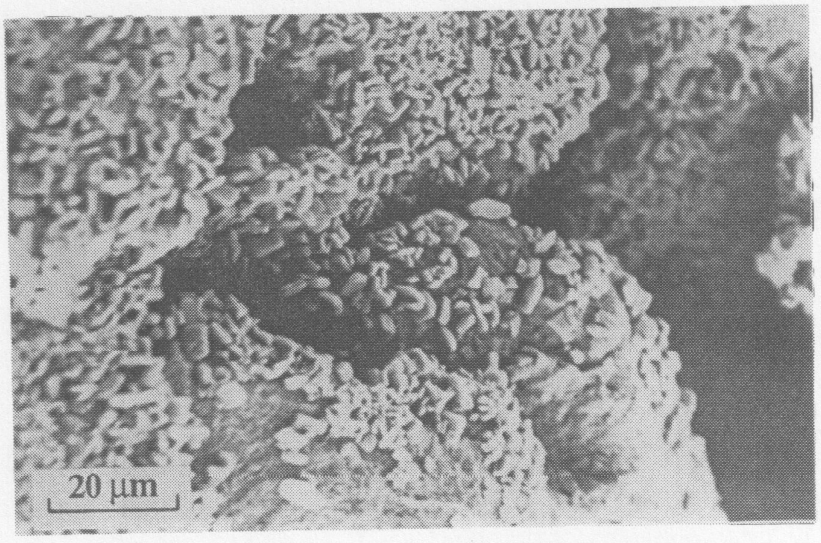

Figure 5.2.3.13
SEM micrograph showing precipitated crystals covering the surfaces of Synroc powders as a result of hydrothermal chemical attack.

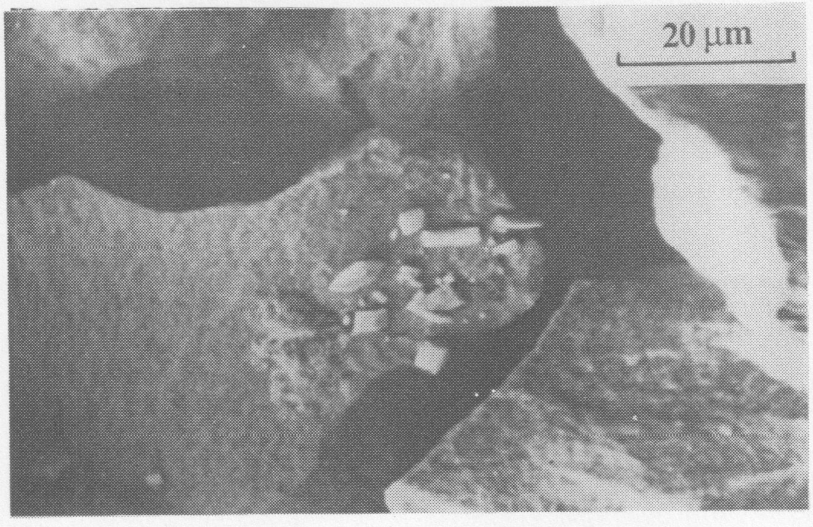

Figure 5.2.3.14
SEM micrograph showing a much less extent of precipitated crystal than that of figure 5.2.3.13.

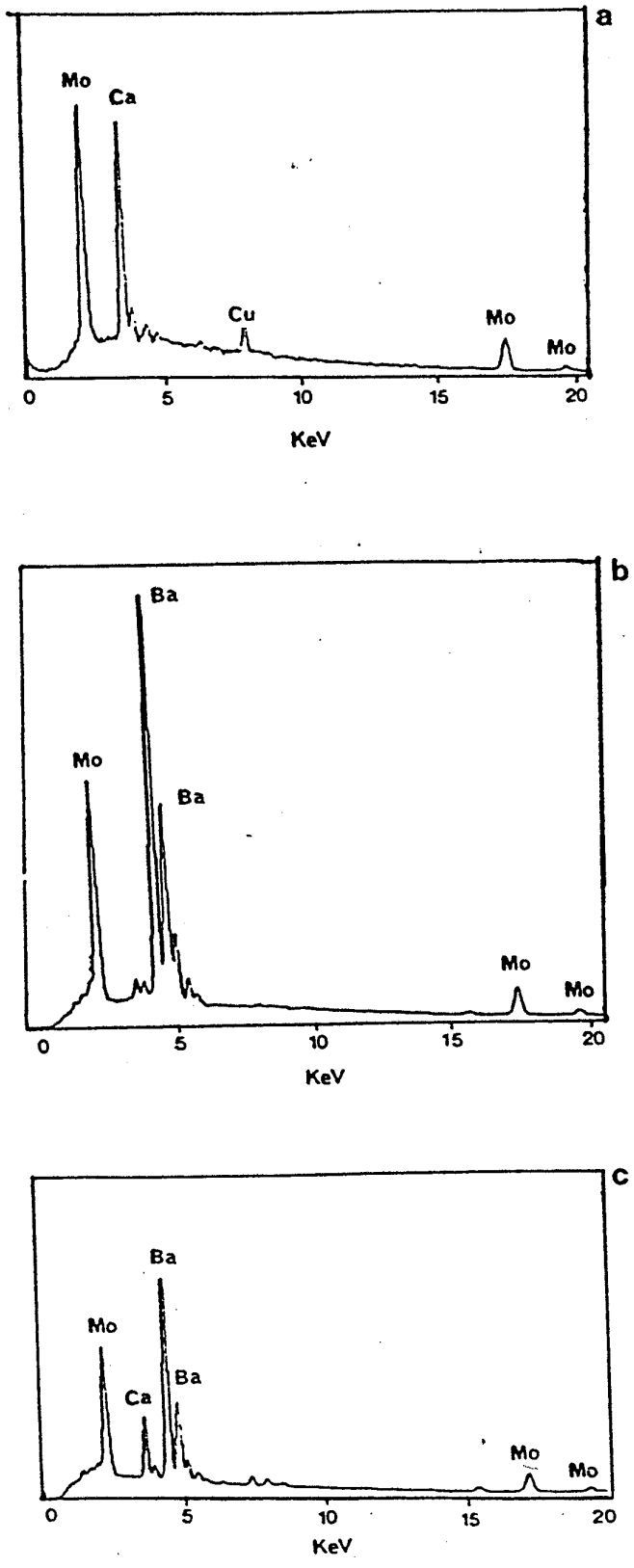

Figure 5.2.3.15
Representative EDS spectra of surface precipitate.

5.2.4 Discussion

5.2.4.1 Effects of Quenching

For runs at 90°C, solution analysis results (R3) indicated conclusively that cooling to ambient temperatue had no recognisable effect on the solution composition.

For runs at 150 and 190°C, almost all potential precipitate phases such as alkaline-earth carbonates and molybdates, Al-containing phases, etc., as were identified by EQ3NR and SEM/EDS, have inverse solubility relationship with temperature (i.e., the solubility decreases with increasing temperature). The detection of these precipitates by SEM/EDS, and the observation of the increase in the values of Mo/Ti, Al/Ti, etc., by XPS, therefore, cannot be an artefact of the cooling process. Furthermore, solution analyses showed that elements which gave rise to precipitate phases generally levelled out at values lower than those found in experiments with shorter durations. This observation, coupled with the solubility-temperature characteristics of the precipitate phases as mentioned above, suggest that the back-reactions during the cooling process, if any, would not significantly alter these conclusions. This argument is also supported by the results from runs R2,where analyses of the precipitating elements (such as Ba, Mo , Ca) gave concentrations which were independent of the SA/V parameter, once the system approached the saturation limits. Also, the secondary solid phases were generally similar for all runs at both temperatures. These observations suggest that even if back reactions had occurred, the rates at which a particular element was released into solution through back reaction processes would have been similar for all runs. Coupled with the fact that the cooling process was identical for all runs (30min in ambient air), these arguments suggest that the trends exhibited by the measured levels of elements in solution taken after the cooling process would reflect correctly the evolution of the fluid phase at higher temperatures.

5.2.4.2 Saturation and Precipitation Effects

Calcium, Barium, Strontium and Molybdenum

At 90°C, concentrations of Ca in solution had values around 6ppm. Computer simulations indicated that the solutions were saturated or supersaturated with calcium carbonate or molybdate phases. It is therefore likely that the Ca concentrations in solution at this temperature were controlled by the saturation and precipitation of these phases. In the cases of Ba and Sr, the saturation index data also suggest saturation or supersaturation for carbonates or molybdates of these elements. Solution analysis results, however, showed increases in concentrations of these elements with duration of attack, suggesting an overall dominance of dissolution kinetics. Examination by SEM/EDS of the powders after chemical attack at 90°C did not identify any distinct precipitate crystals. Therefore, it must be assumed that kinetic constraints are apparently important in the precipitation / crystallisation processes of these phases.

At 150 and 190°C, concentration data for these elements showed an overall dominance of dissolution kinetics during the initial period (with the exception of Ba at 190°C, which had concentrations of about 7.5ppm). Further attack beyond this stage had the effect of decreasing the concentrations of these elements, until finally became steady with the progress of chemical attack. At these temperatures, saturation index data indicated that the solutions were saturated (or slightly supersaturated) with respect to carbonates and molybdates of Ca and Sr. The formation of Ba carbonate and molybdate precipitates was also predicted at 150°C, while only Ba carbonate was thermodynamically favoured at 190°C. These data are in accord with the results obtained by SEM/EDS, which showed

crystals containing Ca-Mo, Ba-Mo, Sr-Ca-Mo, Sr-Ba-Mo, Ca, Ba (the last two are presumably $CaCO_3$ and $BaCO_3$ phases) after attack at 150°C. In the case of attack at 190°C, the majority of Mo precipitates contained Ca. Most of the Ba precipitates at this temperature were (presumably) $BaCO_3$ crystals since SEM/EDS revealed only a Ba peak. The totality of results suggests that, in the long term, the concentrations of Ca, Ba, Sr and Mo in solution are buffered by the precipitation of carbonates and molybdates.

Previous studies have established that the majority of Sr is accomodated in the perovskite phase [Fielding and White 1987], and that Ca and Sr should be released at the same normalised rate, i.e., congruently, at low SA/V ratio and undersaturated conditions[Myhra et al., 1988]. In this study, the precipitation processes obscured the congruency.

Mo has been known to form alloys with elements such as Ru, Fe,Ag [Myhra et al., 1987]. These alloy phases, when in the surface, are substantially oxidised on exposure to air, leading to unexpected and relatively high initial loss rates of Mo from Synroc in the case of low SA/V ratio. The presence of Mo alloy phases in Synroc material used in this study was confirmed by SEM/EDS; and, as inferred from the low SA/V case, these phases might be primarily responsible for the increase in the concentration of Mo in solution to ≈ 60ppm after about 20d and 4d of attack at 150 and 190°C, respectively. However, these alloy phases did not appear to dissolve readily at 90°C, as indicated by the gradual increase of Mo concentrations up to a maximum of ≈ 18ppm after about 90d of attack at this temperature. This is in contrast to the case of low SA/V, which showed loss of Mo from alloy phases within the first day of contact with an aqueous solution. The reasons for the different behaviour at high SA/V ratio are not clear, but it is possible that the solution chemistry, i.e., the presence of a variety of other species in solution at high concentrations, might have limited the dissolution rates of these phases.

The totality of the solution analysis results for Ca, Sr (the majority of which is incorporated in perovskite) and Ba (which is largely immobilised in the hollandite-type phase) suggests that most of the dissolution of perovskite and hollandite-type phases (presumably in the near - surface regions) occurred within the first 10d of aqueous attack at temperatures > 150°C. It is noteworthy that it took about 90d or more of attack at 90°C for Sr and Ba to attain extents of dissolution equivalent to the corresponding peak values (i.e., saturation maxima) in the higher temperture cases (which were achieved within the first 10d). Given that the precipitation / crystallisation kinetics at 90°C were slower than those at higher temperatures, it is reasonable to argue that the rates of dissolution of perovskite and hollandite -type phases were drastically reduced at the lower temperature. There is still some uncertainty, however, as to whether the "long term" steady-state concentrations for these elements were due to equal rates of dissolution and precipitation, or to the attainment of thermodynamic equilibrium of the total system, thus inhibiting further attack.

Aluminium

Al is a matrix element in Synroc assemblage, the majority of which is incorporated in the hollandite-type phase. Al is also known to be present in "glassy" triple points and intergranular films. Concentration data for Al at all three temperatures indicated that this element followed trends similar to those for Mo and Sr. At 90°C, dissolution kinetics dominated in all cases, while at 150 and 190°C, dissolution kinetics was prominent in the initial stage of the attack, followed by steady concentration of Al. Saturation index data suggest that the solutions were saturated or slightly supersaturated with respect to AlO(OH), $Al(OH)_3$, and sometimes Al_2O_3 as in the cases of attack at 150 or 190°C. These theoretical predictions were supported by the detection of crystals showing only the Al peak in EDS spectra. These results suggest that the long term concentration of Al in solution is controlled by precipitation of oxides or hydroxides. It is noteworthy that AES and SEM in

combination have detected the formation of Al_2O_3 (or AlO(OH)) on the hollandite phase after hydrothermal attack under low SA/V condition [Myhra et al., 1984].

Cesium, Sodium and Silicon

Cs is one of the most leachable waste elements, at least in the initial phase of attack [31]. It is immobilised in the hollandite-type phase. "Glassy" triple points, intergranular films and porosity also selectively segregate this element [Cooper et al., 1984]. Na and Si are contaminants incorporated during the fabrication process. They are also found in intergranular films and "glassy" triple point regions. Na can enter perovskite in a one-to-one molar ratio with trivalent rare-earth elements. The minor phase freudenbergite ($Na_2Fe_2Ti_6O_{16}$) is thought to be the major host for Na in Synroc formulation [Warmeant et al., 1986]. The totality of experimental data suggests that Cs and Na remained undersaturated in solution. Dominance of dissolution kinetics is seen in the increase in concentration of these elements with the progress of chemical attack. For Si, the concentration and saturation index data suggest that the solution should be saturated with respect to SiO_2 phases in most cases.

Discussion of XPS Results

XPS results for the values of the Ca/Ti, Ba/Ti, Mo/Ti, and Al/Ti ratios on the surfaces of monolithic disks which had undergone different hydrothermal treatments are consistent with the arguments made above, relating to the saturation and precipitation of secondary phases containing Ca, Ba, Mo and Al.

Discussion of pH Results

Finally, the pH-time graphs presented in Fig. 5.2.3.12 show a number of similarities between different experimental temperatures. Firstly, there was a progressive increase in pH over the first 10d for both 90 and 150°C. It is likely that this initial stage reflects an ion-exchange mechanism between the alkali and alkaline earth cations of the solid and the protons of the fluid phase, leading to a decrease in hydrogen ion activity. In the second stage, this process is superceded so that attainment of the equilibria of the dissolved species (i.e., hydrolysis reactions) results in a net transfer of protons into solution rather than out of solution, resulting in a decrease in pH. Based on the evidence presented concerning precipitation of secondary solid phases, the most likely means of achieving proton production (or hydroxyl consumption) is through reactions such as:

$$Al^{3+} + 2H_2O \longrightarrow AlO(OH) + 3H^+$$
$$2Al^{3+} + 3H_2O \longrightarrow Al_2O_3 + 6H^+$$
$$Al^{3+} + 3H_2O \longrightarrow Al(OH)_3 + 3H^+$$

or reactions which produce alkaline-earth carbonates such as:

$$Ca^{2+} + HCO_3^- \longrightarrow CaCO_3 + H^+$$

It is also likely that base catalysed hydrolysis reactions of the titanate structure, which produce $Ti(OH)_x^{(4-x)+}$ species in the surface, have the effect of decreasing the solution pH. These reactions could therefore be among those causing the observed long term trend of pH. It is not clear, however, why the pH of solutions after chemical attack at 190°C exhibited trends different from those at 90 and 150°C.

5.2.5 Concluding Remarks and Further Work

The data presented in this preliminary study demonstrate clearly the importance of saturation of elements in solution and precipitation of secondary solid phases in evaluating the performance of Synroc. It is primarily these phases which will determine the extent of near-field retardation of radionuclides in solution vis a vis migration into the far-field regions throughout the repository core.

Generally, there is a good agreement between the theoretical model concerning the predicted products and the experimental results throughout this study. However, further work to determine the actual structures of the precipitate phases is necessary. Also, a lack of understanding of the effects of solution chemistry on the reactivity of the titanate phases and of microstructural features such as intergranular films, pores and "glassy" triple points has hindered further interpretation of the experimental data and limited the correlation with results from low SA/V conditions. In addition, lack of knowledge concerning precipitation / crystallisation kinetics of various secondary solid phases has introduced further uncertainties. These are the more important aspects that have to be resolved for a more complete picture.

Another factor that complicated the interpretation is the presence of CO_2 in solution. Atmospheric CO_2 might be absorbed into the starting solution, or adsorbed onto Synroc powder surfaces (as CO_3^{2-} and HCO_3^-) before commencement of the experiments. Definition of the effects of CO_2 is therefore essential, not only for the concerns of this study but it is also relevant to realistic repository conditions, where ground water is expected to contain a substantial amount of dissolved CO_2. Within this context, the effects of silica and the interactions between Synroc and repository rock minerals should be investigated, so that these factors can be incorporated into long term extrapolation models. Experiments at higher temperatures (in the range 250 - 350°C) should also be conducted since these temperatures may occur in "fresh" waste disposal strategies and could alter reaction paths in the system.

In parallel with the experiments described above, studies to investigate the temperature - pressure characteristics of solid precipitates should be carried out. This is important in reliable long term extrapolation, and may be achieved by experimental work on simple systems and by consideration of the geological occurences of "natural analogues" of the solids. More thermodynamic data for species and minerals relevant to Synroc (e.g. Ti, Zr, Ni) should be added to the database of EQ3NR.

REFERENCES

1. Appleman, D. E. & Evans, H.T., Jr. 1973. Indexing and least squares refinement of powder diffraction data, U.S. Technical Report.

2. Apted, M.J., McKay, G.L., Wald, J.W., 1986, Release of actinides from defence waste glass under simulated repository conditions, Nucl. Technol., **73**, pp. 165-178.

3. Ball, C. J. , Blake, R.G., Cassidy, D.J., Woolfrey, J.L., 1988, "Neutron irradiation effects in perovskite.", J. Nuc. Mat., **151**,pp. 151-161.

4. Ball, C. J. , Buykx, W.J., Dickson, F.J., Hawkins, K., Levins, D.M., Smart, R.StC., Smith, K.L., Stevens, G.T., Watson, K.G., Weedon, D., White, T.J., 1989, "Titanate ceramics for the stabilization of partially reprocessed nuclear fuel elements.", J. Amer. Ceram. Soc., **72**,(3): pp. 404-414.

5. Buykx, W. D. , Woolfrey, J.L., Bartlett, J., Seatonberry, B.W., 1988, "Ceramic powders from alkoxides.", The Material Wealth of the Nation (Proc. Bicentennial Conf.), Sydney, May,1988.

6. Buykx, W. J. , Levins, D.M., Smart, R.StC., Smith, K.L., Stevens, G.T., Watson, K.G., Weedon, D., White, T.J., 1989, "Interdependence of phase chemistry, microstructure and oxygen fugacity in titanate nuclear waste ceramics.", J. Amer. Ceram. Soc., in press.

7. Buykx, W. J. , Levins, D.M., Smart, R.StC., Smith, K.L., Stevens, G.T., Watson, K.G., White, T.J., 1989, "Processing impurities as phase assemblage modifiers in titanate nuclear waste ceramics.", J. Amer. Ceram. Soc., in press.

8. Buykx, W. J. , Hawkins, K., Levins, D.M., Mitamura, H., Smart, R.StC., Stevens, G.T., Watson, K.G., Weeton, D., White, T.J., 1988, "Titanate ceramics for the immobilisation of sodium-bearing high level nuclear waste.", J. Amer. Ceram. Soc., **71**,(8): pp. 678-678.

9. Coles, D. G. & Bazan, F., 1982, "Continuous flow leaching studies of crushed and cored Synroc.", F. Nuclear Technology, **56**,pp. 226-238.

10. Cooper, J. A. , Cousens, D.R., Hanna, J., Lewis R.A., Myhra, S., Segall, R.L., Smart, R.StC., Turner, P.S., White, T.J., 1986, "Intergranular films and poor surfaces in Synroc C. Structure, composition, and dissolution characteristics.", J. Amer. Ceram. Soc., **69**,pp. 347-352.

11. Cooper, J. A. , Cousens, D.R., Lewis, R.A., Myhra, S., Segall, R.L., Smart, R.StC., Turner, P.S., White, T.J., 1985, "Microstructural characterisation of Synroc C and E by electron microscopy.", J. Amer. Ceram. Soc., **68**, pp. 64-70.

12. Costello, J. M., Jan/Oct,1984, "Current state of the art in high-level radioactivewaste disposal.", Atomic Energy in Australia, pp. 17-40.

13. Cousens, D. R. , Lewis, R.A., Myhra,S., Segall,R.L., Smart, R.StC., Turner, P.S., "Evaluating glasses for high level radioactive waste immobilisation.", Radioactive Waste Management, 2, 1981.

14. Cousens, D. R. , Lewis, R.A., Myhra, S., Segall, R.L., Smart, R.StC., Turner, P.S., White, T.J., 1985, ".Microstructural characterisation of Synroc C and E be electron microscopy.", J. Amer. Ceram. Soc., **68**, pp. 64-70.

15. Cousens, D. R. , Lewis, R.A., Myhra, S., Segall, R.L., Smart, R.StC., Turner, P.S., 1982, "The chemical durability of some HLW glasses: effects of hydrothermal conditions and ionising radiation.", Scientific Basis for Radioactive Waste Management, 5.

16. Cousens, D. R. , Penrose, J., Segall, R.L., Smart, R.StC., Turner, P.S., 1982, "The microstructure of Synroc.", Scientific Basis for Radioactive Waste Management, 5.

17. Dickson, F. J. , Mitamura, H., White, T.J., 1989, "Radiophase development in hot-pressed alkoxide derived titanate ceramics for nuclear waste stabilization.", J. Amer. Ceram. Soc., 72, pp. 1055-1059.

18. Dickson, R. J. , Hawkins, K.D., White, T.J., 1988 submitted, "Calcium Uranium titanate- A new Pyrochlore.", J. Sol. State Chem.

19. Dosch, R. G. & Lynch, A.W., 1981.

20. Dosch, R. G. et. al., 1983.

21. Fielding, P. E. , & White, T.J., 1987, "Crystal Chemical Incorporation of High-Level Waste Species in Aluminotitanate Based Ceramics: Valence, Location, Radiation Damage and Hydrothermal Stability.", J. of Materials Research , 2, pp.387-414.

22. Fielding, P. E., 1989. Incorporation of lanthanide elements in Zirconolite, AINSE Report.

23. Fyfe, W. S. & Verhoogen, J., 1958, "Metamorphic Reactions and Metamorphic Facies.", Geological Soc. of Amer. Memoir , **73**, pp. 53.

24. Jostsons, A. &. Reeve, K.D., "Immobilisation of high-level waste in Synroc.", 6th Pacific Basin Nuclear Conf., Beijing, China, 5-11 September, 1987.

25. Kastrissios, T. Stephenson , M., Turner, P.S., White, T.J., 1987, "Hydrothermal dissolution of perovskite. Implications for Synroc formulation.", J. Amer. Ceram. Soc., **70**, pp. 144-146.

26. Levins, D. M. & Smart, R.StC., 1984, "Effects of acidification and complexation from radiolytic reactions on leach rates of Synroc C and nuclear waste glass.", Nature, **309**, (5971): pp. 776-778.

27. Levins, D. M. , Reeve, K.D., Buykx, W.J., Ryan, R.K., Seatonberry, B.W., Woolfrey, J.L., Hart, K.P., "Fabrication and performance of Synroc.", Specrum 86, Proc. Int. Topical Meeting on Waste Management, Niagra Falls, 14-18 Sept., 1986, CONF 86095.

28. Levins, D. M. & Jostons, A., "Syroc-Radiological implications of high-level wastemanagement strategies.", Int. Conference of Radiation Protection in Nuclear Energy, Sydney, April, 1988. IAEA-CN-51/103.

29. Lewis, R. A. & Smart, R.StC., 1983, "Experimental factors in glass leaching at high temperatures.", Physics and Chemistry of Glasses, **24**, (4): pp. 93-97.

30. Lewis, R. A. , & Segall, R.L., 1982, "Pressure dependence of glass dissolution: its bearing on nuclear waste disposal.", Nature, **299**, pp. 140.

31. Lewis, R. A. , Myhra, S., Segall, R.L., Smart, R.StC., Turner, P.S., 1982, "The surface layer formed on zinc-containing glass during aqueous attack.", J. of Non-Crystalline Solids, **53**, pp. 299-313.

32. Lutze, W., & Ewing, R.C., 1988, Radioactive Waste Forms of the Future, pp. 699-740., eds. Lutze & Ewing, North-Holland Physics Publishings., Amsterdam.

33. Macedo, P. B.et. al., 1982, Nuclear Chem. Waste Management , **3**, pp. 13.

34. Matzke, Hj Ray , I.L.F., Seatonberry, B.W., Thiele, H., Trisolio, H., Walker, C.T., White, T.J., 1989, "The incorporation of transuranic elements in titanate nuclear waste ceramics.", J. Amer. Ceram. Soc., in press.

35. MCC. 1983. MCC-1P Static Leach Test Method (Rev. 1), Materials Characterisation Center, Battelle Northwest Laboratory, Richland, W.A.

36. MCC. 1984. MCC-2S Agitated Powder Leach Test Method (Appendix A), Materials Characterisation Center, Battelle Northwest Laboratory, Richland, W.A.

37. Mendel, J. E., 1982, "The Measurement of Leach Rates: A Review.", Nucl. Chem. Waste Management , **3**, pp. 117-123.

38. Mitamura, H. Matsumoto , S., Buykx, W.J., Tashiro, S., 1988 submitted,"Fabrication of a curium-doped Synroc for an Alpha Radiation Stability Test.", J. of Nuc. Technology.

39. Myhra, S. et al., 1987. Aust. Govt. Publishing Officer.

40. Myhra, S. Segall , R.L., Smart, R.StC., Stephenson, M., Turner, P.S., White, T.J., "Characterisation of Synroc microstructure and durability and its influence on final disposal of radioactive waste products.", Radioactive Waste Products, Julich, 1986.

41. Myhra, S. White , T.J., Kesson, S., Riviere, J.C., 1987, "Direct identification of Ti valence states in a titanate mineral (Hollandite).", Amer. Mineralogist , **73**, pp.161.

42. Myhra, S. Pham , D.K., Smart, R.StC.,Turner, P.S., "Dissolution mechanisms of Perovskite and Hollandite phases in the Synroc assemblage.", 13th Int. Symp.Sci. Bases for Nuclear Waste Management, Boston, November, 1989.

43. Myhra, S. Bishop , H.E., Riviere, J.C., 1985, "Features of fracture faces in Synroc C.", Surf. Techn , **25**, pp. 259-272.

44. Myhra, S. Bishop , H.E., Riviere, J.C., 1987, "Hydrothermal dissolution of perovskite ($CaTiO_3$).", J. Mater. Sc , **22**, pp. 3217-3226.

45. Myhra, S. Segall , R.L., Smart, R.StC., Turner, P.S., White, T.J., "Intergranular films and pore surfaces in Synroc C.", Scientific Basis for Nuclear Waste Management, 90 Materials Research Society, 1986.

46. Myhra, S. Bishop , S.E., Riviere, J.C., 1983, "Investigation by X-ray Photoelectron Spectroscopy of surface features of some titanate Minerals.", Surf. Techn , **19**, pp. 161.

47. Myhra, S. Delogu , P., Giorgi, R., Riviere, J.C., 1988, "Scanning andhigh-resolution Auger analysis of zirconolite//perovskite surfaces following hydrothermal treatment.", J. Mater. Sc., **23**, pp. 1514-1520.

48. Myhra, S. Bishop , H.E., Riviere, J.C., 1983, "Surface Analysis of Features of Synroc B and C.", Surf. Techn , **19**, pp. 145.

49. Myhra, S. Atkinson , A., Riviere, J.C.,1984, "Surface analytical study of Synroc subjected to hydrothermal attack.", J. Amer. Ceram. Soc , **67**, pp. 223-227.

50. Myhra, S. Savage , D., Atkinson, A., Riviere, J.C., 1984b, "Surface modification of some titanate minerals subjected to hydrothermal chemical attack.", Amer. Mineralogist , **69**, pp. 902-909.

51. Myhra, S. Segall , R.L., Smart, R.StC., Turner, P.S., 1984, "The adequacy of glassas a solid for high level radioactive waste disposal.", Atomic Energy in Australia , **27**, pp. 42-47.

52. Myhra, S. Smart , R.StC., Turner, P.S., 1988, "The surfaces of titanate minerals, ceramics and silicate glasses.", Scanning Microscopy , **2**, pp. 715.

53. Oversby, V. M. & Ringwood, A.E., 1982, Radioactive Waste Management , **2**, (2):

54. Pham, D. K., 1989, "Chemical durability of perovskite ($CaTiO_3$) and thermodynamic factors affecting Synroc dissolution.", Griffith University, Queensland, Australia.[Ph.D Thesis.]

55. Pham, D. K. , Neall, F.B., Smart, R.StC., Turner, P.S., "Dissolution mechanisms of $CaTiO_3$- solution analysis, surface analysis and electron microscope studies-implications for Synroc.", Mat. Res. Soc. Symp. Proc, 1989.

56. Pham, D. K. , Myhra, S., Neall, F.B., Smart, R.StC., Turner, P.S., 1990a, (submitted), "The chemical durability of Perovskite ($CaTiO_3$): Solution and analytical studies.", J. Amer. Ceram. Soc.

57. Pham, D. K. , Myhra, S., Neall, F.B., Smart, R.StC., Turner, P.S. 1990b, (submitted), "The chemical durability of Perovskite ($CaTiO_3$): Solution and analytical electron microscopy.", J. Amer. Ceram. Soc.

58. Reeve, K. D. , Levins, D.M., Seatonberry, B.W., Ryan, R.K., Hart, R.K.,Stevens,G.T."Fabrication and performance of raadioactive Synroc.", The Material Wealth of the Nation (Proc. Bicentennial Conf.), Sydney, 1988.

59. Reeve, K. D. , Levins, D.M., Seatonberry, B.W., Ryan, R.K., Hart, K.P., Stevens, G.T. "Fabrication and leach testing of Synroc containing actinides and fission products.", Scientific Basis for Nuclear Waste Management,12, Berlin, October, 1988.

60. Reeve, K. D. et. al. 1987. Fabrication and Study of Synroc containing radioactive waste elements, NERDDC Report, Grant 498.

61. Reeve, K. D. , Levins, D.M., Seatonberry, B.W., Ryan, R.K., Hart, K.P., Stevens, G.T., 1988. Fabrication and study of Synroc containing radioactive waste elements, AAEC/ C60.

62. Reeve, K. D. et. al. 1983. Synroc fabrication development.

63. Ridal, A. Ramm , E.J., Reeve, K.D.,"Full scale fabrication of Synroc in a non-radioactive plant.", The Material Wealth of the Nation (Proc. Bicentennial Conf.), Sydney, 1988.

64. Ridal, A. Ramm , E.J., Reeve, K.D., 1988, "Full scale fabrication of Synroc in a Non-Radioactive Plant.", The Material Wealth of the Nation. (Pro. Bicentennial Conf), Sydney, May, 1988.

65. Ringwood, A. E., 1984. Nuclear waste immobilisation.

66. Ringwood, A. E., 1987. Nuclear waste immobilistion in Synroc, December 1985.

67. Ringwood, A. E. , Kesson, S.E., Reeve, K.D., Levins, D.M., Ramm, E.J. 1988, Radioactive Waste Forms for the Future, Chpt. 4, 'Synroc', pp. 223-334. Amsterdam: North-Holland Physics Publishing.[Chpt. 4, 'Synroc', pp. 223-344.]

68. Ringwood, A.E., Oversby, V.M., Kesson, S.E., Sinclair, W., Ware, N.G., Hibberson, W.D., Major, A., 1981, Immobilisation of high -level nuclear wastes in Synroc: A current appraisal., Nuclear and Chem. Waste Management., **2**, pp. 287-305.

69 Roberts, R. D. , White, G.K., Buykx, W.J., Cassidy, D.J., 1987, "Thermal expansion of Synroc minerals.", J. of Nuc. Materials, **148**, pp. 353-355.

70. Roussouw, C. J. , Turner, P.S., White, T.J. "Site identification of impurities of perovskite by ALCHEMI using zone axis diffraction conditions.", Int. Conf. on Anal. Electron Microscopy, Hawii, U.S.A, 1987.

71. Savage, D. 1984. British Geological Survey Report.

72. Segall, R. L. et al. 1983. Evaluation of critical properties of Synroc for disposal of high level radioactive waste.

73. Segall, R. L. , Smart, R.StC., Turner, P.S., 1988, "Surface and near-surface chemistry of oxide materials.", Oxide surfaces in solution, pp. 827-576. Elseviere:[invited review.]

74 Smart, R. StC et al. 1987. Scientific and technical evaluation of the Synroc fabrication program, Griffith University.

75. Smart, R. StC. 1988. Scientific and technical evaluation of the Synroc fabrication program, Griffith University, NEERDDP Report, EG89/809.

76. Smart, R. StC. 1985, "The validity of SIMS observations of alkali metal segregation into intergranular regions of ceramics.", Applications of Surface Science , **22/23**, pp. 90-99.

77. Stevens, G. T. & Reeve, K.D. "Microstructure aspects of Synroc manufacture.", 1987 Australasian Conf., Proc. of Institute of Metals and Materials, Australasia, Christchurch, New Zealand, 24-26 August, 1987.

78 Stevens, G.T., Watson, K.G., Bellrose, A., 1987, Synroc from Sandia Percursor II. Some effects of impurities.

79. Stewart, M. W. A. & Buykx, W.J. "Synroc preperation from a conventional ceramic precursor.", The Material Wealth of the Nation (Proc. Bicentennial Conf.), Sydney, 1988.

80. Sykes, R. F. R. 1965, "Seperation of Glass Grain Samples for Durability Tests.", Glass Technology, **6**, pp. 178-183.

81. Szjaman, J. Smart , R.StC., Myhra, S. 1987, "X-Ray photoelectron spectroscopy studies of valence states of cerium and uranium in Synroc C.", Surface and Coatings Technology, **30**,pp. 333-342.

82. Turner, P. S. , Jones, C.F., Myhra, S., Neall, F.B., Pham, D.K., Smart, R.StC. "Dissolution mechanisms of oxides and titanate ceramics- electron microscope and surface analytical studies.", Proceedings of the NATO Advanced Study Institute on Surfaces and Interfaces of Ceramic Materials, Sept. 1988.

83. Warmeant, J.H. et al., 1986, Synroc Progress Note No. 87.

84. White, T. J. , Segall, R.L., Turner, P.S. 1985, "Radwaste immobilization by structural modifications - the crystallochemical properties of Synroc, a titanate ceramic.", Angewandte Chemie. Int. Edn. Engl., 24, pp. 357-365.

85. Wolery, T. J. 1979. The EQ3/6 Software Package,

86. Woolfrey, J. L. , Levins, D.M., Smart, R.StC., Stephenson, M. 1989, "Effect of hot-pressing conditions on the structure and leaching of Synroc.", Amer. Ceram. Soc. Bull , **66**, (12):pp. 1739-1746.

87. Woolfrey, J. L. , Bartlett, J.R., Buykx, W.J., "Preparation of multi-component ceramic powders by alkoxide hydrolysis: The prepartion of Synroc.", 2nd Int. Conf. on Ceramic Powder Processing Science, Berchetsgaden, 12-14 October, 1988.

88. Woolfrey, J. L. , Cassidy, D.J., Buykx, W.J., Dickson, F., White, T.J., "The Calcination of Synroc powders.", The Material Wealth of the Nation (Proc. Bicentennial Conf.), Sydney, 1988.